CRYSTALLINE AND GLASSY STATES OF ULTRACOLD ATOMIC SYSTEMS

BY

SARANG GOPALAKRISHNAN

DISSERTATION

Submitted in partial fulfillment of the requirements
for the degree of Doctor of Philosophy in Physics
in the Graduate College of the
University of Illinois at Urbana-Champaign, 2012

Urbana, Illinois

Doctoral Committee:

Professor Eduardo Fradkin, Chair
Professor Paul Goldbart, Director of Research
Professor Brian DeMarco
Professor John Stack

Abstract

Spatially modulated ordered states, such as crystals, liquid crystals, and antiferromagnets, are ubiquitous in nature but relatively difficult to realize in ultracold atomic systems. In the present work, we present a scheme for generating controllable cavity-mediated interactions between atoms, and show that these interactions give rise to a crystallization transition in the case of a transversely pumped optical cavity. We focus on the case of multimode cavities, in which the interactions are relatively local and the range of possible ordered configurations (and consequently of low-energy fluctuations) is large; as we show, the crystallization transition for a Bose-Einstein condensate in a multimode cavity is driven first-order by fluctuations, through the Brazovskii effect. The ordered state to which this crystallization transition gives rise is a "supersolid" [1], possessing both superfluid and solid order. We address the crystallization transition and the properties of the ordered state, discuss the experimental feasibility of observing these, and finally show how ordering in layered systems of atoms is geometrically frustrated. We then introduce a more straightforward realization of frustrated cavity-mediated interactions, viz. systems of randomly-positioned spins in multimode cavities. We show by means of a mapping to a variant of the Hopfield associative-memory model [2, 3] that such systems exhibit a spin-glass phase. Finally, we consider a different ultracold-atomic setting—that of spin-orbit-coupled Bose gases—in which the Brazovskii effect has a profound influence on the low-temperature phases, leading to a universal preference for stripe-like ordering at zero temperature and bosonic pair condensation at nonzero temperatures.

Acknowledgments

Thou shalt not do as the dean pleases,
Thou shalt not write thy doctor's thesis ...

— W.H. Auden, "Under Which Lyre"

First things first: I was exceedingly lucky to have had Paul Goldbart for an advisor. The extent of this good fortune is only clear in retrospect. Working with Paul was always enjoyable—he had something unexpected and interesting to say about almost anything, and was always encouraging—but I did not realize at the time how profoundly he was shaping my sensibility as a physicist. One cannot summarize these things easily, so I will simply note that his example gave me the courage to be curious about problems in which I had no specific expertise, and left me with the sense that one *could* often say a great deal about a system on general grounds. And I am grateful that Paul knew when I could be left to my own devices, and even more grateful that he sensed when I couldn't.

I have been fortunate in my collaborators. Benjamin Lev and I have been exchanging ideas, arguing, and conspiring to publish papers for almost as long as I have been a graduate student; much of the work presented in this thesis was originally his idea, and I have learned most of what I know about atomic and optical physics from him. He has also been, over the years, a fount of brilliant ideas and enthusiasm. The rest of the work presented here (i.e., the chapter on spin-orbit coupled condensates) was done in collaboration with Austen Lamacraft, from whom I learned much about how to fuse a love of elegant mathematics with an interest in real systems.

I am equally grateful for the collaborations that are not documented in this thesis (chiefly because each of them would have entailed a separate introductory chapter). Serena Eley and Nadya Mason were very generous with their time and their wonderful data on superconducting island arrays; I only wish I had done a better job of explaining it. My conversations with Nadya taught me a great deal, especially about how the scientific method at its best *works* in practice. I am also grateful to Matt Brenner and Alexey Bezryadin, and to Nayana Shah, for our long collaboration on nanowire-based resonators; they were all more patient

with me than I deserved. And I am grateful to Siddhartha Lal and Pouyan Ghaemi for many things, not least for sustaining my interest in the Kondo problem.

Nigel Goldenfeld, Tony Leggett, Eduardo Fradkin, and Brian DeMarco taught me most of the graduate-level physics I still remember; a paean to each would be in order, but is beyond my abilities. The latter two, as well as John Stack, have been good-humored about being on my committee and dragging themselves through my prelim paper and thesis. And I have acquired a great deal of practical knowledge from the grad students in the DeMarco and Lev labs, particularly David McKay, Matt Pasienski, Carrie Meldgin, and Alicia Kollár.

I had the rare good luck to spend the fall of 2010 at the Kavli Institute for Theoretical Physics in Santa Barbara as a Graduate Fellow. I had a good time there—perhaps too much of one—but nevertheless learned a lot. For the good time, I am grateful to my fellow Fellows, Steve Avery, Claudia De Grandi, and especially John Biddle; to Roman Lutchyn, Ann Kallin, and Roger Melko; and to the grad students and postdocs at UCSB. (SungBin Lee and Hyejin Ju hosted an especially memorable Halloween party.) I learned much from the faculty at UCSB: Leon Balents descanted memorably on many topics; Cenke Xu was incredibly generous with his time and ideas; and Matthew Fisher patiently explained d-wave Bose metals to me, more than once. I am greatly indebted to the organizers of the KITP conference on optical lattices—Ehud Altman, Maciek Lewenstein, and Vincent Liu—for involving me in their program, and to Ehud and Maciek for their many insightful comments on my research. I can no longer remember all those I met there and learned from, but even the most partial of such lists must include Carlos Bolech, Gabriele De Chiara, Pietro Massignan, Roderich Moessner, Helmut Ritsch, and Hui Zhai.

To this list, I must add an equally partial one, of others who have directly or indirectly sharpened the arguments presented here: Ferdinand Brennecke, Dan Crow, Jonathan Keeling, Mikhail Lukin, Giovanna Morigi, Subir Sachdev, Philipp Strack, and Hakan Türeci.

And now for those whose friendship helped me cling to what remnants of sanity I have retained after more than five years in Urbana. Jeremy and Jenny McMinis did more than anyone else; I cannot imagine how I would have managed without them. Matt Pasienski was an invaluable source of company, rides, bad puns, and references to *Finnegans Wake*. Wade DeGottardi and Ben Hsu provided good cheer when I needed or wanted it; so—when I could find them—did Stephanie Law, Carrie Meldgin, John Nichol, Tomoki Ozawa, Kevin Roberts, Norm Tubman, and Jitong Yu. My officemate Zeb Rocklin was always informative, especially about Mathematica and Intrade. My parents have been remarkably patient and long-suffering.

Lastly, a number of brilliant people have regaled me with banter and book recommendations on the internet. My life would have been much drabber had it not been for Calista McRae, dolphin/truffle-hog ex-

traordinaire, and her continual disgorging of "bright trouvailles" (some of which appear as chapter epigraphs). My college friends Dave Gottlieb, Alan Lawn, James McDonnell, Carson Mitchell, Daisuke O, Zach Sachs, and Kit Wallach have stayed in touch, refuting the conventional wisdom that no one does. (Kit, Carson, and Tal Liron were also generous with their couches when work or the prospect of seeing them took me to Boston, New York, or Chicago.) And then there are all those I would never have known in a world devoid of blogs and Twitter—I am thinking in particular of Steph Bernhard, Jenny Davidson, Elisa Gabbert, David Hayden, and Paraic O'Donnell.

I am grateful to Paul Goldbart, Carrie Meldgin, and Calista McRae for proofreading a draft of this thesis and noticing various things that were wrong with it. Any lingering howlers or delinquencies are, of course, entirely my fault.

I was funded as a graduate student by the University of Illinois Graduate College through an Illinois Distinguished Fellowship; by Amherst College through a Forris Jewett Moore alumni scholarship; by the National Science Foundation under Grants No. NSF DMR09-06780 and NSF PHY11-25915 (the latter at KITP); and by the US Department of Energy, Division of Materials Sciences under Grant No. DE-FG02-07ER46453, through the Frederick Seitz Materials Research Laboratory at the University of Illinois at Urbana-Champaign.

S.G.

Table of Contents

List of Tables

List of Figures

Chapter 1

Introduction: the appeal of ultracold atoms

It is difficult even to choose the adjective
For this blank cold.

— Wallace Stevens, "The Plain Sense of Things"

The history of ultracold atomic systems can be divided roughly into two parts: in the first part, which runs from the 1960s until the achievement of Bose-Einstein condensation (BEC) in 1995, the objective [5] was to cool gases of atoms down to the regime of quantum degeneracy (i.e., the "ultracold" regime); in the second part, which is still in progress, the quest has been to coax ultracold atomic gases into displaying interesting quantum-mechanical behavior. While the initial BECs [6, 7] and degenerate Fermi gases [8] were weakly interacting, it was soon realized that, by imposing optical lattices and by manipulating the atomic structure (e.g., through Feshbach resonances [9]), one could realize strongly correlated states such as Mott insulators, Tonks-Girardeau gases, and unitary Fermi gases (for a review of these developments see Ref. [10]). These correlated states have been of longstanding theoretical interest in condensed matter physics but—in several cases—were not previously experimentally realizable. Expanding the range of realizable systems remains an active enterprise; recent proposals on this front include using alkaline-earth atoms, to realize $SU(N)$ spin systems [11]; atoms with strong dipole moments, to realize liquid-crystalline phases (see, e.g., Ref. [12]); multiple-laser configurations, to simulate magnetic fields and spin-orbit coupling [13]; and—as in the bulk of this thesis—optical cavity photons, to mediate interatomic forces that lead to crystallization and glassiness [14, 15, 16].

1.1 Why ultracold atoms?

Why is it worthwhile to realize condensed-matter phenomena using ultracold atoms? An important initial motivation was the prospect of quantum simulations of condensed-matter models. The idea is as follows: many phenomena in condensed matter physics are hard to understand because, in a typical setting, there

is simply too much going on. For instance, the conduction electrons in a metal interact with one another, with lattice vibrations and dislocations, with static impurities, and with electrons in other bands. When the metal exhibits unexpected properties (e.g., high-temperature superconductivity), it is usually challenging to decide which aspects of the system are responsible for such properties. Yet it is almost always necessary to simplify one's model of the system drastically before one can solve it even approximately, and if such approximate solutions do not describe the phenomena of interest, one can rarely tell whether the fault lies in one's model or one's approximations. This difficulty is exacerbated by the fact that first-principles computer simulations of quantum many-body physics are only tractable for systems of relatively few particles—and are plagued, in general, by "sign problems" [17]. From this point of view, the appeal of ultracold atomic simulations stems from the fact that for these one *does* know the microscopic Hamiltonian very well, and can tune almost all the parameters in it by manipulating the atomic level structure (e.g., by means of magnetic fields) or the intensities of lasers. Thus, one can seek to address open questions in condensed-matter physics such as the following: does the standard simplified model of high-temperature superconductivity (i.e., the Hubbard model) in fact possess a superconducting phase, or is it an oversimplification? Furthermore, cold atomic systems often allow the experimental exploration of regions of parameter space beyond those achieved in solid-state systems, thus enabling one to study the crossovers and transitions between various phases: the classic achievement to date, on this front, has been the characterization of the weak-to-strong-coupling (i.e., BCS-BEC) crossover in fermionic superfluids.

A second advantage of ultracold atomic systems as "quantum simulators" is the availability of probes that have no direct analog in condensed-matter physics. That such probes exist has been known since the early interference experiments [18], which were subsequently adapted to yield a novel way of visualizing vortex-unbinding transitions [19]; however, even such simple probes as a time-of-flight measurement (which yields a momentum distribution) can reveal information that is difficult to access in condensed matter systems. Many properties of a system that were formerly regarded as essentially unmeasurable—such as "string order parameters"—can in fact be extracted from experiments with ultracold atoms [20]. (By contrast, many condensed-matter probes, such as transport measurements, are difficult to implement: one cannot readily hook up leads to a dilute gas suspended in vacuum.)

A related, but conceptually distinct, way of thinking about ultracold atomic systems—as well as, e.g., coupled superconducting-qubit arrays—is as part of a general intellectual project that can be described as *controlled* quantum many-body physics. This project can be regarded as an offshoot of the experimental advances that have made it possible to realize simple, isolated systems—e.g., a single atom interacting with a single photon—in the laboratory. These discrete elements can be assembled into many-body systems that

differ from conventional materials in that one can choose which elements of complexity to put in. Thus, effects that would typically have occurred imperceptibly fast, or that would been swamped by noise, can be sequestered and studied; among these effects, many of the most striking involve the nonequilibrium behavior of almost isolated, or controllably environment-coupled, many-body systems. Traditional many-body physics has focused on the study of systems in or near equilibrium; however, many basic questions about the approach to equilibrium in a quantum-mechanical system remain imperfectly understood, and examples exist—among integrable systems, as well as glassy systems of the kind we shall consider later [21]—of systems that apparently do not approach equilibrium. Investigations of this sort, which address the origins of decoherence, are potentially of great practical use; it is hoped, moreover, that they will shed light on the foundations of quantum statistical mechanics.

1.2 Finite-wavevector instabilities: solids, stripes, and glasses

The simplest ordered states of many-body systems—e.g., ferromagnets and neutral superfluids—preserve the translational symmetries of the underlying Hamiltonians. For example, in a ferromagnet, each spin in the lattice points in the same direction. Thus, the local magnetization $M(\mathbf{x})$ of a ferromagnet (or more generally the order parameter of an ordered state) is constant in space; in momentum space, correspondingly, ordering is associated with an instability of the zero-momentum Fourier component $M_{\mathbf{k}=\mathbf{0}}$ of the magnetization. A richer variety of ordered states, including antiferromagnets, charge density waves, liquid crystals, and solids, exhibit spatially modulated patterns that spontaneously break translational symmetry. Thus, e.g., antiferromagnetic spin ordering corresponds to a situation in which one or more Fourier components of the magnetization satisfying $M_{\mathbf{k}\neq 0}$ simultaneously become unstable. The ordering vector $\mathbf{k}$ is inversely proportional to the wavelength of the modulation (e.g., the lattice spacing of the emergent crystal).

To date, most ordered states realized in ultracold atomic systems have been zero-momentum, uniform states. One can understand why this is so on quite general grounds, at least for *bosonic* systems. The generic Hamiltonian for a standard ultracold atomic system can be written in the schematic form:

$$H = \text{kinetic energy} + \text{contact repulsion}. \tag{1.1}$$

For a system to be unstable toward crystallization, at least one of these terms must have a minimum at a finite wavevector. In general, however, the kinetic energy is minimized by a spatially uniform state rather than a crystal; similarly, a *contact* interaction does not favor crystallization because it does not set a preferred interparticle distance (unlike, e.g., a Lennard-Jones potential). Thus, in order to achieve crystallization, one

must alter the structure of either one or both of these terms. (In the case of fermions, this argument does not work, as the Fermi momentum sets a preferred scale for modulation; however, the temperature scales for the associated instabilities are too low to be realizable at present.)

1.2.1 Interaction-energy-based approaches

An essential feature of the Lennard-Jones interatomic potential, or any other simple potential that can give rise to a solid, is that it is attractive at some distances and repulsive at others; therefore, it sets an optimal, nonzero interparticle spacing. While the *true* interactions between the alkali atoms are of this form (and, indeed, the *true* thermodynamic ground state of these systems is a solid), the atoms in typical ultracold gases are too far apart ($\sim$ 1 micron), and too cold, to resolve the details of the interatomic potential; instead, they experience it entirely as an effective contact potential characterized by an s-wave scattering length. The primary beyond-contact interactions *intrinsic* to ultracold atoms are the long-range dipole-dipole interactions in some atoms and molecules; however, these are always attractive in some separation directions and always repulsive in others, and therefore do not set an optimal interparticle spacing (although an ingenious scheme has been proposed for achieving a form of "crystallization" via dipolar interactions in one dimension [22]).

We have adopted an alternative approach, which is to study *mediated* interactions; in particular, interactions, mediated by optical cavity modes. As we shall see, these modes have spatial profiles that vary rapidly (on the scale of a micron, i.e., a typical interparticle spacing), and the interactions they mediate vary correspondingly rapidly in strength and sign. Thus, they are conducive to the realization of crystalline phases, as was demonstrated—in a particularly simple case with only two possible crystalline arrangements—in the paper by Baumann et al. [23]. The work presented in Chapters 2-4 studies cavity-mediated interactions and cavity-mediated crystallization in more generality, and finally discusses how one might proceed from crystalline to glassy states.

1.2.2 Kinetic-energy-based approaches

The alternative to modifying the structure of the interactions is to modify the structure of the kinetic energy (i.e., the single-particle dispersion relation) so that it favors a $k \neq 0$ state; this can be done in at least two experimentally feasible ways. The first is to subject the atoms to a light-induced spin-orbit coupling, via appropriately chosen Raman transitions [24]. The second, conceptually simpler, approach is to load the atoms into the upper bands of an optical lattice, whose minima are typically not at $k = 0$: owing to the extreme isolation of ultracold atomic systems from the environment, the rate at which the atoms decay into

the lowest band is extremely small. Both approaches permit the realization of almost rotationally-invariant (i.e., circular or spherical) dispersion minima, which are the case of greatest theoretical interest.

1.3 Payoff: fluctuations and glassiness

Many phenomena in condensed-matter physics depend crucially on the fact that crystal lattices are responsive, dynamical entities: a particularly well-known example of such a phenomenon is conventional phonon-mediated superconductivity. Therefore, the ability to realize dynamically responsive, compliant lattices is an important prerequisite for general simulations of condensed-matter phenomena using ultracold atoms. More generally, the ability to realize crystallization and liquid-crystallization paves the way for realizing an entirely different branch of condensed-matter physics using ultracold atoms. Whereas research with ultracold atoms has focused on using atoms to simulate the quantum dynamics of electrons propagating in a static lattice, one can now imagine using atoms to simulate the behavior of atoms and molecules, thus bringing the tools of atomic physics to bear on problems in *soft* condensed matter physics. Part of the value of realizing soft matter using ultracold atomic systems is that such systems—unlike traditional soft matter—are naturally in the quantum limit, and thus offer the prospect of studying phenomena such as crystallization for particles that are strongly quantum mechanical. The only condensed-matter system that has these properties is ^{4}He, in which the interplay between superfluidity and crystallization potentially gives rise to a new phase of matter, the supersolid [1]. It is plausible that the interplay of quantum mechanics with phenomena such as liquid-crystallization, etc., will lead to yet more new phases of matter.

In this dissertation, I shall discuss two specific ways in which crystallization and related effects enable the realization of *qualitatively* different physics from that observed so far in ultracold atomic systems. The first of these relates to the crystallization transition itself (or, more accurately, the liquid-to-smectic transition); the character of this transition, and of the realizable liquid-crystalline phases, is qualitatively altered by fluctuation effects. In particular, the crystallization transition, though continuous at the mean-field level, is driven first-order by fluctuations through the Brazovskii effect; moreover, as discussed in Chapter 5, the mean-field phase diagram changes its morphology, even at zero temperature, once fluctuations are incorporated. The second way in which realizing crystalline phases can lead to qualitatively new physics is if one pairs it with frustration, geometrical or otherwise; as discussed in Chapters 3 and 4, frustration gives rise to glassy behavior. The isolated quantum dynamics of glassy systems has been a topic of considerable interest in recent years: a question of particular conceptual interest is whether such systems are capable of approaching thermal equilibrium.

1.4 Overview of the dissertation

This thesis is built around two themes: (i) the theme of *extrinsically mediated* interactions—in particular, cavity-mediated interactions—in ultracold atomic systems, and (ii) the theme of fluctuations in crystallizing systems, in which the low-lying degrees of freedom lie on a momentum-space surface. These themes are intertwined in Chapters 2 and 3, which address crystallization *through* cavity-mediated interactions. Chapter 2 aims to be a heuristic introduction to cavity-mediated interactions and how they give rise to crystallization; Chapter 3 first covers the same ground more carefully and then turns to an analysis of fluctuation effects and their dramatic impact on crystallization. In the next two chapters, the themes are developed separately: Chapter 4 is about cavity-mediated interactions and how they can be used to realize spin glasses, whereas Chapter 5 is about universal fluctuation-governed physics near the liquid-crystallization transition, in the setting of spin-orbit coupled Bose gases. Finally, in Chapter 6 I conclude with a summary and a list of open questions.

Chapters 2-4 are based on a series of papers [14, 15, 16] that I wrote with Benjamin Lev and Paul Goldbart, and Chapter 5 is based on a paper [25] that I wrote with Austen Lamacraft and Paul Goldbart.

Chapter 2

The physics of many atoms in a cavity

Why does the air grow cold
in the region of mirrors?

— Geoffrey Hill, "Damon's Lament for his Clorinda, Yorkshire 1654"

In this chapter, we introduce the physics of cavity-mediated interactions between atoms, and of the self-organization transition that these interactions give rise to. We begin by reviewing a few general properties of light-atom interactions, and proceed to the specific case of atoms in a transversely pumped optical cavity. We outline a simple classical analysis of these interactions, and exploit this to discuss how cavity photons mediate interatomic interactions; how these interactions can give rise to a crystallization (or "self-organization") transition [26]; and how this crystallization transition is enriched by the presence of multiple cavity modes. We then briefly sketch how the classical results can be arrived at quantum-mechanically; a more detailed quantum-mechanical treatment is deferred until the next chapter. The quantum-mechanical derivation enables us to discuss how the self-organization of a Bose-Einstein condensate (BEC) can be regarded as a quantum phase transition. Finally, we touch upon the experimentally relevant parameter regimes, and connect our work to related problems such as the Dicke phase transition [27] and polariton condensation [28].

It should be emphasized that the discussion here does not aim to be a comprehensive overview of self-organization or of cavity-mediated atom-atom interactions. Our focus is on a particular regime—the "dispersive" limit, in which all relevant frequencies are far-detuned from one another—which, as we shall see, has the advantage of favoring the persistence of quantum coherence for long times, and also allows a simple theoretical description.

2.1 Light-atom interactions

Alkali atoms can be regarded as two-level systems having a ground and excited state—denoted $|g\rangle$ and $|e\rangle$ respectively—separated by an optical-frequency transition (e.g., the $5s \rightarrow 5p$ transition for rubidium

atoms) [29]. Transitions from the ground to the excited state are assumed to be driven by a pump laser that is near resonance with this transition. In what follows, we shall assume that the steady-state population of the excited state (i.e., the population inversion) is small, because the pump laser is either weak or off resonance [1]. In this limit, one can approximate the laser-driven two-level atom as a damped, driven harmonic oscillator. Formally, this approximation amounts to the introduction of many fictitious excited states that are not populated; however, the atomic oscillator can be understood physically as an electric dipole oscillating in response to the sinusoidal electric field due to the laser. The dynamics of this dipole can be understood classically, via the standard equation of motion:

$$\ddot{\mathcal{X}}(t) + 2\gamma\dot{\mathcal{X}}(t) + \omega_A^2\mathcal{X}(t) = \Omega\omega_L \sin(\omega_L t), \tag{2.1}$$

where $\mathcal{X}$ is the displacement of the atomic dipole; γ is its damping rate (corresponding to the linewidth of the atomic transition); ω_A and ω_L are the frequencies of the atomic transition and the pump laser respectively; and Ω is the Rabi frequency [2] of the pump laser. (Note that Ω^2 is proportional to the intensity of the pump laser.) The *polarization* of the electric field is not relevant for our purposes, and we shall always take the polarizations of all the fields to coincide, as is standard with optical cavities [30]. Note that, here and in all equations below, we assume that $\omega_L \leq \omega_A$, i.e., the laser is *red-detuned* from the atomic transition. The steady-state solution to Eq. (2.1) takes the general form (for $\Delta_A \equiv \omega_A - \omega_L \ll \omega_A$):

$$\mathcal{X}(t) = \frac{\Omega}{\sqrt{\gamma^2 + \Delta_A^2}} \sin(\omega_L t + \phi), \tag{2.2}$$

where ϕ is a phase shift that is $\pi/2$ at resonance and approaches the value γ/Δ_A for large detunings, i.e., for $\gamma/\Delta_A \ll 1$. In the regime of large detunings, which is of primary interest for our purposes, we can write $\mathcal{X}(t)$ simply in terms of an "in-phase" component which oscillates with the laser and an "in-quadrature" component that is phase-shifted by $\pi/2$:

$$\mathcal{X}(t) = \mathcal{X}_1(t) + \mathcal{X}_2(t), \tag{2.3}$$

$$\mathcal{X}_1(t) = \frac{\Omega}{\Delta_A} \sin(\omega_L t), \tag{2.4}$$

$$\mathcal{X}_2(t) = \frac{\Omega}{\Delta_A}\frac{\gamma}{\Delta_A} \cos(\omega_L t). \tag{2.5}$$

[1] This might seem to contradict the previous remark that the laser is near resonance. However, it is possible for the detuning from resonance to be at once (i) much smaller than the resonant frequency itself, and (ii) much larger than any other energy scale in the problem. Typical scales are indicated in Table 2.1.

[2] Ω is defined by $\Omega \equiv \mathbf{E}_0 \cdot \langle g|\mathbf{x}|e\rangle$, where $\mathbf{E}_0$ is the amplitude of the electric field and the matrix element that multiplies it is the polarizability of the atom.

The components $\mathcal{X}_1$ and $\mathcal{X}_2$ differ in their dynamical consequences. To see this, we observe, first, that the interaction energy of a dipole in the electric field due to the laser is given by

$$U \sim -\mathbf{p} \cdot \mathbf{E} \sim -\mathcal{X}(t) \times \Omega \sin(\omega_L t). \tag{2.6}$$

When the energy is averaged over a cycle, only the in-phase component given by $\mathcal{X}_1(t)$ survives, so that

$$U \sim -\frac{\Omega^2}{\Delta_A}. \tag{2.7}$$

This energy shift is also known as the a.c. Stark shift, or light shift. (Note that we have set $\hbar = 1$, as most of the relevant energy scales are naturally interpreted as frequencies.) The crucial feature of U is the following: if the laser strength Ω is spatially varying, atoms are drawn to regions of high laser intensity. This fact is the basis of optical traps and optical lattices; it is also, as we shall see, the basis of cavity-mediated interactions.

Although $\mathcal{X}_1(t)$ determines the energy of an atom in the presence of the laser, it does not affect the power Γ dissipated by the system, which is proportional to the force times the *velocity*, i.e.,

$$\Gamma \sim \Omega \sin(\omega_L t) \times \left[\mathcal{X}_1 \omega_L \cos(\omega_L t) - \mathcal{X}_2 \omega_L \sin(\omega_L t)\right]. \tag{2.8}$$

Evidently, the power dissipated depends only on $\mathcal{X}_2$; consequently, it takes the form

$$\Gamma \sim \frac{\gamma \Omega^2}{\Delta_A^2}. \tag{2.9}$$

What are the physical implications of this term? Heuristically, one can understand these as follows: the power dissipated is proportional to the flux of photons from the laser into free space electromagnetic modes, i.e., to the amount of spontaneous emission. Because each scattering event imparts a random momentum kick to the atoms, thus heating them, it follows that Γ sets a heating rate, at least if the initial temperature of the atoms is sufficiently low (i.e., $\ll \hbar\Gamma/k_B$). At higher temperatures, the heating is balanced by Doppler cooling [29], a process whereby atoms with kinetic energies $\sim \Delta_A$ absorb a laser photon at frequency ω_L and re-emit it at a frequency ω_A, thus lowering their kinetic energy by Δ_A. However, the lowest steady-state temperatures achievable via Doppler cooling are too high to be relevant for ultracold atomic experiments; therefore, the heating associated with Γ is best regarded as determining an effective lifetime for experiments with ultracold atoms. In other words, the states of interest in a typical ultracold-atomic experiments are best regarded as *transients* that are eventually destroyed by heating, not as nonequilibrium steady states.

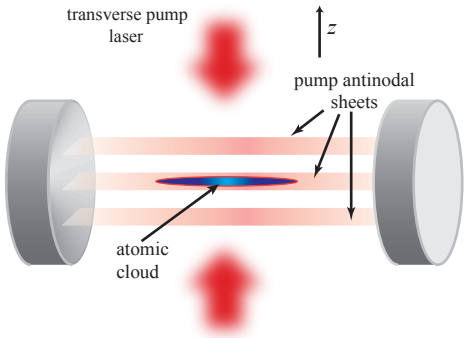

Figure 2.1: Experimental setup considered in this thesis for realizing cavity-mediated atom-atom interactions. Note that the pump laser is oriented *transverse* to the cavity axis.

2.2 Light-atom-cavity interactions

We now adapt the discussion of the previous section to the case of an atom (or multiple atoms) in an optical cavity that is transversely pumped by a laser. An optical cavity is an arrangement of two or more highly reflective mirrors that, between them, support localized modes of the electromagnetic field; these modes can be treated as harmonic oscillators. Because the vacuum energy density of such localized modes is much higher than that of free-space modes, an atom is likelier to emit photons into a cavity mode than into any particular free-space mode. Indeed, in the "strong-coupling" regime of cavity QED, the rate of emission into the cavity exceeds the rate of emission into *all* free-space modes combined (i.e., the total rate of spontaneous decay). For the present, we shall assume the system is in the strong-coupling regime and neglect spontaneous decay; as discussed in Chapter 3, this assumption is experimentally reasonable.

The experimental geometry we consider is that shown in Fig. 2.1, with the pump laser oriented *transverse* to the cavity axis; in this geometry, the laser and cavity are only coupled *through* the atom(s). We assume that the pump laser frequency, ω_L, is relatively near, but red-detuned from, the resonance frequency of a particular cavity mode ω_C, so that $\omega_C - \omega_L \ll \Delta_A$. Assuming that $\gamma/\Delta_A \ll 1$, as before, one can neglect spontaneous emission, so that the atomic dipole amplitude $\mathcal{X}(t)$ can be approximated as $\mathcal{X}_1 \sin(\omega_L t)$; it is this atomic dipole, driven by the laser, that in turn drives the cavity mode $\mathcal{Y}(t)$, as follows:

$$\ddot{\mathcal{Y}}(t) + \kappa\,\dot{\mathcal{Y}}(t) + \omega_C^2\,\mathcal{Y}(t) = g\omega_L\mathcal{X}_1 \sin(\omega_L t), \tag{2.10}$$

where g is the atom-cavity coupling; and κ, the linewidth of the cavity mode, is proportional to the rate at which photons leak out through the cavity mirrors. Note that we have *neglected* the influence of the cavity mode itself on the atomic oscillator; this neglect is justifiable in the regime of primary interest in this work, in which the electric field due to the pump laser is much stronger than that due to the cavity. Inserting the

expression $\mathcal{X}_1 = \Omega/\Delta_A$, we find that the atomic drive is formally identical to the drive term in Eq. (2.2) if one makes the replacement $\Omega \to \Omega(g/\Delta_A)$. In particular, the cavity mode amplitude $\mathcal{Y}$, like the atomic dipole displacement $\mathcal{X}$, has an in-phase component

$$\mathcal{Y}_1(t) = \frac{g\Omega}{\Delta_A \Delta_C} \sin(\omega_L t) \tag{2.11}$$

that is conservative, and an in-quadrature component

$$\mathcal{Y}_2(t) = \frac{\kappa g\Omega}{\Delta_A \Delta_c^2} \cos(\omega_L t) \tag{2.12}$$

that dissipates power. As before, in the limit $\kappa/\Delta_C \ll 1$, the dissipative component is suppressed relative to the conservative one by a factor of κ/Δ_C.

As with the atom-light interaction, one can relate the energetics of the atom in a cavity to $\mathcal{Y}_1$, as follows. The total atom-field interaction energy averaged over a cycle (i.e., retaining only the terms that are in phase with the pump laser) is given by

$$U \sim -p(E_L + E_c) \sim -\mathcal{X}_1 \times (\Omega + g\mathcal{Y}_1) \sim -\frac{\Omega^2}{\Delta_A} - \frac{\Omega^2 g^2}{\Delta_A^2 \Delta_C}. \tag{2.13}$$

Note that the coupling g multiplying the cavity amplitude $\mathcal{Y}_1$ captures the fact that the electric field strength of a cavity photon is enhanced relative to that of a free-space photon, owing to the localization of the cavity mode.

Moreover, the dissipative processes governed by $\mathcal{Y}_2(t)$, corresponding ultimately to the transfer of photons from the laser to free-space modes, lead to the heating of atoms via recoil, precisely as in the case of the atom-light interaction. This heating rate, given by

$$\Gamma_c = \kappa \frac{\Omega^2 g^2}{\Delta_A^2 \Delta_C^2}, \tag{2.14}$$

determines a lifetime for experiments with ultracold atoms in cavities. As in the case of the atom-light interaction, this heating is eventually balanced by a process analogous to Doppler cooling (the details are discussed in Refs. [26, 31]). The lowest achievable steady-state temperatures are of order $T_\kappa \approx \kappa/(2k_B)$. Unlike the Doppler cooling limit mentioned above, T_κ is not *necessarily* lower than the temperature scales relevant for Bose condensation; however, as discussed in Sec. 3.9, it is difficult to simultaneously achieve a sufficiently low κ in a system that, at the same time, has a sufficiently strong coupling g to be in the strong-coupling regime. Thus, we shall, as before, regard the heating rate Γ_c as potentially determining a

lifetime for experiments with ultracold atoms in cavities, and thus as something to be minimized, e.g., by working at large detunings $\Delta_C/\kappa \gg 1$. (As shown in Sec. 3.9, however, spontaneous decay rather than cavity photon leakage is the dominant dissipative mechanism for typical experimental parameters.)

Note that the above discussion has been simplified considerably by neglecting the effects of the cavity on the atomic dipole $\mathcal{X}_1(t)$; as we shall see, these effects *are* typically insignificant in the regimes of interest, *except* insofar as the presence of an atomic cloud in the cavity changes its refractive index, and thereby shifts the resonance frequency (and hence Δ_C). However, this shift can be accounted for via a redefinition of Δ_C; we shall assume, except when otherwise noted, that Δ_C refers to the corrected rather than the bare detuning.

2.3 Cavity-mediated interactions between atoms

So far, we have discussed the similarities between the light-atom interaction and the light-atom-cavity interaction, in the case where the *spatial profiles* of both were taken to be constant. However, the typical spatial profile of an optical cavity mode is rapidly varying (on a scale set by an optical wavelength, $\sim 1\mu$m); as we discuss in this section, this spatial variation can have particularly significant consequences in systems with multiple atoms in a cavity.

In order to generalize the results of the previous section to the case of both multiple atoms and varying mode profiles, one needs only to replace the single-atom-cavity coupling g with the collective atoms-cavity coupling $\sum_i g(x_i)$. We assume for simplicity that the cavity mode function has the simple standing-wave form $g_0 \cos(kx)$; that the atoms are confined to the line $y = z = 0$, and that the pump laser is oriented along the z axis, so that its spatial variation does not affect the atoms. (Spatial variation in the pump laser profile can be introduced straightforwardly.) Under these assumptions, the last term of Eq. (2.13) takes the form

$$U_c = -\frac{\Omega^2 g_0^2}{\Delta_A^2 \Delta_C} \left(\sum_i \cos(kx_i) \right)^2 . \tag{2.15}$$

This expression can be seen to have the following properties: (i) For a single atom in a cavity, the energy varies spatially as $-\cos^2(kx)$, and is consequently highest when the atom is at an antinode and lowest when it is at a node. (ii) For two atoms, the interaction takes the form $-[\cos^2(kx_1)+\cos^2(kx_2)+2\cos(kx_1)\cos(kx_2)]$; the last term is minimized when the atoms are both at even antinodes or both at odd antinodes, i.e., when the two atoms are a whole number of wavelengths apart. Thus, each atom exerts a force on every other atom. (iii) For a large number of atoms, the diagonal terms in the sum are outweighed by the off-diagonal terms; therefore, U_c can be regarded purely as an interatomic interaction. If we introduce the standard

density operator

$$n(x) = \sum_i \delta(x - x_i), \tag{2.16}$$

we can rewrite Eq. (2.15) as

$$U_c = -\frac{\Omega^2 g_0^2}{\Delta_A^2 \Delta_C} \int dx\, dx'\, n(x) n(x') \cos(kx) \cos(kx'), \tag{2.17}$$

which has the form of an infinite-range density-density interaction, which is repulsive when the atoms are an odd number of half-wavelengths from each other, and attractive when they are separated by a whole number of wavelengths. (Note that, owing to the infinite range of the interaction, the appropriate definition of the thermodynamic limit is subtle; in general, as explained in Sec. 3.1, we shall take $g_0^2 N$ to be held constant as $N \to \infty$.)

2.4 The self-organization transition(s)

The cavity-mediated interaction energy is minimized when the atoms form a λ-spaced lattice, i.e., if all the atoms are at even antinodes or all the atoms are at odd antinodes. Thus, it favors spontaneous symmetry-breaking between the even and odd antinodes; on general grounds, one expects this symmetry-breaking to occur in a system of noninteracting thermal particles either as the temperature is lowered or as the interaction strength is increased (e.g., by increasing the laser intensity). This "self-organization" transition was theoretically investigated by Domokos and Ritsch [26, 31] and subsequently experimentally verified by Black et al. [32]. These results were extended, both theoretically [33] and experimentally [23], to the quantum dynamics of a Bose-Einstein condensate (BEC) in a cavity; in this case, the interaction energy competes, not with the temperature, but with the kinetic energy of the BEC, which favors a uniform distribution. In what follows, we briefly discuss the thermal case and then turn to the quantum-mechanical case, which is the primary focus of this thesis.

2.4.1 Transition for a classical gas

For a classical gas at an initial temperature T, one can estimate the threshold for self-organization by considering the conditions under which the optical well depth created by an atomic modulation becomes comparable to the thermal energy of the atoms, viz.

$$\frac{\Omega^2 g^2 N}{\Delta_A^2 \Delta_C} \simeq k_B T. \tag{2.18}$$

At shallower depths or higher temperatures, the optical wells are no longer deep enough to trap atoms, so that the cloud delocalizes. The work of Refs. [26, 31] was motivated by a potential application of self-organization to cavity-mediated cooling: as discussed in Sec. 2.2, cavity-mediated cooling is an analogous process to Doppler cooling, and can be used to cool a system to a minimum temperature of order κ/k_B if the detuning Δ_C is of order κ. (Thus, setting $\kappa = \Delta_C$ in Eq. (2.18) yields, to within factors of order unity, the threshold expression given in Eq. (19) of Ref. [26].)

While the dissipative dynamics studied in Refs. [26, 31] is beyond the scope of the present work, it is instructive to note that the *utility* of self-organization for cavity-mediated cooling schemes is due to the following fact: self-organization is accompanied by a macroscopic increase in the photon population in the cavity, which leads—owing to the Bose statistics of photons—to a superradiant enhancement of the atom-cavity coupling, and thus to increased rates of emission and thus of cooling. Thus, cavity-mediated cooling exploiting self-organization has been suggested as a possible method for cooling atomic species such as dysprosium [34], which have intricate level structures that make standard laser-cooling techniques difficult to apply.

2.4.2 Properties of deeply self-organized states

In the preceding discussion of cavity-mediated interactions and self-organization, we neglected the effects of the cavity field on the amplitude of the atomic dipole $\mathcal{X}_1(t)$ [see, e.g., Eq. (2.13)]. This neglect is permissible as long as the electric field due to the pump laser greatly exceeds that due to the cavity, as it always does sufficiently near threshold (where the cavity field is small). Deep in the ordered state, however, one cannot, a priori, neglect the effects of the cavity field on the atomic dipole. In the ordered state, the total trapping potential on an individual atom in the cavity is simply given by the total electric field due to both the pump laser and the cavity:

$$U_c(x) \sim -(E_L + E_C \sin(kx))^2 \sim -E_L^2 - 2E_L E_C \sin(kx) - E_C^2 \sin^2(kx). \tag{2.19}$$

In this expression, the cavity field E_C is an order parameter for the crystallization transition, and thus rises above the self-organization threshold as $E_C \sim (\Omega - \Omega_c)^\beta$ for some critical exponent β (which happens to be $\frac{1}{2}$, as discussed in Ref. [31]). Thus, near the transition, $E_C \ll E_L$ for all parameter values. We now turn to the opposite limit, in which self-organization is essentially complete and the atoms are all situated at the

appropriate antinodes. Here, the cavity field is of order $E_C \sim g(\Omega g N/\Delta_A \Delta_C)$ [from Eq. (2.11)], whereas the laser field is of order $E_L \sim \Omega$. So long as the inequality

$$Ng^2 \leq \Delta_A \Delta_C \tag{2.20}$$

holds (i.e., in the regime of large detunings, which we consider here) the cavity field is weaker than the laser field, and neglecting it makes no *qualitative* difference. We shall assume this inequality is satisfied in most of what follows, as (for reasons discussed above) the large-detuning limit is that in which heating is minimized. However, we note that if the inequality (2.20) does not hold, then the optical potential in Eq. (2.19) develops the superlattice structure shown in Fig. 2.2. Then, at sufficiently low temperatures or high fields, even the minority wells in Fig. 2.2 become deep enough to trap thermal atoms; thus, metastable states with a substantial number of atoms trapped in the minority wells begin to proliferate, so that the relaxational dynamics of the self-organized state changes its character. To summarize, regardless of the values of detuning, E_C can always be neglected near threshold. However, for small detunings or very strong atom-cavity coupling, the arguments above suggest a crossover between a regime without metastable states and one with them: whether this regime persists once quantum mechanical fluctuations are included is an interesting question for future work.

2.4.3 Transition for a Bose-Einstein condensate

We now turn to the case of a Bose-Einstein condensate (BEC) at zero temperature, subject to the cavity-induced coupling from Eq. (2.17). In second-quantized notation, the Hamiltonian, expressed in momentum space, reads:

$$\mathcal{H} = \int d^d k \psi^\dagger(\mathbf{k}) \left(\frac{k^2}{2M} \right) \psi(\mathbf{k}) - \frac{\zeta}{4} \left\{ \int d^d k \psi^\dagger(\mathbf{k}) [\psi(\mathbf{k}+\mathbf{K}_0) + \psi(\mathbf{k}-\mathbf{K}_0)] \right\}^2, \tag{2.21}$$

where $\zeta \equiv g^2\Omega^2/(\Delta_A^2 \Delta_C)$ and $\mathbf{K}_0$ is the wavevector of the cavity mode. This Hamiltonian can be diagonalized by means of a Bogoliubov transformation (see, e.g., Ref. [35]); we consider, in particular, the hybrid excitation at momenta $\pm\mathbf{K}$, whose energy is given by:

$$E_1 \sim \sqrt{\frac{K_0^2}{2M} \left(\frac{K_0^2}{2M} - \zeta N \right)}. \tag{2.22}$$

Thus, when the cavity-mediated interaction is weak, this mode costs an energy $\frac{K_0^2}{2M}$ per particle to populate, but as the interaction strengthens, this mode softens, until it becomes unstable at a critical value of ζ. This

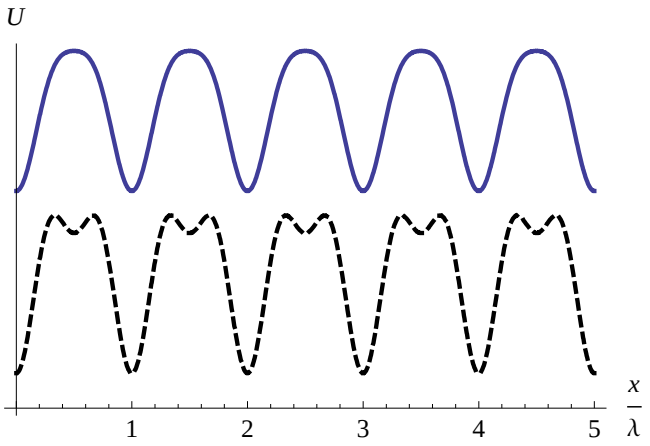

Figure 2.2: Total optical potential on an atom due to the other atoms in the self-organized state, shown in the weakly organized/large-detuning regime (solid curve) and in the regime of small detunings and strong ordering (dashed curve). As discussed in the text, we shall primarily be concerned with the regime described by the solid curve.

instability signals the onset of a crystalline state, in which the density wave corresponding to this mode pattern is macroscopically occupied.

The argument given above is generally expressed in the literature in terms of the Dicke model [27]; we shall return to this formulation, which is based on a quantum-mechanical description of the cavity field, after briefly extending the heuristic considerations given above to the case of multimode cavities.

2.4.4 Case of multimode cavities

For the purposes of the present discussion, a multimode cavity is one that supports multiple degenerate modes, the profiles of which are orthogonal to one another; we shall turn to a discussion of realistic multimode geometries later. The general question that arises when one attempts to extend the idea of crystallization to the setting of multimode cavities is this: Which mode(s) do the atoms crystallize into? In this subsection, we offer some heuristic considerations aimed at addressing this issue. We shall return to this question in the specific context of the concentric cavity in more detail, once we have developed the relevant field-theoretic techniques.

Traveling waves

The argument given in the previous sections for self-organization in a single-mode cavity proceeds similarly for the case of multimode cavities, except that the individual mode-function $\cos kx$ must be replaced by the (as yet unspecified) set of cavity mode functions $\{g_\alpha(\mathbf{x})\}$. There are, however, two crucial differences. The first is pertinent whenever the cavity supports traveling-wave modes (e.g., the ring cavity). In this case, the

potential energy is given by

$$\mathcal{E} \sim -\int d^d x\, g_\alpha(\mathbf{x})\, n(\mathbf{x}) \int d^d x'\, g_\alpha(\mathbf{x}')^*\, n(\mathbf{x}'), \tag{2.23}$$

and the dynamics of each mode is coupled to that of its partner under time-reversal. This has an important consequence, which is easiest to illustrate in the case of the ring cavity. Here, $g_\alpha = \exp ikx$, and $\mathcal{E}$ is invariant under the transformation $n(x) \to n(x+\epsilon)$, which involves shifting the atomic distribution along the cavity axis (and adjusting the antinodes of the cavity mode accordingly). Therefore, crystallization in multimode cavities having traveling-wave modes necessarily involves the spontaneous breaking of a continuous translational symmetry.

Mode selection

If two cavity mode functions $g_\alpha(\mathbf{x})$ and $g_{\alpha'}(\mathbf{x})$ are associated with a pair of frequency-degenerate harmonic solutions of the wave equation for the same (homogeneous) boundary conditions, any linear combination $C_\alpha\, g_\alpha(\mathbf{x}) + C_{\alpha'}\, g_{\alpha'}(\mathbf{x})$ is also a legitimate cavity mode. Therefore, it might seem that, in an N-fold degenerate cavity, any normalized mode of the form $\sum_\alpha C_\alpha\, g_\alpha(\mathbf{x})$ would be an "equally good" arrangement for crystallization, i.e., there is an N-dimensional degenerate subspace. This is *not* generally true, as a result of terms in the energy, omitted so far in the present section, that lift this degeneracy, such as the interatomic contact repulsion. Consider the extreme simplification involving two modes having the respective mode functions $\cos kx$ and $\cos ky$ (as would arise, e.g., from two cavities, perpendicular to one another and to the laser): any function of the form $(C_\alpha, C_{\alpha'}) \equiv C_\alpha \cos(kx) + C_{\alpha'} \cos(ky)$, with $C_\alpha^2 + C_{\alpha'}^2 = 1$, is a legitimate mode function. If the atoms are self-organized in the state $(C_\alpha, C_{\alpha'})$, the atomic density is given by $n(\mathbf{x}) \sim A + B\,[C_\alpha \cos(kx) + C_{\alpha'} \cos(ky)]$, and the typical interatomic contact interaction energy [see, e.g., Eq. (3.5)], goes as $\int d^d x\, |n^2$. This can readily be checked to be smallest when either $C_\alpha = 0$ or $C_{\alpha'} = 0$, i.e., for a stripe-like arrangement along either the x axis or the y axis.

A similar effect arises from the mode-mode scattering term (i.e., the E_C^2 term),

$$\int d^d x\, n(\mathbf{x})\, g_\alpha(\mathbf{x})\, g_{\alpha'}(\mathbf{x}). \tag{2.24}$$

In the two-mode example discussed in the previous paragraph, in which the modes are at right angles to one another, this term is almost diagonal in the mode indices for either of the stripe-like states. Suppose, however, that the two cavities lie at a small angle θ rather than at right angles to one another, so that the modes are $\cos(\mathbf{k} \cdot \mathbf{x})$ and $\cos(\mathbf{k}' \cdot \mathbf{x})$ with $\mathbf{k} \approx \mathbf{k}'$. In this case, atomic density fluctuations of wave-vector

$|\mathbf{k} - \mathbf{k}'| \approx |\mathbf{k}|\theta$—which, for small θ, could be excited either thermally or quantum-mechanically—would suffice to mix the cavity modes. The effect of such mixing would be to lock the relative phases of the two modes.

2.4.5 Shaping interactions via multimode cavities

The previous subsection addressed the fact that an atomic cloud in a multimode cavity can order in many different ways. The present subsection addresses a different point regarding multimode cavities, which is that cavities having *many* degenerate modes can in fact mediate relatively local interatomic interactions. The considerations here differ from those in the previous section in two ways: (a) they depend essentially on having a large number of near-degenerate cavity modes (i.e., modes that are closely spaced relative to Δ_C), but (b) they do not depend on exact degeneracy of these modes.

We begin with the obvious generalization of Eq. (2.17) to the multimode case:

$$U_c = -\frac{\Omega^2 g_0^2}{\Delta_A^2} \sum\nolimits_\alpha \int dx\, dx'\, \frac{1}{\Delta_\alpha}\, n(x) n(x') \Xi_\alpha(kx) \Xi_\alpha(kx'), \tag{2.25}$$

where Ξ_α is the appropriately normalized mode profile of cavity mode α, and Δ_α is its detuning from the laser. We shall consider expressions like this, in the realistic case of concentric cavities, in a subsequent chapter; for now, however, let us simplify the problem further and assume that the cavity mode functions are $\Xi_\alpha \sim \cos(k_\alpha x)$, where $k_\alpha = k_0 \times 1, 2, 3 \ldots$ runs over a wide range of modes. (This situation approximately describes an atom coupled to higher-angular-momentum modes in a confocal or concentric cavity [30].) Now if Δ_α is taken to be independent of α, this interaction involves a sum over all α; thus the interaction in this case is short-range, i.e., *contact*, in character; likewise, if the Δ_α are taken to increase with α as a power law, the interaction decays as a power law with distance. (In the extreme limit where Δ_α is small for only one cavity mode, one arrives at an infinite-range interaction as expected.)

Thus, by tuning the resonances of various cavity modes with respect to one another, one can tune the nature of the interaction mediated by the cavity. Such tuning is in fact *feasible*: as discussed in Ref. [30], the resonances are chiefly a function of mirror spacing, and therefore it should be possible to dynamically alter the range of cavity-mediated interactions even during an experiment—this fact is an especially striking illustration of the new possibilities that ultracold atomic systems offer for studying many-body physics.

2.5 Quantum-mechanical treatment

The discussion given above was phrased entirely in terms of a classical picture of the atom-light interaction. In what follows, we first briefly sketch the standard quantum-mechanical treatment of the atom-light interaction and extend it to the case of cavities; next, we discuss why, and in what sense, the self-organization transition can be regarded as a quantum phase transition.

2.5.1 Atom-light interactions

We consider the case of a two-level atom interacting with a single, macroscopically populated, mode of the electromagnetic field. The energy spacing of the two atomic states is $\hbar\omega_A \approx \hbar \times 10^{15}$ Hz, and the linewidth of the transition (i.e., the rate at which an excited-state atom decays) is $\gamma \approx 10^6$ Hz. (In what follows, we shall set $\hbar = 1$, as most energy scales can naturally be understood as frequencies and/or rates.) In the situations we shall consider, the atoms are taken to be interacting with a laser (or lasers) of spatially varying intensity at the frequency ω_L, where $\Delta_A \equiv \omega_A - \omega_L \approx 10^{10}$ Hz: i.e., the laser is "red-detuned" from the atomic transition. The Hamiltonian for a two-level atom interacting with a laser mode is

$$H = \left[\omega_A \sigma_z + \omega_L a_L^\dagger a_L + i\widetilde{\Omega}(a_L^\dagger \sigma_- - \text{h.c.})\right]. \tag{2.26}$$

Here, the σ's are Pauli matrices acting on the internal state of the atom, a_L is the annihilation operator for laser photons, and $\widetilde{\Omega}$ is the coupling constant between atoms and the laser mode. (A more physically relevant parameter is the Rabi frequency $\Omega \equiv \widetilde{\Omega}\sqrt{n}$, where n is the average number of photons in the laser mode.) A typical value of Ω in the setup we shall consider is about 1 GHz For $\widetilde{\Omega} = 0$, the eigenstates of H form Δ_A-spaced 2×2 subspaces of the form $\{|g\rangle|n+1\rangle, |e\rangle|n\rangle\}$; these subspaces are separated from one another by $\omega_L \gg \Omega$, and are therefore unmixed by the atom-light interaction. By diagonalizing the Hamiltonian in any one subspace, one finds that the lower of the two atom-photon states (which, for $\Omega \ll \Delta_A$, is essentially the atomic ground state) decreases in energy by Ω^2/Δ_A. This effect is called the a.c. Stark shift or light shift.

The analysis given above is strictly true only for a stationary atom. However, as Δ_A greatly exceeds the typical kinetic energy of the atoms $\sim k_B \times 100$ nK, atoms virtually excited by the laser must decay on a timescale that is rapid compared with the atomic motion (by the uncertainty relation, $\Delta t \sim 1/\Delta_A$). Therefore the light shift can be thought of as providing an effective *local* potential $V(\mathbf{x}) \equiv \Omega(\mathbf{x})^2/\Delta_A$ acting on the atoms at position $\mathbf{x}$.

Dissipative aspects

The treatment sketched so far assumes that the laser and atom form a closed system; this assumption is not quite true, because the atomic excited state is also coupled to a continuum of free-space electromagnetic modes, into which it can scatter laser photons. In general, therefore, the atomic excited state is to be regarded, not as an infinitely sharp level, but as a Lorentzian resonance of linewidth γ (which is of order a few megahertz for most commonly used transitions [29]). Given the lineshape, one can use Fermi's Golden Rule to get a rough estimate of the atomic scattering rate:

$$\Gamma \sim \Omega^2 \rho(\Delta_A) \sim \Omega^2 \frac{\gamma}{\Delta_A^2 + \gamma^2} \tag{2.27}$$

where $\rho(\Delta_A)$ is the density of available states at the detuning Δ_A. In particular, when $\Delta_A \gg \gamma$, the scattering rate $\Gamma \sim \gamma\Omega^2/\Delta_A^2$, as derived using the classical model.

2.5.2 Light-atom-cavity interactions

In this section, we generalize the discussion of light-atom interactions to the case in which the atoms are coupled both to a laser and to an optical cavity mode. We shall assume that the atoms can be treated as purely polarizable particles whose primary effect is to generate matrix elements connecting the laser mode to the cavity mode (this is known as the "adiabatic elimination" of the atomic dipole, and is discussed further in the next chapter). Under this assumption, the coupled laser-cavity Hamiltonian $\mathcal{H}'$ can be written as:

$$\begin{aligned} \mathcal{H}' &= \sum_\alpha \Delta_\alpha a_\alpha^\dagger a_\alpha + \frac{\Omega^2}{\Delta_A}\int d^d x n(\mathbf{x}) + \frac{\Omega}{\Delta_A}\sum_\alpha a_\alpha^\dagger \int d^d x g_\alpha(\mathbf{x}) n(\mathbf{x}) + \text{h.c.} \\ &\quad + \frac{1}{\Delta_A}\sum_{\alpha,\alpha'} \int d^d x g_\alpha(\mathbf{x}) n(\mathbf{x}) \int d^d x' g_{\alpha'}(\mathbf{x}') n(\mathbf{x}') \end{aligned} \tag{2.28}$$

where Δ_α is the detuning of cavity mode α from the laser. The first interaction term (second term overall) represents the dipole potential acting on the atoms due to the laser. The second interaction term describes the scattering of photons between the laser and the cavity, and the third describes the scattering of photons between cavity modes. We shall consider the limit of a strongly pumped system, in which the last term is negligible; thus, the effective Hamiltonian can be simplified to the following approximate form:

$$\mathcal{H}'' = \sum_\alpha \left\{ \Delta_\alpha a_\alpha^\dagger a_\alpha + \left(\frac{\Omega \int d^d x g_\alpha(\mathbf{x}) n(\mathbf{x})}{\Delta_A} \right) a_\alpha^\dagger + \text{h.c.} \right\} \tag{2.29}$$

In the limit of large Δ_α, the population of the cavity modes is small; thus, to a reasonable approximation, one can treat each cavity mode as a two-level system, containing either zero photons or one. (The converse approximation, i.e., treating a two-level atom as an oscillator with the appropriate frequency, is commonly used at small population inversion [29].)

Thus, in this regime one can think of each cavity mode as a two-level system, having linewidth κ and detuning Δ_α, and driven with an "effective Rabi frequency" Ω', given by

$$\Omega' = \frac{\Omega \int d^d x g_\alpha(\mathbf{x}) n(\mathbf{x})}{\Delta_A}. \tag{2.30}$$

In their regime of validity, the arguments above establish a correspondence between the atom-mediated laser-cavity interaction and the standard atom-light interaction; therefore, one can apply the results of Sec. 2.5.1 to the present case simply by the replacements $\Omega \leftrightarrow \Omega'$, $\Delta_A \leftrightarrow \Delta_\alpha$, and $\gamma \leftrightarrow \kappa$. This mapping immediately reproduces Eqs. (2.13) and (2.14), and therefore completes our parallel quantum-mechanical derivation of the arguments of Sec. 2.2.

2.5.3 Self-organization as a quantum phase transition: toy model

Now that we have a quantum-mechanical model of both the atoms and the light, we can address the problem of self-organization as a quantum phase transition. This point is normally discussed via a mapping to the Dicke model, first proposed by Nagy et al. [27], which we shall touch on below; however, from the point of view of the present discussion, it is more natural to take a different approach (from Appendix A of Ref. [15]). We saw in Sec. 2.4.3 that the physics of self-organization can be understood as the softening of a phonon-like atomic excitation because of its coupling to optical modes. We shall use this observation to construct a simple, but fully quantum-mechanical, toy model of the self-organization transition; this model helps us elaborate on the connection between quantum phase transitions in quasi-equilibrium cavity QED settings and the conventional theory of quantum phase transitions as level-crossings (as discussed, e.g., in Ref. [36]), by means of a toy model. This toy model has the following components: (i) a laser mode of frequency ω_L, (ii) a cavity mode of wavevector k and frequency $\omega_C = \omega_L + \Delta_C$, and (iii) an anharmonic atomic phonon of wavevector k and frequency ω_p. The Hamiltonian for the model is given by:

$$H = \omega_L a_L^\dagger a_L + \omega_C a_C^\dagger a_C + \omega_p b^\dagger b + \lambda (b^\dagger b)^2 + \Gamma (a_L^\dagger a_C + \text{h.c.})(b^\dagger + b), \tag{2.31}$$

where Γ is the photon-phonon coupling constant, and λ is a parameter describing the extent of anharmonicity of the phonon. In what follows we shall rescale all energies by ω_p, in order to de-dimensionalize them; the

dimensionless parameters will be denoted as $\tilde{\omega}_L$ etc. As H commutes with the total number of photons, $\mathcal{N} \equiv a_L^\dagger a_L + a_c^\dagger a_c$, one can diagonalize it in a space of fixed total photon number $\mathcal{N}$. (For sufficiently large $\mathcal{N}$, the difference between number and coherent states is irrelevant.) Let us attempt to find the ground state for a particular value of $\mathcal{N}$. It is helpful to simplify further and treat the phonons as being "classical," by taking the commutator $[b^\dagger, b] = 0$; this is equivalent to rewriting $b = \sqrt{m\omega/2}[x + i(p/m\omega)]$ and taking the $m \to \infty$ limit. In this limit, all terms depending on p in the Hamiltonian are suppressed; thus the Hamiltonian can be rewritten, in terms of $x \propto b + b^\dagger$, as

$$H = \tilde{\omega}_L(a_L^\dagger a_L + a_C^\dagger a_L) + \tilde{\Delta}_L a_C^\dagger a_L + x^2 + \tilde{\lambda}x^4 + 2\tilde{\gamma}x(a_C^\dagger a_L + \text{h.c.}). \tag{2.32}$$

In this expression, the prefactors accompanying x have been absorbed as appropriate into the various coupling constants. The first term is simply a constant times $\mathcal{N}$, and can be ignored for our purposes. As x is also a good quantum number, it is now possible to diagonalize H in a manifold of fixed $\mathcal{N}$ and x. This can be achieved via canonical transformation from from $a_{L/C}$ to $A_{1/2}$:

$$a_L = \alpha A_1 + \sqrt{1-\alpha^2}A_2, \tag{2.33}$$

$$a_C = -\sqrt{1-\alpha^2}A_1 + \alpha A_2 \tag{2.34}$$

where

$$\alpha^2 = \frac{1}{2}\left(1 \pm \frac{\tilde{\Delta}_C}{\sqrt{4\tilde{\gamma}^2x^2 + \tilde{\Delta}_C^2}}\right). \tag{2.35}$$

In terms of A_1 and A_2, the Hamiltonian H has the form

$$H = \Delta_C\mathcal{N} + x^2 + \tilde{\lambda}x^4 + \frac{4\tilde{\gamma}^2x^2 - \tilde{\Delta_C}^2}{\sqrt{\tilde{\Delta}_C^2 + 4\tilde{\gamma}^2x^2}}(A_1^\dagger A_1 - A_2^\dagger A_2). \tag{2.36}$$

Expanding in powers of x, one finds that the coefficient of x^2 in the Hamiltonian is now given by

$$1 + (A_1^\dagger A_1 - A_2^\dagger A_2)\frac{6\tilde{\gamma}^2}{\tilde{\Delta}_C}. \tag{2.37}$$

For a fixed $\mathcal{N}$, the smallest value that the last term can attain is

$$-\frac{6\tilde{\gamma}^2}{\tilde{\Delta}_C}\mathcal{N}. \tag{2.38}$$

Thus, when $6\tilde{\gamma}^2/\tilde{\Delta}_C \leq 1/\mathcal{N}$, the coefficient of x^2 is always positive; hence the ground state always lies in the $x = 0$ manifold. However, for $6\tilde{\gamma}^2/\tilde{\Delta}_C > 1/\mathcal{N}$, the ground state is that in which $A_2^\dagger A_2 = \mathcal{N}$, and

$$x^2 = \frac{\frac{6\tilde{\gamma}^2}{\tilde{\Delta}_C}\mathcal{N} - 1}{2\tilde{\lambda}}. \tag{2.39}$$

Hence, as $\tilde{\gamma}$ is increased, the ground-state value of x (for fixed $\mathcal{N}$) becomes nonzero, singularly. In other words, the lowest level of the $x = 0$ manifold and that of an $x \neq 0$ manifold cross at the critical value of $\tilde{\gamma}$: such a level crossing is known as a "quantum phase transition" [36]. Although the phenomenon of self-organization in a multimode cavity involves substantially more than a single photon and a single phonon, its essential character in the equilibrium limit, for a classical laser, is also that of a ground-state level-crossing at some fixed photon number $\mathcal{N}$.

Effect of temperature and dissipation

At this point, we should briefly discuss a possible objection to the above description, which is that, in any realistic system, photons *do* leak out of the cavity, so that the assumption of fixed total photon number is unrealistic. In this thesis, we take the perspective (partly substantiated in the next chapter) that dissipation plays a similar role to that played by temperature near equilibrium quantum phase transitions [36]. In the equilibrium case, it is well understood that, although experiments only address systems at $T > 0$ and quantum phase transitions only occur at $T = 0$, the quantum phase transitions nevertheless *influence* the $T > 0$ properties of systems in measurable ways; these are normally understood via the renormalization-group idea of "crossovers" near phase transitions. A similar argument applies here, if one replaces the notion of temperature with that of cavity photon loss. In particular, (a) as discussed in the next chapter, there is a window of timescales and energy scales on which the dynamics is essentially quantum; and (b) sufficiently close to a putative critical point, various observables should have a universal dependence on the decoherence rates (just as, near an equilibrium quantum critical point, various observables have universal dependences on temperature). The latter issue is not discussed at length in the present work because, as we shall see, the quantum phase transition in a multimode cavity is not a critical point, being driven first-order by fluctuation effects.

Table 2.1: Estimates of the frequency scales corresponding to the parameters involved in cavity-mediated interactions.

Quantity	Expression	Typical frequency (in Hz)
Optical frequencies	$\omega_L, \omega_C, \omega_A$	10^{15}
Atom-laser detuning	Δ_A	10^{12}
Cavity-mode spacing ("free spectral range")		$10^{10} - 10^{11}$
Laser Rabi frequency	Ω	10^9
Laser-cavity detuning	Δ_C	$10^8 - 10^9$
Atom-cavity coupling	g	$10^6 - 10^7$
Loss/decay rates	κ, γ	$10^5 - 10^6$
Recoil energy; threshold scale	$K_0^2/(2M)$, ζN	10^5
Temperatures, heating rates	T, Γ, Γ_c	10^2

2.6 Experimental realization

Having discussed the physics of the self-organization transition, we now briefly describe some questions regarding its experimental realization. This discussion naturally consists of two parts: first, a discussion of the relevant energy scales and the criteria for them to be well-separated, and second, a few remarks on how the transition can be detected. We discuss both topics at a heuristic level; a more detailed discussion is presented in the next chapter.

2.6.1 Parameter regimes

We first discuss the parameter regime in which the considerations of previous sections apply. To summarize the assumptions we have made so far: in order for a quasi-equilibrium treatment to apply, the heating rates must be slow compared with the coherent coupling rates, so that the inequalities $\kappa \ll \Delta_C$ and $\gamma \ll \Delta_A$ must hold; furthermore, to eliminate the atoms before the cavity photons, we assumed that $\Delta_C \ll \Delta_A$. Prior to any of these assumptions, we implicitly assumed that all detunings were much smaller than the actual optical frequencies of the laser and the cavity modes, i.e., $\Delta_A, \Delta_C \ll \omega_L, \omega_C$. And finally, in order to explore the *quantum* regime, we assumed that the heating rates were small compared with the recoil energy, $\Gamma, \Gamma_c \ll 1/(2M\lambda_c^2)$. Table 2.1 provides order-of-magnitude estimates of all of these quantities (in units of frequency), indicating how it is possible for all these inequalities to be satisfied at once. We shall return to this question in Sec. 3.9, after having estimated the size of fluctuation effects, in order to discuss the feasibility of detecting such effects. Note that the frequency-space window of most interest is between the smallest "fast" scale (i.e., the atomic recoil energy, which is one of the two competing terms involved in the phase transition) and the largest decohering scale, which is either the system temperature or the scattering rate set by the leading decay process.

2.6.2 Detection channels

The most obvious channel for detecting self-organization experimentally involves monitoring the emission of photons through the cavity mirrors. When self-organization takes place, it leads to the macroscopic population of the cavity mode(s) with photons, and therefore—given that the modes have a finite decay rate—to a sudden increase in the total number of photons emitted from the cavity. This sudden increase was first observed by Black et al. [32], and later by Baumann et al. [23]. In the experiment of Baumann et al., the self-organizing system was a Bose condensate; in this case, one can measure the self-organization of the atomic cloud directly via time-of-flight imaging, which maps out the atomic momentum distribution. As the self-organized state is an emergent density wave, the Bragg peaks corresponding to this density wave should appear concomitantly with the self-organization transition. This expectation was borne out in the experiments of Ref. [23]: the onset of the satellite Bragg peaks coincided with the sudden increase in photon emission.

Although these measurements are sensitive to the onset of self-organization, they do not distinguish between the distinct possible self-organized states, especially in the case of a single-mode cavity. One simple approach that accomplishes this is to measure the phase of the emitted cavity photons with respect to the pump laser; the two self-organized configurations (i.e., even and odd antinodes) emit with a phase difference of π relative to one another [32]. The *spontaneity* of the symmetry breaking between even and odd antinodes can be tested by repeatedly "melting and refreezing" the emergent crystal; the protocols for this differ depending on whether one is considering a thermal gas or a BEC.

Finally, the recent work of Mottl et al. [37] offers a novel way of looking at the progressive softening of the Bogoliubov excitation in Sec. 2.4.3, by probing its influence on the cavity resonance. Because it is sensitive to the properties of the uniform state as well as the self-organized state, this approach is likely to be especially valuable for studying fluctuation effects, as we shall discuss in the next chapter.

2.7 Other perspectives

We now close this heuristic discussion of the physics of self-organization with some remarks on its relation to two other phenomena: (a) Dicke superradiance, originally studied in the context of masers [38], but to which the self-organization transition can be mapped; and (b) polariton condensation [28], which is analogous in that it involves quantum coherence and condensation in an intrinsically lossy system.

2.7.1 Dicke model mapping

In the vicinity of the self-organization transition, the two atomic modes at low energies are the uniform mode at $k = 0$ and the "softening" mode that hybridizes with the photons, $\psi_1(x) \sim \cos(kx)$. Thus, one can write the Bose field for the atoms as $\Psi(x) = c_0 + c_1 \cos(kx)$. If one defines the pseudospin operators $S_x \equiv c_0^\dagger c_1 + \text{h.c.}$, $S_y = i(c_0^\dagger c_1 - \text{h.c.})$ and $S_z \equiv c_1^\dagger c_1 - c_0^\dagger c_0$, one can write the full Hamiltonian for atoms and photons in the form:

$$H_{\text{Dicke}} = \Delta_C a_C^\dagger a_C + \frac{K^2}{2M} S_z + \frac{\Omega g}{\Delta_A} S_x (a_C^\dagger - a_C) + \frac{g^2}{\Delta_A}(S_z + N/2), \tag{2.40}$$

where a_C are cavity-mode creation and annihilation operators. This spatially zero-dimensional Hamiltonian, a version of the Dicke model, has been studied extensively, so that various properties of its dynamics are known, and can be generalized to the case of a dissipative system [39, 40, 41]. For our purposes, however, the Dicke model is not the most convenient approach, for two reasons: (i) for the reasons previously mentioned, we are most interested in the case of large Δ_C; in this regime, the cavity mode can be adiabatically eliminated to yield an atom-only theory with cavity-mediated interactions; (ii) the Dicke model does *not* allow for nontrivial spatial dependence in the cavity mode amplitudes. In its original application to microwave cavities, this neglect was well motivated, and for a single-mode optical cavity one can remove the spatial dependence by means of the transformation introduced in Ref. [27]. However, the spatial structure of modes in multimode cavities cannot in general be transformed away, so that it is necessary to work with a more general Hamiltonian.

2.7.2 Polariton condensation: similarities and differences

At first sight, the physics of a BEC in a cavity bears some resemblance to that of "polariton condensates," i.e., systems of laser-pumped excitons in a semiconductor microcavity (for a general review of these systems, see Ref. [28]). The aspect of these systems that is relevant here is that they, too, involve BECs in dissipative environments. Thus, there are parallels between the nonequilibrium field-theoretic approaches of Ref. [42] and of Chapter 3 (or Ref. [15]). A crucial distinction must be kept in mind, however: in polariton BECs, the pump laser *creates* the particles that condense; therefore, in the absence of a pump laser there would be no $U(1)$ symmetry breaking. By contrast, in the case of a crystallizing BEC, the BEC (and hence the symmetry-breaking) exists even in the absence of pumping. (In this sense, the case of spin ordering discussed in Chapter 4 is closer to that of polariton condensation.)

2.8 Summary

In this chapter, we have provided a heuristic introduction to the ideas behind cavity-mediated interactions and self-organization in cavities. The main points can be listed as follows:

1. An atom in a transversely pumped cavity (i.e., in the geometry of Fig. 2.1) both scatters photons into free space through the cavity and "feels" an energy shift that is closely analogous to the light shift. Both processes are maximal when the atoms are located at antinodes of the cavity mode. When the laser-cavity detuning is large, the conservative energy shift dominates the dissipative scattering.

2. In particular, dissipative processes due to cavity photon loss can be regarded as analogous to dissipative processes due to spontaneous decay: they set an experimental lifetime beyond which the physics is heating-dominated. A particularly important consequence is that the states of interest (whether uniform or self-organized) are long-lived *transients* described by effective equilibrium theories, and *not* nonequilibrium steady states.

3. In systems with many atoms in a single-mode cavity, this energy shift depends on the location of all the atoms; thus, it can be regarded as mediating an infinite-range interatomic interaction [as in Eq. (2.17)]. This interaction favors spontaneous symmetry-breaking and the formation of a density wave. In cavities with multiple modes, the cavity-mediated interaction is shorter-ranged.

4. As the laser intensity is increased, there is a transition between a uniform state with a depopulated cavity mode and a spatially modulated state with a macroscopically occupied cavity mode. This transition can be understood as a quantum phase transition—*qua* ground-state level crossing—in the limit of zero dissipation.

Chapter 3

The liquid-crystallization transition for atoms in a concentric cavity

Shiftings of an inchoate crystal tableau ...
The slight incipiencies, of which the form,
At last, is the pineapple

— Wallace Stevens, "Someone puts a pineapple together"

The work presented in this chapter is reprinted with minor changes from the following publication: Sarang Gopalakrishnan, Benjamin L. Lev, and Paul M. Goldbart, Phys. Rev. A 82, 043612 (2010). Copyright (2010) by the American Physical Society. In this chapter, we depart from the convention used in the rest of the thesis, and explicitly write out all factors of $\hbar$; this is chiefly in order to present our results in a form that facilitates estimates of experimental feasibility.

In this chapter, we develop a fully nonequilibrium, field-theoretic description of the atom-cavity system that was introduced in previous chapters, using the Schwinger-Keldysh functional-integral formalism [43, 44], and use it to address the self-organization transition. We show that the nonequilibrium description can be reduced, in the regime in which the cavity's photon loss rate is narrower than the timescales for atomic motion, to an effective equilibrium description; we then analyze this effective equilibrium theory using diagrammatic and renormalization-group techniques to establish the nature of the self-organization transition, in the specific case of a concentric cavity. Finally, we reintroduce the nonequilibrium effects, due to the leakage of photons out of the cavity, using perturbation theory, and account for their effects on critical behavior near the self-organization transition.

Our analysis of the equilibrium theory exploits a variant of Shankar's renormalization-group treatment of the Fermi liquid [45], to establish that for an interacting Bose-Einstein condensate the self-organization transition is always discontinuous in a concentric cavity. Furthermore, we show that the chief consequence of nonequilibrium effects is to decohere quantum correlations on a timescale related to the linewidth of the cavity; thus, the self-organization transition is always *classical* on the longest timescales. (For sufficiently high-finesse cavities, there should, however, be an extended crossover regime of timescales for which the

phase transition appears quantum.)

After presenting our analysis of the phase transition itself, we turn to the properties of the ordered (i.e., self-organized) state. We show that the ordered state has low-lying excitations, associated with the continuous symmetry-breaking, that resemble the excitations of smectic liquid crystals. We also observe that, for a Bose-condensed atomic cloud, the ordered state would be a "supersolid" (or, more accurately, a "super-smectic") in that it simultaneously possesses emergent (liquid-)crystalline and superfluid order. The properties and even the existence of supersolidity in ^{4}He are much-discussed topics in the condensed-matter literature [1, 46, 47, 48, 49]; the appeal of ultracold-atomic realizations is that one can explore the characteristic *phenomenology* of supersolids in contexts where it is less challenging to establish that they do in fact possess supersolidity. In order to explore the relevant phenomenology, it is necessary that the solidity be associated with a broken *continuous* spatial symmetry; for this purpose a continuum supersolid such as the one explored in the present work should serve as a more suitable setting than would, e.g., the lattice supersolids proposed in Refs. [50, 51]. The present scheme has the added advantage of being more readily realizable. The self-organization of a BEC in a cavity was demonstrated experimentally by Baumann et al. [23] for the case of a *single-mode* cavity; generalizing this experiment to the multimode case, in which one has continuous symmetry-breaking, should be technically straightforward. Continuing with the theme of supersolidity, we propose a scheme for detecting such as state, and develop a schematic phase diagram for the system (Fig. 3.11), which exhibits three phases: the supersolid, the normal solid, and the uniform superfluid. The phase diagram for a multimode cavity differs from that for a single-mode cavity in that the *multimode* case features a direct transition from the uniform superfluid to the normal solid, whereas in the single-mode case there is always a supersolid regime separating the uniform superfluid and the normal solid.

This chapter is organized as follows: In Sec. 3.1 we describe the microscopic model of the atom-cavity system that formalizes the ideas discussed heuristically in the previous chapter. In the next three sections we construct and analyze a nonequilibrium field-theoretic formulation of this model: Sec. 3.2 introduces the relevant field-theoretic formalism, Sec. 3.3 applies this formalism to derive an atoms-only action, and Sec. 3.4 describes the quasi-equilibrium limit of the atoms-only action. In Sec. 3.5 we derive an effective Ginzburg-Landau free energy, valid near the phase transition, which realizes a version of Brazovskii's model [52] of ordering at a finite wavelength, and analyze the effects of fluctuations on the self-organization transition in both the classical ($T > 0$) and quantum ($T = 0$) cases. In Sec. 3.6 we turn to the effects of departures from equilibrium, both on the fluctuations near the transition and (following the work of Hohenberg and Swift [53]) on the nucleation of ordered states. In the next two sections we focus the properties of the ordered state: Sec. 3.7 reviews the properties and elementary excitations of the ordered state, and Sec. 3.8

discusses the supersolid aspects of the ordered state. In Sec. 3.9 we discuss the experimental feasibility of the phenomena that we are investigating, showing that most of them should be readily detectable in the laboratory. In Sec. 3.10 we briefly consider the case of strongly layered three-dimensional systems, which have the feature that geometrical factors tend to frustrate the development of globally coherent long-range order. Finally, in Sec. 3.11 we summarize the results of this work, and discuss its relationship with other problems involving phase transitions and related collective effects in atom-light systems.

3.1 Model

The system analyzed in this chapter consists of N two-level atoms confined in a multimode optical cavity, together with the electromagnetic modes of the cavity. The system is pumped by an external laser, which is oriented transverse to the cavity axis, as shown in Fig. 3.1. In addition, the system is coupled to a set of extracavity electromagnetic modes, which constitute a bath for the system. The complete Hamiltonian $\mathcal{H}$ governing the system and bath comprises three elements—viz., $H_{\rm at}$, the atoms-only Hamiltonian; $H_{\rm em}$, the light-only Hamiltonian; and $H_{\rm int}$, the atom-light interaction Hamiltonian—which we discuss in detail in the rest of this section.

Two-level atoms

The atoms are described by the Hamiltonian

$$H_{\rm at} = \sum_{n=1}^{N} \left(\frac{\mathbf{p}_n^2}{2M} + \frac{\hbar\omega_A}{2}\left(1+\sigma_n^z\right) \right) + \overline{U} \sum_{1\le n<n'\le N} \delta(\mathbf{x}_n - \mathbf{x}_{n'}), \tag{3.1}$$

where N is the number of atoms (indexed by $n = 1, \ldots, N$), each of which has mass M; the position and momentum of atom n are, respectively, $\mathbf{x}_n$ and $\mathbf{p}_n$. The operator σ_z denotes the Pauli operator, which acts on the internal state of the atoms, which, for the sake of simplicity, we take to be two-state atoms, with $\hbar\omega_A$ being the energy splitting between the ground (g) and excited (e) states. (Our conclusions do not hinge in any essential way on this restriction to two states.) We model the interaction between atoms via a repulsive contact potential, which is parametrized in terms of the (positive) parameter $\overline{U}$. To ensure the correct handling of the Bose-Einstein quantum statistics of the atoms, we employ the framework of second

quantization. Thus, $H_{\rm at}$ becomes

$$\begin{aligned} H_{\rm at} &= -\frac{\hbar^2}{2M}\int d^dx\big\{\Psi_g^\dagger(\mathbf{x})\nabla^2\Psi_g(\mathbf{x}) + \Psi_e^\dagger(\mathbf{x})\nabla^2\Psi_e(\mathbf{x})\big\} \\ &\quad +\hbar\omega_A\int d^dx\,\Psi_e^\dagger(\mathbf{x})\Psi_e(\mathbf{x}) + \frac{\overline{U}}{2}\int d^dx\big(\Psi_g^\dagger\Psi_g^\dagger\Psi_g\Psi_g + \Psi_e^\dagger\Psi_e^\dagger\Psi_e\Psi_e + 2\Psi_g^\dagger\Psi_e^\dagger\Psi_e\Psi_g\big)\,, \end{aligned} \tag{3.2}$$

in which the pair of bosonic field operators, $\Psi_g(\mathbf{x})$ and $\Psi_e(\mathbf{x})$, respectively represent the ground- and excited-state atoms. In the last line of Eq. (3.2), all the coordinate indices are $\mathbf{x}$, as the interaction is taken to be local in space.

Next, we assume that the density of excited-state atoms is sufficiently low that collisions between such atoms can be neglected. This assumption necessarily holds in the low-temperature regime, which is the regime of primary interest to us, because the rate of spontaneous decay (which is proportional to the number of excited atoms) must be kept low in order to avoid the heating associated with it. With this regime in mind, we approximate the interaction term as

$$\frac{\overline{U}}{2}\int d^dx\,\left(\Psi_g^\dagger\Psi_g^\dagger\Psi_g\Psi_g + 2\Psi_g^\dagger\Psi_e^\dagger\Psi_e\Psi_g\right). \tag{3.3}$$

In what follows we shall replace $\overline{U}$ by the *frequency* $U \equiv \overline{U}/\hbar$, in order that its magnitude be expressed in the same units as those conventionally used to describe the atom-cavity coupling.

Electromagnetic modes

Optical cavities typically consist of two or more mirrors that support localized modes of the electromagnetic field between them [30]. The modes might be standing waves, as in the single-mode cavity, or the traveling waves that one can have in the ring cavity. In general, we shall be concerned with transverse electromagnetic (TEM) modes. The vector character of the electromagnetic field can be absorbed into the effective atom-mode coupling [54]; hence, such modes can effectively be described in terms of harmonic solutions to the scalar wave equation [30]. Furthermore, as the mirrors are not perfectly reflective, these modes are in fact weakly coupled to the extracavity modes, and thus cavity-mode photons tend to "leak" out of the cavity at some nonzero rate κ (which sets the intrinsic linewidth of the cavity). These considerations lead us to model the electromagnetic field—both intracavity and extracavity—in terms of the Hamiltonian

$$H_{\rm em} = \sum_{\alpha\,\text{in cav.}}\hbar\omega_\alpha a_\alpha^\dagger a_\alpha + \sum_{\varepsilon\,\text{in env.}}\hbar\omega_\varepsilon A_\varepsilon^\dagger A_\varepsilon + \left(\sum_{\alpha,\varepsilon}\hbar\kappa_{\alpha\varepsilon}A_\varepsilon^\dagger a_\alpha + \text{h.c.}\right), \tag{3.4}$$

where a_α and A_ε respectively represent the intracavity and extracavity photons, ω_α and ω_ε are the intracavity and extracavity mode frequencies, and $\kappa_{\alpha,\varepsilon}$ describes the coupling between the intracavity mode α and the extracavity mode ε. We assume that the intracavity-extracavity coupling is weak enough (i.e., the cavity is of sufficiently high finesse) that it is meaningful to separate the modes into intracavity and extracavity ones.

The modes of a generic standing-wave cavity are not frequency-degenerate: the typical frequency spacing, or *longitudinal* "free spectral range," is of order c/L, where L is the linear dimension of the cavity: e.g., for a 1 cm cavity, the free spectral range is about 15 GHz. For such a cavity, the frequency spacing between higher-order *transverse* modes is an appreciable fraction of this number; thus there are no degenerate modes. However, certain specific cavity geometries do support degenerate modes. The simplest of these is the ring cavity, which is a three-mirror arrangement that supports two counterpropagating traveling-wave modes (see Fig. 3.1a). Even larger degeneracies are possible, e.g., in confocal or concentric cavities. Let us label the cavity-mode structure by the integers (q, m, n), where q is the number of nodes along the axial direction, and (m, n) are the numbers of nodes along the transverse directions; see Fig. 3.1. (The corresponding mode functions are approximately sinusoidal in the axial direction, and Hermite-Gaussian (or Laguerre-Gaussian) in the transverse directions, although this approximation breaks down in the limit of a concentric cavity.) In the confocal cavity, the condition for frequency degeneracy is that $q + ((m+n)/2) = M$ (see, e.g., Ref. [30]) for some fixed integer M; in the concentric cavity, the condition becomes $q+m+n = M$. In principle, these conditions imply that there are of order M^2 degenerate modes, where M is roughly the number of optical wavelengths across the cavity, commonly 10^4 or more. In practice, higher-order modes are increasingly lossy, because their profiles (i.e., spot sizes) are larger, and therefore more of their light leaks out of the sides of the cavity mirrors, which typically occupy only a modest amount of solid angle. We approximately account for this effect by assuming that M_0 of the modes have a common loss rate κ, and that the other modes are perfectly lossy (i.e., for them $\kappa = \infty$).

Atom-light interactions

In the dipole and rotating-wave approximations [54], the atom-light coupling has the generic form $i\sigma_- \, a_n^\dagger \, g_n(\mathbf{x}) -$ h.c., where the σ operators raise or lower the atomic internal state; a_n is either an intracavity or extracavity mode; and $g_n(\mathbf{x}) \equiv g\,\Xi(\mathbf{x})$, in which g is the coupling between the atom and the mode, and Ξ is an appropriately normalized mode function. Note that g is proportional to $1/\sqrt{V}$, where V is the system volume [54]; hence $g^2 N$ stays finite in the thermodynamic limit. In the special case of the pump laser mode, we shall treat the corresponding a_n as a classical variable, so that the atom-laser coupling takes the form $\Omega(\mathbf{x}, t)\sigma_- +$ h.c., where $\Omega(\mathbf{x}) \equiv \Omega(\mathbf{x})e^{-i\omega_L t}$, with $\Omega(\mathbf{x})$ being the local Rabi frequency (which is proportional to the local

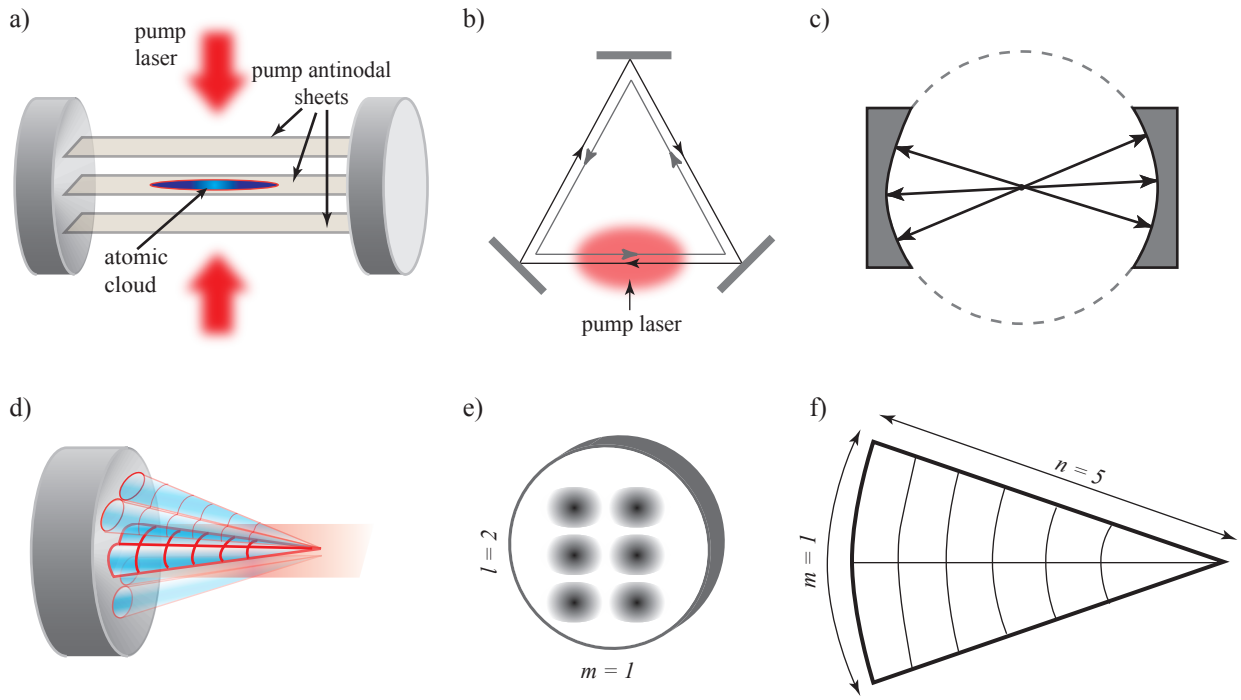

Figure 3.1: (a) The transversely pumped, quasi-two-dimensional geometry primarily discussed in this paper. (b) Ring cavity geometry. The pump laser beam is perpendicular to the plane defined by the three mirrors, as indicated in the figure. (c) Schematic representation of a concentric cavity, showing the partial rotational symmetry that such a cavity inherits from the sphere of which both cavity mirrors are arcs. (d) Three-dimensional view of a representative mode function for the concentric cavity. This mode function is labeled by $(l, m, n) = (2, 1, 5)$, or alternatively by TEM_{21}. The three numbers enumerate the nodes (one fewer than the number of lobes) in the pump (z), angular, and radial directions, respectively. The axial mode index n is fixed by the requirement that $l+m+n$ be constant for a family of degenerate modes, and can therefore be suppressed. (e) The intensity profile of the representative mode TEM_{21} at one of the cavity's end mirrors. (f) The intensity profile of the mode TEM_{21} in the equatorial (i.e., $z = 0$) plane of the cavity.

amplitude) of the laser. In our analysis, we shall largely neglect the term that governs spontaneous atomic emission into extracavity modes (i.e., spontaneous decay); this term is proportional to the linewidth of the transition, which is denoted as γ. The reason we can neglect spontaneous decay processes is not that such processes are always weak. Rather, it is that their effects amount to the heating up of the sample via the random impulses they give to the atoms, and therefore the timescale for spontaneous decay [which is given by $1/R_\gamma = \Delta_A^2/(\gamma\Omega^2)$] acts as an upper limit on the duration of an experiment: quantum dynamics on timescales slower than R_γ is likely to be washed out as a result of spontaneous decay. Neglecting, then, spontaneous decay processes, the Hamiltonian governing the atom-light interactions is given by

$$H_{\rm int} = i\hbar \int d^d x\, \Psi_e^\dagger(\mathbf{x})\Psi_g(\mathbf{x}) \left[\sum_{\alpha\in{\rm cav.}} g_\alpha(\mathbf{x})\, a_\alpha^\dagger + \Omega(\mathbf{x},t) \right] - {\rm h.c.} \tag{3.5}$$

3.2 Field-theoretic formulation

Our objective in this and the subsequent two sections, Sec. 3.3 and Sec. 3.4, is to construct a useful field-theoretic formulation that will enable us to explore the quantum statistical mechanics of correlated many-atom, many-photon systems in multimode cavities. Having done that, in Sec. 3.5 we employ this formulation to address issues such as the emergence and nature of the spatial structure and spatio-temporal atomic and photonic correlation properties of such systems, focusing on the vicinity of the transition to the self-organized state. The atom-cavity systems of interest here are neither closed nor in thermal equilibrium, because they are driven by an external pump laser (which adds energy) and leak photons into the continuum of modes that lie outside the cavity (hence losing energy); thus, even in its steady states there is a flux of energy through the system. For these reasons, the structure and correlation properties must be computed within a nonequilibrium formalism. The one we employ is the closed-time-path formalism, due to Schwinger [43] and Keldysh [44], which enables the use of diagrammatic methods as well as renormalization-group techniques to analyze fluctuations. (For a discussion of the differences between the equilibrium and nonequilibrium formalisms, see Sec. 3.4 and Ref. [4].)

Although, as we have just discussed, a full analysis of the problem demands a nonequilibrium approach, we find that, for systems that are near the threshold for self-organization and in the dispersive regime (i.e., the pump laser is far-detuned from the atomic resonance), an effective equilibrium description is valid, to a reasonable approximation. As we shall see, e.g. in Sec. 3.6, the description of this regime can be improved, and other regimes (such as the strongly organized regime) can be analyzed, using the full machinery of the Schwinger-Keldysh nonequilibrium approach.

3.2.1 Schwinger-Keldysh functional integral

The quantities of interest in quantum many-body dynamics are the expectation values of observables and their response and correlation functions. Formally, the task of computing these may be stated as follows: suppose that we know the state of the system in the infinite past, as described by its density matrix $\rho(t = -\infty)$, when it is taken to be isolated and noninteracting. The system is then coupled to an environment (or environments), which generically force the composite of system and environment(s) to be out of equilibrium, and the intra-system interactions are adiabatically switched on. The question then becomes: What are the expectation values and response and correlation functions of the various *system* observables, once the system and environment have relaxed to a steady state?

Let us first consider the case of a single harmonic oscillator with Hamiltonian $H = \hbar\omega_0\, b^\dagger\, b$, i.e., a free bosonic degree of freedom having the characteristic frequency ω_0. Suppose, as a simple example, that we are interested in the expectation value of some observable $A(t)$ at time t, given that the system was at some time $t_i < t$ in a thermal state at temperature T, i.e., governed by the density matrix $\rho(t_i) \propto \exp(-\hbar\omega_0 b^\dagger b/k_B T)$. Thus, we wish to compute the quantity

$$\langle A(t)\rangle \equiv \mathrm{Tr}\left[\rho(t_i)A(t)\right]. \tag{3.6}$$

One can expand the trace in terms of bosonic coherent states [55] at the times t_i and $t_f > t$, thus arriving at the expression

$$\frac{1}{(2\pi)^4} \int d\tilde{w}_f d\tilde{w}_f^* d\tilde{w}_i\, d\tilde{w}_i^* dw_i\, dw_i^* dw_f dw_f^* \tag{3.7}$$
$$e^{-|\tilde{w}_f|^2-|\tilde{w}_i|^2-|w_i|^2-|w_f|^2}\langle w_i|\rho(t_i)|\tilde{w}_i\rangle \times \langle\tilde{w}_i|\tilde{w}_f\rangle \times \langle\tilde{w}_f|1|w_f\rangle \times \langle w_f|A(t)|w_i\rangle.$$

Note that the primary motivation for inserting the complete set of states $|w_f\rangle$ is to make the above expression more symmetric between initial and final times. (Note also that we have adopted the normalization convention of Ref. [55], in which the norm of a coherent state $|z\rangle$ is given by $\langle z|z\rangle = e^{|z|^2}$. In the quantum optics literature, by contrast, coherent states are conventionally normalized to unity. This difference in conventions leads to some apparent discrepancies with standard quantum-optics formulas.) The relevant matrix element of the initial density matrix is given by $\exp(-\beta\hbar\omega_0 w_i^*\tilde{w}_i)$, the overlap $\langle\tilde{w}_f|1|w_f\rangle$ is given by $\exp(-\tilde{w}_f^* w_f)$, and the two other expressions, which are transition amplitudes, can be rewritten as coherent-state path integrals:

$$\langle \tilde{w}_i|\tilde{w}_f\rangle\langle w_f|A(t)|w_i\rangle = \int_{z_+(t_i)=\tilde{w}_i}^{z_+(t_f)=\tilde{w}_f} D(z_+,z_+^*)e^{iS[z_+,z_+^*]} \int_{z_-(t_i)=w_i}^{z_-(t_f)=w_f} D(z_-,z_-^*)A(z_-,z_-^*)e^{-iS[z_-,z_-^*]}, \quad (3.8)$$

in which the $\pm$ signs indicate whether the final state is the ket $(+)$ or the bra $(-)$; the functions $A(z_\pm, z_\pm^*)$ represent the matrix elements $\langle z_\pm|A|z_\pm\rangle$; and the action S is given by

$$S[z_\pm, z_\pm^*] = \int_{t_i}^{t_f} dt\, z_\pm^*(i\partial_t - \omega_0)z_\pm. \quad (3.9)$$

One can thus rewrite Eq. (3.6) as follows:

$$\begin{aligned}\langle A(t)\rangle \;=\; & \int d(\tilde{w}_f\tilde{w}_f^*\tilde{w}_i\,\tilde{w}_i^* w_i\, w_i^* w_f w_f^*)\, e^{-|\tilde{w}_f|^2-|\tilde{w}_i|^2-|w_f|^2-|w_i|^2} e^{-\beta\hbar\omega_0 w_i^*\tilde{w}_i}\, e^{-w_f\tilde{w}_f^*} \\ & \int_{z_+(t_i)=\tilde{w}_i}^{z_+(t_f)=\tilde{w}_f} D(z_+,z_+^*) \int_{z_-(t_i)=w_i}^{z_-(t_f)=w_f} D(z_-,z_-^*) \frac{\delta}{\delta\xi_-(t)}\bigg|_{\xi_\pm=0} e^{iS[z_+,z_+^*]-iS[z_-,z_-^*]+\int dt\xi_-(t)A_-(t)+\xi_+(t)A_+(t)}.\end{aligned} \quad (3.10)$$

If we omit the functional derivative $\delta/\delta\xi_-(t)$ from the right hand side of Eq. (3.10), the remaining formula is the quantity commonly denoted as Z (by analogy with the partition function). Z is a generating functional for the correlation functions of the oscillator: it can be differentiated repeatedly with respect to either of the two source functions $\xi_\pm(t)$ in order to generate all requisite correlation functions of A. By differentiating with respect to the $+$ and $-$ sources appropriately, one can compute expectation values that involve various orderings of the operators, e.g., the time-ordered, retarded, and advanced Green functions. By contrast, in the zero-temperature and Matsubara nonzero temperature equilibrium formalisms, the only correlation functions that can be computed directly are the time-ordered ones; the (physically relevant) retarded Green functions are then to be inferred using identities that hold in equilibrium or at zero temperature.

Because, in Eq. (3.10), the initial and final values of the paths are integrated over (with an exponential measure), the path integral in Eq. (3.10) is in effect an *unconstrained* path integral over the two sets of paths $z_\pm$. Moreover, these paths are uncoupled from one another *except* at the two endpoints of the path integrals. For the oscillator in question one can write the action in the form

$$S = \begin{pmatrix} z_+^* & z_-^* \end{pmatrix} \begin{pmatrix} S_{++} & S_{+-} \\ S_{-+} & S_{--} \end{pmatrix} \begin{pmatrix} z_+ \\ z_- \end{pmatrix}, \quad (3.11)$$

in which integration is implied over time. We shall sometimes denote as $\mathbf{S}$ the matrix comprising the four block matrices $S_{\pm\pm}$. The diagonal blocks S_{++} and S_{--} are given by Eq. (3.9); the off-diagonal blocks S_{+-}

and S_{-+} are zero, except at the time-endpoints; they cannot, however, be neglected, because the presence of such off-diagonal terms changes the *inverse* of $\mathbf{S}$, denoted $\mathbf{G}$, which contains the two-point correlation functions and has the following structure:

$$G_{+-}(t,t') = n_B(\omega_0)e^{-i\omega_0(t-t')} = \langle z(t)z^*(t')\rangle, \tag{3.12a}$$

$$G_{-+}(t,t') = (n_B(\omega_0)+1)\,e^{-i\omega_0(t-t')} = \langle z^*(t)z(t')\rangle, \tag{3.12b}$$

$$G_{++}(t,t') = \Theta(t-t')G_{+-} + \Theta(t'-t)G_{-+}, \tag{3.12c}$$

$$G_{--}(t,t') = \Theta(t-t')G_{-+} + \Theta(t'-t)G_{+-}, \tag{3.12d}$$

where $n_B(\omega_0)$ is the Bose-Einstein distribution function. Evidently, G_{++} and G_{--} are the time-ordered and anti-time-ordered Green functions. It is convenient for our purposes to rotate $z_\pm$ into its "classical" and "quantum" components, defined as follows: $z_c \equiv (z_+ + z_-)/2$, $z_q \equiv (z_+ - z_-)/2$, in Eq. (3.11). This has the advantage of reducing the number of independent Green functions by one:

$$\mathbf{G} = \begin{pmatrix} G_K & G_R \\ G_A & 0 \end{pmatrix}, \tag{3.13}$$

where

$$G_K \equiv \langle z_c^*(t)z_c(t')\rangle = -i\big(2n_B(\omega_0)+1\big)e^{-i\omega_0(t-t')}, \tag{3.14a}$$

$$G_R \equiv \langle z_c^*(t)z_q(t')\rangle = -i\Theta(t-t')e^{-i\omega_0(t-t')}, \tag{3.14b}$$

$$G_A \equiv \langle z_q^*(t)z_c(t')\rangle = i\Theta(t'-t)e^{-i\omega_0(t-t')}. \tag{3.14c}$$

G_R and G_A are the retarded and advanced Green functions—which describe the *response* of the system to an external perturbation—whereas G_K, the "Keldysh Green function," depends on the system's initial density matrix and its *correlations*. For a system in equilibrium with a bath, the correlations and response are related by the fluctuation-dissipation theorem; by contrast, for an isolated, noninteracting (and hence nonequilibrating) system such as the harmonic oscillator, the two properties—response and correlation—are independent. In *interacting* systems that are away from equilibrium, there is in general a complicated interplay between the correlations and the response; therefore, all the Green functions contain information about both correlations and response. The nature of this relation, however, varies from system to system, and hence the information contained in the three Green functions is not redundant.

3.2.2 Application to atom-photon system

The prescription for proceeding from the second-quantized Hamiltonian for a generic set of bosonic degrees of freedom $\{\phi_i(t)\}$ to the appropriate coherent-state path integral (in real time) is as follows:

$$\begin{aligned} S &= \int dt \sum_r \phi^*_{r,+}(t)\, i\partial_t \phi_{r,+}(t) - H\big(\{\phi^*_{r,+}(t), \phi_{r,+}(t)\}\big) \\ &\quad + \sum_r \mu_r |\phi_{r,+}(t)|^2 - (+ \leftrightarrow -). \end{aligned} \tag{3.15}$$

In this expression, μ_r is the chemical potential for field r—in the present case, the chemical potential for the photons is zero, whereas that for the atoms determines the atomic density—and the symbol $(+ \leftrightarrow -)$ indicates a formally identical set of terms in which + fields are replaced by the corresponding − fields. This prescription can be carried out for each of the terms in the Hamiltonian $\mathcal{H}$ introduced in Sec. 3.1, and generates all the $++$ and $--$ components of the action. The off-diagonal ($+-$ and $-+$) blocks in the bare (i.e., microscopic) theory depend on the appropriate Bose-Einstein distributions of the free photonic modes and the free atomic modes. Because these blocks are infinitesimal (as they arise from the end-point couplings discussed in the previous section), it is more useful to write down the relevant blocks in the inverse action, viz., the bare Green functions G_{+-} and G_{-+}. For the cavity photon modes these have precisely the forms in Eqs. (3.12), i.e.,

$$G_{+-}(t,t') = n_B(\omega_C) e^{-i\omega_C(t-t')}, \tag{3.16}$$

$$G_{-+}(t,t') = \big(n_B(\omega_C)+1\big) e^{-i\omega_C(t-t')}, \tag{3.17}$$

whereas for bosonic atoms (in their internal ground state) and in a single-particle eigenstate of the kinetic energy having eigenvalue E, these have the form

$$G_{+-}(t,t') = n_B(E-\mu) e^{-i(E-\mu)(t-t')/\hbar} \tag{3.18}$$

$$G_{-+}(t,t') = \big(n_B(E-\mu)+1\big) e^{-i(E-\mu)(t-t')/\hbar}. \tag{3.19}$$

Other degrees of freedom can be treated similarly.

3.3 Constructing the atoms-only action

In this section we derive an effective action, involving the ground-state atoms, which we shall use to determine expectation values and correlators involving atoms and/or intracavity photons. This is accomplished by integrating out all other degrees of freedom—a task that is straightforward, owing to the fact that they appear quadratically in the complete action.

3.3.1 Eliminating the atomic excited state

As we see from Eqs. (3.15), (3.2), and (3.5), the complete action involves the atomic excited state in the following terms:

$$\int dt\, d^d x \Psi^\dagger_{e,\pm}(\mathbf{x},t)\left(i\partial_t + \frac{\hbar\nabla^2}{2M} - \omega_A\right)\Psi_{e,\pm}(\mathbf{x},t) + i\Big[\sum_\alpha g_\alpha(\mathbf{x})\Psi_{g,\pm}(\mathbf{x},t)\Psi^\dagger_{e,\pm}(\mathbf{x},t)a_{\alpha,\pm}(t) - \text{h.c.}\Big]$$
$$-U|\Psi_{g,\pm}(\mathbf{x},t)|^2|\Psi_{e,\pm}(\mathbf{x},t)|^2 + \cdots . \tag{3.20}$$

The functional integral over the quadratically occurring $\Psi_{e,\pm}$ in Eq. (3.20) can be performed exactly. In the regime of interest, the atom-laser detuning $\hbar\Delta_A \equiv \hbar\omega_A - \hbar\omega_L$ is much greater than the energy scale associated with atomic motion; therefore, one can simplify matters by dropping the gradient term for Ψ_e. (Put heuristically, excited-state atoms, being short-lived and massive, "decay" before they have time to move, so that the interactions they mediate are local in space and time.) Thus, one can integrate out the excited state, determining the necessary kernel via the standard technique of solving the classical equations of motion for $\Psi_{e,\pm}$ and $\Psi^\dagger_{e,\pm}$ to obtain

$$\Psi_{e,\pm}(\mathbf{x},t) = i\frac{\sum_\alpha g_\alpha(\mathbf{x})a_\alpha(t)\Psi_{g,\pm}(\mathbf{x},t)}{\Delta_A + U|\Psi_{g,\pm}(\mathbf{x},t)|^2}, \tag{3.21}$$

where, for convenience, we have made the change of photon variables $a_\alpha \to a_\alpha\, e^{-i\omega_L t}$ to enable us later to exploit the approximate degeneracy of the laser and cavity modes. By inserting the classical solutions, Eq. (3.21) into the action, Eq. (3.20), we arrive at the following contributions to the action:

$$\int dt\, d^d x\, \Psi_{g,\pm}(\mathbf{x},t)\left(i\partial_t + \frac{\hbar\nabla^2}{2M} - U|\Psi_{g,\pm}(\mathbf{x},t)|^2 + \mu\right)\Psi_{g,\pm}(\mathbf{x},t)$$
$$+\sum_\alpha \frac{g_\alpha(\mathbf{x})\Omega}{\Delta_A + U|\Psi_{g,\pm}(\mathbf{x},t)|^2}|\Psi(\mathbf{x},t)_\pm|^2 a^\dagger_{\alpha,\pm}(t) + \text{h.c.}$$
$$+\sum_{\alpha\beta} \frac{g_\alpha(\mathbf{x})g^*_\beta(\mathbf{x})}{\Delta_A + U|\Psi_{g,\pm}(\mathbf{x},t)|^2}|\Psi_{g,\pm}(\mathbf{x},t)|^2 a^\dagger_{\alpha,\pm}(t)a_{\beta,\pm}(t). \tag{3.22}$$

In what follows we shall approximate $\Delta_A + U|\Psi_{g,\pm}(\mathbf{x},t)|^2$ by Δ_A, using the fact that the interatomic interaction is typically many orders of magnitude weaker than Δ_A.

3.3.2 Eliminating the photon states

Next, we integrate out the photon states, doing so in two steps: (i) by integrating out the environment modes to arrive at an effective action for the cavity photons, and (ii) by integrating out the cavity photon modes to arrive at an effective action for ground-state atoms alone. To achieve step (i) we use the result of Caldeira and Castro-Neto [i.e., Eqs. (36) of Ref. [56] in the limit $\hbar\omega_C \gg k_B T$] for the path integral over extracavity modes, and thus we identify the following contributions to the action that involve the cavity modes:

$$\sum_\alpha \int dt \begin{pmatrix} a^*_{\alpha,+}(t) & a^*_{\alpha,-}(t) \end{pmatrix} \begin{pmatrix} i\partial_t - \omega_C + i\kappa & 0 \\ 2i\kappa & -i\partial_t + \omega_C + i\kappa \end{pmatrix} \begin{pmatrix} a_{\alpha,+}(t) \\ a_{\alpha,-}(t) \end{pmatrix} \tag{3.23}$$
$$+\frac{1}{\Delta_A}\left[\sum_\alpha \int dt\, d^d x (\Omega e^{i\omega_L t} g_\alpha(\mathbf{x}) n_+(\mathbf{x},t) a^*_{+,\alpha}(t) + \text{h.c.})\right.$$
$$\left. + \sum_{\alpha,\beta}\int dt\, d^d x\, a^*_{\alpha,+}(t)a_{\beta,+}(t)g_\alpha(\mathbf{x})g^*_\beta(\mathbf{x})n_+(\mathbf{x},t) - (+\leftrightarrow -)\right],$$

where $n_\pm(\mathbf{x},t) \equiv \Psi^*_\pm(\mathbf{x},t)\Psi_\pm(\mathbf{x},t)$ is the local atomic density. Note that we have dropped the atomic internal-state index g (i.e., we have made the relabeling $\Psi_{g,\pm} \to \Psi_\pm$).

To achieve step (ii), we observe that the action is quadratic in the cavity photon modes, so they too can be integrated out, to produce the desired atom-only action which, for convenience, we express in terms of the classical-quantum (i.e., $c-q$) basis for the fields rather than the $\pm$ basis (see Sec. 3.2):

$$
\begin{aligned}
S^{\rm eff} &= \int dt\, d^dx \Psi_c^*(\mathbf{x},t)\left(i\partial_t + \frac{\hbar\nabla^2}{2M} + \mu\right)\Psi_q(\mathbf{x},\mathbf{t}) \\
&\quad - U\Psi_c^*(\mathbf{x},t)\Psi_q^*(\mathbf{x},t)[\Psi_c(\mathbf{x},t)^2 + \Psi_q(\mathbf{x},t)^2] + \text{h.c.} + \frac{1}{2}\text{Tr}\ln\mathbf{M} \qquad (3.24)\\
&\quad + \int d^dx\, d^dx'\, d\omega\, d\omega' \sum_\alpha \frac{\Omega^2 g_\alpha^2(\mathbf{x})}{\Delta_A^2}\begin{pmatrix} n_1(\mathbf{x},\omega) & n_2(\mathbf{x},\omega)\end{pmatrix}\left[\mathbf{M}(\omega,\omega';\alpha,\beta)\right]^{-1}\begin{pmatrix} n_1(\mathbf{x}',\omega') \\ n_2(\mathbf{x}',\omega')\end{pmatrix},
\end{aligned}
$$

in which $\mathbf{M}$ is the matrix

$$
\mathbf{M}(\omega,\omega';\alpha,\beta)\equiv\begin{pmatrix} 0 & \omega-\omega_C+i\kappa \\ \omega-\omega_C-i\kappa & 2i\kappa\end{pmatrix}\delta(\omega-\omega')\,\delta_{\alpha\beta} + \begin{pmatrix} 0 & D_1(\omega'-\omega;\alpha,\beta) \\ D_1^*(\omega'-\omega;\alpha,\beta) & D_2(\omega'-\omega;\alpha,\beta)\end{pmatrix},
$$

and the quantities D_i are defined as follows:

$$
D_i \equiv \frac{1}{\Delta_A}\int d^dx g_\alpha(\mathbf{x})\, g_\beta(\mathbf{x})\, n_i(\mathbf{x},\omega'-\omega), \qquad (3.25)
$$

where the Keldysh components of the atomic density are given by

$$
\begin{aligned}
n_1(\mathbf{x},\omega) &\equiv \int d\omega'\, \Psi_c^*(\mathbf{x},\omega')\Psi_q(\mathbf{x},\omega-\omega') + \text{h.c.}, \qquad (3.26)\\
n_2(\mathbf{x},\omega) &\equiv \int d\omega' \Big\{\Psi_c^*(\mathbf{x},\omega')\Psi_c(\mathbf{x},\omega-\omega') \\
&\qquad + \Psi_q^*(\mathbf{x},\omega')\Psi_q(\mathbf{x},\omega-\omega')\Big\}. \qquad (3.27)
\end{aligned}
$$

How one should proceed from here depends on the relative magnitudes of κ, Δ_C, and g^2N/Δ_A. Our objective in this paper is to analyze the self-organization transition in a multimode cavity. Physically, this transition is associated with the laser-cavity interference term, as discussed in Chapter 2, and is most straightforward to analyze when $E_L \gg E_C$ (i.e., when $\Omega \gg g_\alpha$); moreover, as discussed in Ref. [26] (and as we shall show), the steady-state temperature of the system is proportional to $\hbar\kappa$. Therefore, in order to explore self-organization at low-temperatures, it is natural to take $\Delta_C \gg \kappa, g^2N/\Delta_A$ [1]. We may therefore expand $\ln\mathbf{M}$ and $\mathbf{M}^{-1}$ in

[1] At the mean-field level it is solely the quantity $[\Delta_C - g^2N/\Delta_A]$, i.e., the resonance frequency renormalized by the refractive index of the atoms, that determines the physical properties of the cavity. This is no longer the case when fluctuations in the atomic density are included: the refractive index is then sensitive to these fluctuations, whereas Δ_C is not.

powers of κ/Δ_C and $g^2N/(\Delta_A\Delta_C)$, thus arriving at a simplified atom-only effective action:

$$S_{\rm eff} = S_0 + S_\zeta + S_\xi + S_U + S_\kappa, \tag{3.28}$$

where the five terms—which are labeled by their corresponding coupling constants—respectively account for: S_0, the kinetic energy of the atoms; S_ζ, the λ-periodic interaction caused by the scattering of photons between the laser and cavity modes; S_ξ, the interaction due to the scattering of photons between cavity modes; S_U the contact repulsion between the atoms; and S_κ, dissipative processes due to the leakage of photons through the cavity mirrors. The terms have the following explicit forms:

$$\begin{aligned}
S_0 &= \int d\omega\, d^dx\, \Psi_c^*\left(\omega + \frac{\hbar\nabla^2}{2M} + \mu\right)\Psi_q + \text{h.c.}, \\
S_\zeta &= \zeta\Delta_C \sum_\alpha \int d\omega\, d^dx\, d^dx'\, \Xi_\alpha(\mathbf{x})\Xi_\alpha(\mathbf{x}') \\
&\qquad \times\left\{\frac{n_1(\mathbf{x},\omega)\, n_2(\mathbf{x}',\omega)}{\omega - \Delta_C + i\kappa} + \frac{n_1(\mathbf{x},\omega)\, n_2(\mathbf{x}',\omega)}{\omega - \Delta_C - i\kappa}\right\}, \\
S_\xi &= \xi\Delta_C \sum_{\alpha\beta} \int d^dx\, d^dx'\, \Xi_\alpha(\mathbf{x})\, \Xi_\beta(\mathbf{x})\, \Xi_\alpha(\mathbf{x}')\, \Xi_\beta(\mathbf{x}') \\
&\qquad \times \int d\omega\, d\omega' \frac{n_1(\mathbf{x},\omega)\, n_2(\mathbf{x}',\omega)}{(\omega + \omega' - \Delta_C + i\kappa)(\omega - \Delta_C - i\kappa)}, \\
S_U &= U\int d^dx\, dt\, \Psi_c^*(\mathbf{x}t)\Psi_q^*(\mathbf{x}t)[\Psi_c(\mathbf{x}t)^2 + \Psi_q(\mathbf{x}t)^2] + \text{h.c.}, \\
S_\kappa &= \int d\omega \frac{1}{(\omega - \omega_C)^2 + \kappa^2} \int d\omega\, d^dx\, d^dx'\, g_\alpha(\mathbf{x})\, g_\alpha(\mathbf{x}') \\
&\qquad \times i\,\zeta\,\kappa\,\Delta_C\, \coth(\hbar\kappa/k_BT)\, n_1(\mathbf{x}\omega)\, n_1(\mathbf{x}\omega).
\end{aligned} \tag{3.29}$$

To streamline the notation we have introduced the coupling constants $\zeta \equiv g^2\Omega^2/(\Delta_A^2\Delta_C)$ and $\xi \equiv g^4/(\Delta_A^2\Delta_C)$. For the regime in which Δ_C is large compared with the other frequencies in the effective action (e.g., the typical atomic kinetic energy), a further simplification is possible: the integrals over ω and ω' can be expanded in a gradient expansion in terms of $(1/\Delta_C)\partial_t$. In what follows, we shall keep only the zeroth order term in this expansion, thus arriving at the following "instantaneous" forms of S_ζ and S_ξ, in which we have expanded n_1 and n_2 in terms of the atomic field operators:

$$
\begin{aligned}
S_\zeta &= \zeta \sum_\alpha \int dt\, d^d x\, d^d x'\, \Xi_\alpha(\mathbf{x})\, \Xi_\alpha(\mathbf{x}') \\
&\quad \times \Psi_c^*(\mathbf{x}t)\Psi_q^*(\mathbf{x}'t)[\Psi_c(\mathbf{x}t)\Psi_c(\mathbf{x}'t)+\Psi_q(\mathbf{x}t)\Psi_q(\mathbf{x}'t)]+\text{h.c.} \\
S_\xi &= \xi \sum_{\alpha\beta} \int dt\, d^d x\, d^d x'\, \Xi_\alpha(\mathbf{x})\, \Xi_\beta(\mathbf{x})\, \Xi_\alpha(\mathbf{x}')\, \Xi_\beta(\mathbf{x}') \\
&\quad \times \Psi_c^*(\mathbf{x}t)\Psi_q^*(\mathbf{x}'t)[\Psi_c(\mathbf{x}t)\Psi_c(\mathbf{x}'t)+\Psi_q(\mathbf{x}t)\Psi_q(\mathbf{x}'t)]+\text{h.c.}
\end{aligned}
\tag{3.30}
$$

Note that if we neglect the effects due to S_κ, the nonequilibrium character of the theory would apparently disappear: the nonequilibrium laser- and cavity-mediated interactions S_ζ and S_ξ have precisely the same form in terms of Keldysh and time indices as the contact repulsion S_U; thus, an effective equilibrium description of these terms should be possible. In the rotating-wave approximation (see Sec. 3.4 below and Ref. [54]), the laser, although a nonequilibrium element, only influences the density matrix by raising the system's "apparent" energy eigenvalues by $\hbar\omega_L$. As explained in the following section, we can use this fact to develop an effective equilibrium description of the self-organization transition, to which the effects of a nonzero S_κ can later be added as a perturbative correction.

3.4 Effective equilibrium theory

In this section we offer some considerations on self-organization in pumped cavities in general and, in particular, on the quasi-equilibrium character of this transition in the high-finesse limit. The fundamental difference between the zero-temperature and nonequilibrium formalisms is the assumption—valid in the former case—that the initial state (in this case, the ground state) of the system without interactions evolves adiabatically into a pure energy eigenstate (in this case, the ground state) of the interacting system, provided the interactions are switched on sufficiently slowly. This assumption does not, in general, hold away from equilibrium, but there are certain nonequilibrium systems—e.g., an atom pumped by a far-off-resonant laser—for which it does hold: in this example, Fermi's golden rule implies that the laser does not stimulate *real* transitions between the atomic levels unless the laser is resonant with the atomic transition. (For a broadened atomic level, Fermi's golden rule implies that real transitions are negligible as long as the laser-atom detuning, Δ_A, exceeds the linewidth, γ, of the atomic transition.)

In the present case, the excitation gap between the trivial ground state (i.e., the photon-free cavity and a uniform distribution of atoms) and the lowest excited state, which has photons and a λ-periodic atomic density modulation (a "phonon"), consists of two parts: (i) the energy cost $\hbar\Delta_C$ of adding a cavity photon

and (ii) the energy gain due to the photon-phonon coupling, which in second-order perturbation theory would have the form $\{\hbar^2(\Omega g/\Delta_A)^2\}/\{\hbar^2 K_0^2/2M\}$, where $K_0 \equiv 2\pi/\lambda$. Thus the total gap must have the form:

$$\delta = \Delta_C \left\{ 1 - \text{const.} \times \frac{\hbar\zeta}{\hbar^2 K^2/2M} \right\}. \tag{3.31}$$

For the system at hand, the assumption of adiabaticity holds as long as the cavity is of sufficiently high finesse, i.e., $\delta \geq \kappa$. As we shall see in Sec. 3.9, the self-organization transition is weakly discontinuous, and the range of values of the control parameter Ω over which the ordered and disordered phases coexist can be made larger than κ. Under these conditions, the self-organization transition should be well-described by the effective equilibrium theory sketched in Ref. [14]. Only for large values of κ (i.e., bad cavities) would nonequilibrium effects have a chance of playing a leading role. For an alternative construction of such an equilibrium theory, which illustrates the relation between its quantum phase transitions and conventional equilibrium quantum phase transitions, see Sec. 2.5.3.

The assumption of adiabatic switching implies that if interactions are turned on adiabatically in the distant past and turned off adiabatically in the distant future, an initial energy eigenstate would evolve into itself, up to a (physically unimportant) phase factor [35]. This consequence in turn implies that a *single* path integral can capture all the dynamical information; the second path integral in Eq. (3.9), which was demanded by the necessity of summing over all final states, would be superfluous because the final state would be known. In terms of Green functions, this implies that the components G_{+-} and G_{-+} become redundant; indeed, it can be proved directly, in terms of Keldysh diagrammatics [57], that the expansion for G_{++} (and G_{--}) is closed, containing all information about correlations and response.

Formally, the case of nonzero temperatures is less straightforward because the adiabatic switching assumption is not available for mixed states, and therefore the derivation of the imaginary-time Matsubara formalism from the real-time Keldysh formalism is, in general, nontrivial. In this case, we are guided by the following consideration: if the fluctuation-dissipation theorem holds for the *exact* Green functions, the Matsubara formalism is valid; in the present case, we can use the Keldysh diagrammatic technique (see Sec. 3.6) to show that violations of the fluctuation-dissipation theorem are *small*, and hence that the Matsubara technique is approximately valid. This is what one expects on physical grounds: the chief effect of the laser photons is to mediate an effective atom-atom interaction, rather than to cause an energy flux.

Our strategy in the next section, Sec. 3.5, will be to analyze the equilibrium critical behavior of the system at both $T = 0$ and $T \neq 0$, using established results from statistical mechanics and quantum field theory, and neglecting dissipative processes. After that, we shall return to the Keldysh formalism, in Sec. 3.6,

to reinstate the dissipative processes and explore their consequences.

3.5 Quasi-equilibrium Landau-Wilson description

In this section we derive coarse-grained, Landau-Wilson forms of the atom-only action, Eq. (3.28), both for zero and nonzero temperatures, valid in the quasi-equilibrium regime. These Landau-Wilson actions are closely related to the one first introduced by Brazovskii [52]; we exploit this relationship in order to describe the impact of collective fluctuations on self-organization in multimode cavities. Finally, we discuss how the correlations of these fluctuations can be detected via the light emitted from the cavity.

In an effective equilibrium theory, the prescription for going from the Keldysh to the Matsubara or zero-temperature formalisms is to trace, in reverse, the steps one would have taken to go from the equilbrium to the Keldysh formalism: i.e., keep the (++) component of the action and drop the Keldysh indices [4]. It is, furthermore, convenient to reformulate the action in terms of an order parameter, i.e., a quantity that is zero in the uniform phase and nonzero in the self-organized phase. The considerations of Chapter 2 suggest that the appropriate order parameter for detecting crystallization into cavity mode α should be given by

$$\rho_\alpha(t) \equiv \int d^d x \, \rho(\mathbf{x}) \, g_\alpha(\mathbf{x}). \tag{3.32}$$

The details of this procedure are dependent on the cavity geometry; we shall focus in this work on the case of the concentric cavity, as it is the most straightforward case.

3.5.1 Mode structure of the concentric cavity

A concentric cavity can be thought of as consisting of two mirrors that cover antipodal regions of the same sphere. Its mode structure is derived from the solutions of the Helmholtz equation inside the sphere. The effects of the edges of the cavity mirrors can be hard to compute accurately; the standard technique is to solve the Helmholtz problem approximately, by requiring the electric field to vanish at the mirrors' edges. (As with the subsequent approximations that we shall make, this one works best for large cavities.) As the atomic distribution is quasi-two-dimensional, being confined near the equatorial plane, it breaks the spherical symmetry of the cavity, and it is therefore convenient to employ cylindrical coordinates (r, θ, z). Thus, the planar dependence of the cavity modes takes the form $J_m(k_n r)\cos(m\theta)$, where J_m is a Bessel function, m is quantized by the requirement that $\cos(m\theta_0) = 0$ (see Fig. 3.1), and n by the requirement that the field should vanish at the mirrors. The quantization of solutions along the z direction (i.e., the pump laser axis; see Fig. 3.1) yields a third mode index l. For large cavities, modes having a fixed value of $l + m + n$ are

frequency-degenerate. Because, as discussed in Sec. 3.1, the free spectral range of the cavity is larger than the energy scales relevant to self-organization, we can restrict ourselves to cavity modes having a certain fixed value of $\Lambda_0 \equiv l + m + n$.

The atomic density, which is quasi-two-dimensional, can be expanded over a similar set of mode functions, indexed by (m, n), provided one retains all such modes and not just those satisfying $m+n = \Lambda_0$. In addition, the boundary conditions on these mode functions are not in general the same as those on the cavity modes, as the atoms are confined by an external, confining laser field rather than by the cavity mirrors. For sufficiently large traps, however, this distinction is not expected to have important effects, and we shall neglect it.

The cavity modes for which $l = 0$ are expected to be favored for crystallization, as they have the highest amplitude in the equatorial plane of the cavity, to which the atoms are confined. However, as we shall see, modes having $l > 0$ are also of importance in setting the *range* of the effective atom-atom interaction, and thus in determining, e.g., the extent of the fluctuation-dominated regime, as well as the size and stability properties of droplets of the ordered phase.

In the (m, n) basis for the atomic density, the order parameter, Eq. (3.32), is given by ρ_{mn}. Note, also, that provided that the atomic density is spread out over a large number of optical wavelengths, the following asymptotic result holds:

$$\int d\mathbf{x} \prod_i \Xi_{m_i n_i}(\mathbf{x}) \approx \hat{\delta}_{\sum_i m_i} \hat{\delta}_{\sum_i n_i} . \tag{3.33}$$

In this expression, we have introduced the sign-insensitive Kronecker delta $\hat{\delta}_\Sigma m_i \equiv \frac{1}{4} \sum_\pm \delta_{\sum (-1)^\pm m_i}$. Eq. (3.33) is exact for the angular (m) component, and holds approximately for the radial (n) component, if $n > m$; this is the regime of interest because modes for which $m \geq n$ have large diffractive losses and do not couple to the atoms. Eq. (3.33) is closely analogous to momentum conservation, and simplifies the structure of quartic and higher-order terms in the action.

It is useful, at this point, to specialize to two cases. The first addresses an ultracold gas of bosonic atoms, *without contact interactions*, which may or may not be Bose-Einstein condensed. We have dealt with this case, which involves the introduction of an auxiliary field, in some detail in the Supplementary Information of Ref. [14]; we revisit this case below in Sec. 3.5.2. This approach can, in principle, be generalized to the case of an interacting gas (whether Bose-Einstein condensed or not), but is unwieldy for such systems, in which there are non-cavity-mediated interactions, as it involves the introduction of multiple auxiliary fields. Thus, we treat the *second* case of interest, which is that of an interacting Bose-Einstein condensate (BEC) at temperatures well below the condensation temperature, using an alternative approach that does not involve introducing auxiliary fields. Instead, we exploit the off-diagonal long-range order of the BEC and use a correspondingly modified form of the order parameter. In a BEC that is well below its condensation

temperature, the atomic density factorizes to leading order: $\langle\psi^\dagger(\mathbf{r})\,\psi(\mathbf{r}')\rangle \approx \langle\psi^\dagger(\mathbf{r})\rangle\,\langle\psi(\mathbf{r}')\rangle$. It is clear that, at temperatures much lower than the self-organization energy scale $\hbar^2K_0^2/2M$, the low-energy modes—near the self-organization transition—are those corresponding to two widely separated regimes of "momentum" $m+n$, viz. $m+n \approx 0$ and $m+n \approx K_0R/2\pi$. In the case where the system is Bose-condensed, one can use the presence of off-diagonal long-range order to exchange the order parameter, Eq. (3.32), for the condensate amplitude $\langle\psi_{mn}\rangle$—because self-organization then involves the macroscopic occupation of a mode with $m+n = K_0R/2\pi$ [2]. This exchange considerably simplifies the structure of the theory, and makes it possible to treat the effects of both the contact interaction between the atoms and the cavity-mediated interactions between them in a relatively transparent way. The final structure of the theory is, as we shall see, the same in both cases (i.e., the ultracold noninteracting system and the Bose-Einstein condensed interacting system).

3.5.2 Ideal Bose gas

In the ideal-gas case, we proceed as follows. We note that the cavity-mediated interaction term can be written as $\int d\tau \sum_{mn} \zeta_{mn}\rho_{mn}(\tau)\,\rho_{mn}(\tau)$, where ζ_{mn} is the cavity-mediated interaction favoring atomic modulation at wavenumber $(m+n)$. As mentioned in Sec. 3.5.1, the coupling ζ_{mn} is to be considered as being peaked about modes obeying $m+n = K_0R/2\pi$. Next, we perform a Hubbard-Stratonovich transformation, which involves introducing an additional, Gaussian functional integral into the partition function via the identity [55]

$$\exp\left(\int d\tau\,\zeta_{mn}\,\rho_{mn}(\tau)\,\rho_{-mn}(\tau)\right) = \int D\hat{\rho}_{mn}\,\exp\left(-\int d\tau\,\frac{(k_BT)^2}{\hbar^2\zeta_{mn}}\hat{\rho}_{mn}(\tau)\,\hat{\rho}_{mn}(\tau) + 2\frac{k_BT}{\hbar}\rho_{mn}(\tau)\,\hat{\rho}_{mn}(\tau)\right), \tag{3.34}$$

in order to render the action quadratic in the Ψ variables. The partition function can then be rewritten

$$Z = \int D(\Psi^*,\Psi)D\hat{\rho}\,e^{-S'}, \tag{3.35}$$

where S' is given by

$$\begin{aligned} S' &= \int d\tau \int d^dx\,\Psi^*(\mathbf{x},\tau)\left(\partial_\tau - \frac{\hbar\nabla^2}{2M} - \frac{\mu}{\hbar} + 2\sum_{mn}\frac{k_BT}{\hbar}\hat{\rho}_{mn}(\tau)\,\Xi_{mn}(\mathbf{x})\right)\Psi(\mathbf{x},\tau) \\ &\quad + \int d\tau \sum_{mn}\frac{(k_BT)^2}{\hbar^2\zeta_{mn}}\,\hat{\rho}_{mn}(\tau)\,\hat{\rho}_{mn}(\tau). \end{aligned}$$

[2] This is valid so long as the emergent lattice near the transition is too weak to create a Mott insulator.

Provided the laser strength is below the self-organization threshold and the gas is Bose-condensed, the field operators $\Psi(\mathbf{x},\tau)$ can be expressed in terms of condensate and non-condensate parts as $\Psi(\mathbf{x},\tau) = \sqrt{N_0/\mathcal{A}} + \Phi(\mathbf{x},\tau)$, where $N_0(T)$ is the equilibrium condensate fraction at temperature T and $\mathcal{A}$ is the area occupied by the atoms. Transforming the Bose fields to the basis of (m,n) mode functions and Matsubara frequencies, in which the kinetic energy is diagonal, one has $\Psi_{mn}(\omega_\nu) = \sqrt{N_0}\,\delta_{m,0}\,\delta_{n,0}\,\delta_{\nu,0} + \Phi_{mn}(\omega_\nu)$. Integrating out (Φ^*,Φ), one arrives at the action

$$S'' = \frac{1}{2}\mathrm{Tr}\ln(\mathbf{M}) + \frac{k_B T}{\hbar}\sum_{mn\nu}\left[\frac{1}{\zeta_{mn}}\hat{\rho}_{mn\nu}\,\hat{\rho}_{mn-\nu} - N_0\,\hat{\rho}_{mn\nu}\,(\mathbf{M}^{-1})_{mn\nu,m'n'\nu'}\,\hat{\rho}_{m'n'\nu'}\right], \tag{3.36}$$

where the (infinite-dimensional) matrix $\mathbf{M}$ is defined by

$$\mathbf{M}_{mn\nu,m'n'\nu'} \equiv \left[-i\omega_\nu + \frac{\hbar(m+n)^2}{2MR^2}\delta_{mn,m'n'}\right]\delta_{\nu\nu'} + \frac{2k_BT}{\hbar}\sum_{pq\nu''}\hat{\rho}_{pq\nu''}\,\delta_{mm'+p}\,\delta_{nn'+q}\,\delta_{\nu+\nu'',\nu}. \tag{3.37}$$

Below threshold, so that self-organization is not present and $\langle\hat{\rho}_{mn\nu}\rangle = 0$, it is useful to expand $\mathbf{M}$ in powers of $\hat{\rho}$; the quadratic term in the action is then given by

$$\sum_{mn\lambda}\hat{\rho}_{mn\lambda}\,\hat{\rho}_{-mn-\lambda}\left[\frac{k_BT}{\hbar\zeta_{mn}} - \frac{N_0 k_B T}{-i\omega_\lambda + \frac{\hbar^2(m+n)^2}{2MR^2}}\right. \tag{3.38}$$
$$\left. - \frac{(k_BT)^2}{2\hbar^2}\sum_{pq\nu}\frac{1}{\left(i\omega_\nu - \frac{\hbar(p+q)^2}{2MR^2} - \mu\right)\left(-i\omega_\nu - \frac{\hbar(m+n-(p+q))^2}{2MR^2} - \mu\right)}\right].$$

The last term can be usefully rearranged if one recalls that $(k_BT/\hbar)\sum_{mn\nu}(i\omega_\nu - \frac{\hbar(m+n)^2}{2MR^2} - \mu)^{-1} = N - N_0$ for a Bose-Einstein condensate [55]. (This statement also holds for a non-Bose-condensed gas, if one sets $N_0 = 0$.) We now use the fact that the atoms in a Bose-Einstein condensate typically have energies that are small compared with the recoil energy to approximate the last term, and find that at low temperatures the quadratic part of action is then given by

$$\frac{k_BT}{\hbar}\sum_{mn}\hat{\rho}_{mn\nu}\,\hat{\rho}_{-mn-\nu}\left[\frac{1}{\zeta_{mn}} - \frac{N}{-i\omega_\nu + \hbar(m+n)^2/2MR^2}\right], \tag{3.39}$$

in which the vanishing of the coefficient for any (m,n,ν) signals, at the mean-field level, the instability of the gas towards self-organization in the corresponding mode. (Note that self-organization is therefore possible only in the $\nu = 0$ sector.) To enable an analytic treatment of the transition, we replace the (analytically inaccessible) exact form of ζ_{mn} by the convenient approximate form $\zeta_{mn} = \zeta[1 - \chi(m+n-\Lambda_0)^2]$, where

the parameter $1/\chi$ represents the extent to which the coupling to $l \neq 0$ modes is suppressed (see App. A for further discussion of this point). This approximation captures the fact that the coupling of the atoms to the cavity modes is strongest for the modes that obey $m + n = \Lambda_0$ and otherwise simplifies the structure of the theory without making any drastic modifications to it. (For $\chi = \infty$ the $l \neq 0$ modes are entirely suppressed; for $\chi = 0$ the atoms couple equally strongly to all cavity modes, in which case there is no preferred lengthscale for self-organization.)

Continuing with the expansion of $\ln(\mathbf{M})$ and $\mathbf{M}^{-1}$ in powers of $\hat{\rho}$, assembling the two contributions, and retaining the zeroth-order term in a gradient expansion, we arrive at the following form for the quartic-order term:

$$\frac{(k_B T)^2 N}{\hbar^4 K_0^4/4M^2} \sum_{m_i n_i} \hat{\rho}_{m_1 n_1}\, \hat{\rho}_{m_2 n_2}\, \hat{\rho}_{m_3 n_3}\, \hat{\rho}_{m_4 n_4}\, \hat{\delta}_{\sum m_i}\, \hat{\delta}_{\sum n_i}. \tag{3.40}$$

Finally, we make the rescaling $\hat{\rho} \to \hat{\rho}\sqrt{\hbar\zeta/k_B T\chi}$; in terms of these rescaled fields, the action, to quartic order, assumes the following Landau-Wilson form:

$$\begin{aligned} S_{\rm LW} &= \sum_{mn\nu} \left[\frac{1}{\chi} \left(1 - \frac{N\zeta}{\hbar K_0^2/2M} + \frac{i\omega_\nu \zeta N}{(\hbar K_0^2/2M)^2} \right) + (m + n - (K_0 R/2\pi))^2 \right] \hat{\rho}_{mn\nu}\, \hat{\rho}_{-mn-\nu} \\ &+ \frac{\zeta^2 N}{\chi^2 \hbar^2 K_0^4/4M^2} \sum_{m_i n_i \nu_i} \hat{\rho}_{m_1 n_1 \nu_1}\, \hat{\rho}_{m_2 n_2 \nu_2}\, \hat{\rho}_{m_3 n_3 \nu_3}\, \hat{\rho}_{m_4 n_4 \nu_4}\, \delta_{\sum m_i, 0}\, \delta_{\sum \nu_i, 0}\, \delta_{n_1+n_2, n_3+n_4}. \end{aligned} \tag{3.41}$$

If $T > 0$, we can restrict ourselves to the $\nu = 0$ sector of the order-parameter theory, as this is the only sector of the theory that plays an important role for thermal phase transitions. In this case, $S_{\rm LW}$ is an instance of Brazovskii's free energy [52]. We shall return to this "action" (which is, in effect, a free energy rescaled by $k_B T$) and discuss its implications for the character of the self-organization transition in Sec. 3.5.4, after first deriving a closely analogous effective action in the case of the BEC with contact interactions. The case of $T = 0$ requires extending Brazovskii's analysis to *quantum* phase transitions; we discuss this case in Sec. 3.5.6.

3.5.3 Interacting BEC

For the interacting BEC, one begins with $S_{\rm eff}$ [Eq. (3.28)], as in the previous subsection (Sec. 3.5.2), but proceeds differently. It would be inconvenient to apply the auxiliary-field technique to the present case because the action contains three quartic terms, each having a different "momentum"-space structure; decoupling the action would therefore require the introduction of three auxiliary fields. Instead, we exploit the fact that

the "momentum"-space structure of the action simplifies considerably for the low-energy modes, which are the modes of interest because they are the ones that provide the critical fluctuations. This simplification is analogous to that which arises in Fermi-liquid theory owing to the constraint that all low-energy excitations must have momenta that are approximately equal to the Fermi momentum [45]. In the present case, the operative constraint is that all values of $m + n$ must be either approximately zero or approximately $\Lambda_0 \equiv K_0 R/2\pi$. We denote the $m + n \approx 0$ components of the atomic field by ϕ, and the $m + n \approx \Lambda_0$ components by Φ. "Momentum conservation," i.e., Eq. (3.33), then implies that the following kinds of quartic terms are admissible: (i) four ϕ fields; (ii) two ϕ and two Φ fields; and (iii) four Φ fields. (Processes involving three Φ and one ϕ fields are suppressed because at least one of the Φ fields would have to have $m \geq n$, which would imply large diffractive losses [30].) For terms of type (ii), it is clear that the only kinds of processes that survive to arbitrarily low energies are those in which the two Φ's and the two ϕ's have the same values of (m, n). [In principle, terms involving pairs (Φ, ϕ) having the same value of n/m should also survive to arbitrarily low energies, but they can be shown to have negligible phase space, compared with the other terms mentioned.] Similarly, for terms of type (iii), the only sets of (m, n) that survive to arbitrarily low energies are forward- and backward-scattering processes, viz., those for which $(m_1, n_1) = (m_2, n_2)$ and $(m_3, n_3) = (m_4, n_4)$. The other processes are said to be "irrelevant at tree level," [45] because they become progressively less important at lower energies. (This remark ignores subtleties due to nesting.)

Applying the arguments just given to the three quartic terms in $S_{\rm eff}$, we find: (1) that at low energies the mode-mode scattering term S_ξ is irrelevant for ϕ's (except for the term in which two of the incoming momenta are zero), whereas it *does* survive for Φ's; and (2) that the contact repulsion separates into three parts, and can be written as follows (note that all interactions are local in time; for this reason we have suppressed the time arguments):

$$\frac{S_U}{U} = \sum_{m_i n_i} \phi^*_{m_1 n_1} \phi^*_{m_3 n_3} \phi_{m_2 n_2} \phi_{m_4 n_4} \hat{\delta}_{\Sigma m_i} \hat{\delta}_{\Sigma n_i} + \sum_{m_i n_i} \Phi^*_{m_1 n_1} \Phi^*_{m_3 n_3} \Phi_{m_2 n_2} \Phi_{m_4 n_4} \hat{\delta}_{\Sigma m_i} \hat{\delta}_{\Sigma n_i} \tag{3.42}$$

$$+2 \left(\sum_{mn} \phi^*_{mn} \phi_{mn} \right) \left(\sum_{m'n'} \Phi^*_{m'n'} \Phi_{m'n'} \right) + \left(\sum_{mn} \phi^*_{mn} \phi^*_{mn} \right) \left(\sum_{m'n'} \Phi_{m'n'} \Phi_{m'n'} \right) + \text{h.c.} \tag{3.43}$$

As in Eq. (3.33), we have used the sign-insensitive Kronecker delta, $\hat{\delta}_{\Sigma} m_i \equiv \frac{1}{4} \sum_{\pm} \delta_{\sum (-1)^{\pm} m_i}$. We can now integrate out the ϕ modes, provided we first render the action quadratic in these modes; this can be done either by making the Bogoliubov approximation (see, e.g., Ref. [35]) or, more generally, by exploiting the fact (which follows from Goldstone's theorem [55]) that the low-lying modes of a BEC are linearly dispersing phonons. If this is done, the action for the ϕ fields assumes the form

$$S_\phi = \int d\omega \sum_{mn} \sum_{m'n'} \begin{pmatrix} \phi_{\omega mn} & \phi^*_{-\omega mn} \end{pmatrix} \begin{pmatrix} \mathcal{S} & \mathcal{T} \\ \mathcal{T}^* & \mathcal{S}^* \end{pmatrix} \begin{pmatrix} \phi^*_{\omega' m' n'} \\ \phi_{-\omega' m' n'} \end{pmatrix}. \tag{3.44}$$

This form of the action is, strictly speaking, only appropriate for zero-temperature; for $T > 0$ the integral over ω becomes the discrete sum $k_B T \sum_{\omega_\nu}$. For compactness, we shall present only the expressions for $T = 0$, except when the two cases differ substantively. The blocks $\mathcal{S}$ and $\mathcal{T}$ are given as follows [note that both are diagonal in the (m, n) index; the appropriate delta functions have been omitted for compactness]:

$$\mathcal{S}_{mn}(\omega, \omega') = \left[i\omega + \frac{\hbar(m+n)^2}{2MR^2} + Un_0 \right] \delta_{\omega\omega'} + \sum_{m',n'} \left[U + \zeta(m'+m, n'+n) \right] n_{m'n'}(\omega - \omega'), \tag{3.45a}$$

$$\mathcal{T}_{mn}(\omega, \omega') = Un_0 \delta_{-\omega\omega'} + \sum_{m',n'} \left[U + \zeta(m'+m, n'+n) \right] \nu_{m'n'}(-\omega - \omega'), \tag{3.45b}$$

where n_0 denotes the number-density of particles in the condensate, and

$$n_{mn}(\Omega) \equiv \int d\omega \, \Phi^*_{mn}(\Omega + \omega) \, \Phi_{mn}(\omega), \qquad \nu_{mn}(\Omega) \equiv \int d\omega \, \Phi_{mn}(\Omega - \omega) \, \Phi_{mn}(\omega). \tag{3.45c}$$

We now integrate out the ϕ fields to arrive at the following effective action in terms of Φ:

$$S[\Phi, \Phi^*] = \int d\omega \sum_{mn} \begin{pmatrix} \Phi^*_{mn}(\omega) & \Phi_{mn}(-\omega) \end{pmatrix} \times \mathfrak{M}_{mn\omega} \times \begin{pmatrix} \Phi_{mn}(\omega) \\ \Phi^*_{mn}(-\omega) \end{pmatrix} + \cdots, \tag{3.46}$$

where

$$\mathfrak{M}_{mn\omega} \equiv \begin{pmatrix} i\omega + \frac{\hbar(m+n)^2}{2MR^2} + \mathcal{W} + \mathcal{V} & -\mathcal{W} + \mathcal{V} \\ -\mathcal{W} + \mathcal{V} & -i\omega + \frac{\hbar(m+n)^2}{2MR^2} + \mathcal{W} + \mathcal{V} \end{pmatrix} \tag{3.47}$$

$$\mathcal{V}_{mn} \equiv Un_0 - \zeta_{mn} N_0, \tag{3.48a}$$

$$\mathcal{W}_{mn} \equiv U(n - n_0) + \int d\omega \frac{-\zeta_{mn} Un_0}{\omega^2 + U \frac{\hbar(m+n-\Lambda)^2}{2MR^2}}, \tag{3.48b}$$

with N_0 being the total number of particles in the condensate.

This action, Eq. (3.46), can, once again, be addressed by means of a Bogoliubov transformation. Upon performing such a transformation, we find that, for sufficiently low energies, the quadratic term S_2 in the action can be expressed as follows in terms of the *real* field $\widehat{\Phi}(\omega) \equiv \Phi(\omega) + \Phi^*(-\omega)$:

$$S_2 = \int d\omega \sum_{mn} \widehat{\Phi}_{\omega mn} \frac{\tau + \omega^2 + \frac{\hbar K_0^2}{2M}\zeta N \chi (m+n-\Lambda_0)^2}{\hbar K_0^2/2MR^2} \widehat{\Phi}_{-\omega mn}, \tag{3.49}$$

in which χ again represents the coupling to modes having $l > 0$, but the control parameter τ is now given by

$$\tau = \frac{\hbar K_0^2}{2M}\left(\frac{\hbar K_0^2}{2M} + U - \zeta N\right). \tag{3.50}$$

As for the term quartic in Φ, its leading-order gradient expansion is a contact interaction among the $\widehat{\Phi}$'s, proportional to

$$S_4 = \mathfrak{U} \prod_{i=1}^{4} \int d\omega_i \sum_{M_i, N_i} \widehat{\Phi}_{M_i, N_i, \omega_I} \delta_{\Sigma M_i}\, \delta_{\Sigma N_i}\, \delta(\Sigma \omega_i). \tag{3.51}$$

The coefficient $\mathfrak{U}$ accompanying this term receives contributions arising in two ways: (1) from terms in $S_{\rm eff}$ that are quartic in Φ, and (2) via the integrating out of ϕ. In principle, these each give rise to three terms, one associated with each of the quartic terms in the microscopic action, Eq. (3.28). However, owing to the "momentum"-space structure of this action, S_ζ contributes no terms of type (1), and S_ξ contributes no terms of type (2). On the other hand, S_U contributes both types of term. Of these, the term of type (2) is proportional to the above-the-condensate density, which is expected to be small at the relevant temperatures; hence, this term is subleading, compared with the term of type (1). Putting these facts together, we find that the quartic term, Eq. (3.51), has the coefficient

$$\mathfrak{U} = U - \xi N + \frac{\zeta^2 (N - N_0)^2}{U}. \tag{3.52}$$

At nonzero temperatures and near the self-organization transition, the sum over Matsubara frequencies is dominated by the $\omega = 0$ sector; under these circumstances, the action $S_2 + S_4 + \cdots$ [Eq. (3.46)] has the same form as that for the noninteracting case, and they are both variants of the free-energy functional first analyzed by Brazovskii. At $T = 0$, the situation is somewhat different; we shall return to this case in Sec. 3.5.6.

That the actions have the same form is due to the phenomenon of "universality" near phase transitions: the structure of any theory sufficiently close to a critical point depends only on the symmetries of the order parameter and the free energy (or "action"). In the present case, there are two salient features: (1) that there is a strip of degenerate, low-lying atomic density modes around $2\pi(m+n) = K_0 R$; and (2) that terms cubic in the order parameter, which would be allowed by symmetry, are forbidden because they would involve at

least one mode having $m > n$; such modes have high diffractive losses and cannot, therefore, be effectively populated with photons. These constraints are sufficient to force the action to have the above form near the phase transition.

3.5.4 Classical Brazovskii transition

In this section, we briefly outline our adaptation of Brazovskii's self-consistent analysis of the eponymous model [52] to the present setting. Brazovskii's analysis begins with the following free-energy functional in terms of the real order-parameter field $\psi(\mathbf{x})$ and its Fourier-space counterpart $\psi_{\mathbf{k}} \equiv \int d^d x \, \exp(i\mathbf{k}\cdot\mathbf{x})\,\psi(\mathbf{x})$:

$$F = \int d^d k \, \psi_{\mathbf{k}} \left[\mathcal{R} + (|\mathbf{k}| - k_c)^2\right] \psi_{-\mathbf{k}} + \mathcal{U} \int d^d x \, (\psi(\mathbf{x}))^4 \,, \tag{3.53}$$

where the bare phenomenological parameters $\mathcal{R}$ and $\mathcal{U}$ are, respectively, the control parameter for the transition and the interaction parameter. At the mean-field level, F is minimized for $\mathcal{R} > 0$ by the uniform configuration $\psi(\mathbf{x}) = 0$, and for $\mathcal{R} < 0$ by $\psi_{\mathbf{k}}$ having the nonzero value $\sqrt{-\mathcal{R}/2\mathcal{U}}$ for any one of the momenta $\mathbf{k}$ having magnitude k_c.

In order to adapt Brazovskii's analysis to the present case, we must replace all instances of the momenta $\mathbf{k}$ by the sets of positive mode numbers (m, n). In particular, we must replace the expression $(|\mathbf{k}| - k_c)^2$ by $R^{-2}(m+n-\Lambda_0)^2$, where R is the radius of the concentric cavity. Therefore, the low-lying excitations in the present geometry do not lie on a circular or spherical shell in momentum-space, as they do in the original Brazovskii problem; instead, they lie on a linear ribbon along $m + n = \Lambda_0$ in mode-space (see Fig. 3.2). Thus, the low-energy theory is analogous, not to that of a circular Fermi surface, but to that of a *nested* Fermi surface; the presence of nesting does not, however, qualitatively change the Brazovskii effect at weak coupling.

The primary consequence of order-parameter fluctuations, to leading (i.e., one-loop) order, is to renormalize the bare parameters $\mathcal{R}$ and $\mathcal{U}$ in the free energy Eq. (3.53); thus, the fluctuation-corrected free-energy has the same form as Eq. (3.53), but with corrected parameters r and u instead of $\mathcal{R}$ and $\mathcal{U}$ respectively. For the former, one must evaluate the Feynman diagram in Fig. 3.3a; the result is that r is implicitly given by

$$r = \mathcal{R} + \alpha \, K_0 \, \mathcal{U} \, r^{-1/2}, \tag{3.54}$$

in which the coefficient α in the "self-energy" term is a geometrical factor that, in the present case, is approximately given by the expression

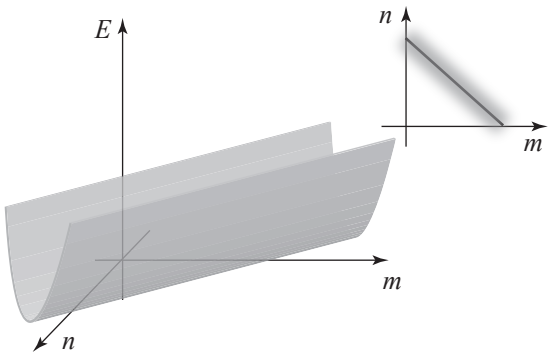

Figure 3.2: Dispersion relation for low-energy atomic excitations, i.e., those that approximately satisfy $2\pi(m+n) = K_0 R$; as discussed in the text, the trough-like form of this dispersion enhances fluctuation effects. The inset shows a "top view" of the dispersion: the black line represents modes at the minimum of the trough, which exactly satisfy $2\pi(m+n) = K_0 R$; self-organization results in the macroscopic occupation of one of these modes.

$$\alpha \approx 4\sqrt{2} n_{\rm modes} \lambda / L, \tag{3.55}$$

with $n_{\rm modes}$ being the number of modes having finesse high enough to be populated. (As one might expect, fluctuation corrections are more important in cavities having a larger number of degenerate modes.) Note that, regardless of the sign of $\mathcal{R}$, the corrected value of r is *positive*; hence the apparent second-order transition out of the disordered state is precluded by fluctuations.

The leading corrections to $\mathcal{U}$ are given, for generic values of m, n, m', n', by Fig. 3.3b. For $(m,n) = (m',n')$ one must also consider the diagrams in Fig. 3.3c. Summing up these series of diagrams, one finds that the corrected value u, for $(m,n) = (m',n')$, is of the form

$$u = \mathcal{U} \frac{1 - (\mathcal{U}/r^{3/2})}{1 + (\mathcal{U}/r^{3/2})}. \tag{3.56}$$

Evidently, u turns negative for sufficiently small r. Naïvely this would mean that the free energy becomes unbounded below; however, perturbative corrections encoded in diagrams such as Fig. 3.3d generate a positive six-point coupling, associated with a coupling denoted as w, which stabilizes the action and gives it the profile with multiple minima shown in Fig. 3.4. This profile for the free energy suggests that any phase transition that the system undergoes is likely to be first-order (i.e., discontinuous).

To determine when the transition becomes energetically favorable *in equilibrium*, one should compare the free energy of the uniform state with that of the possible self-organized states. (We shall revisit this point for the nonequilibrium case in Sec. 3.6.) Let us consider, first, the state in which all the atoms are self-organized in a single mode, so that $\langle \psi_{mn} \rangle = A \, \delta_{m,\tilde{m}} \, \delta_{n,\tilde{n}}$, the coefficient A being the amplitude of the

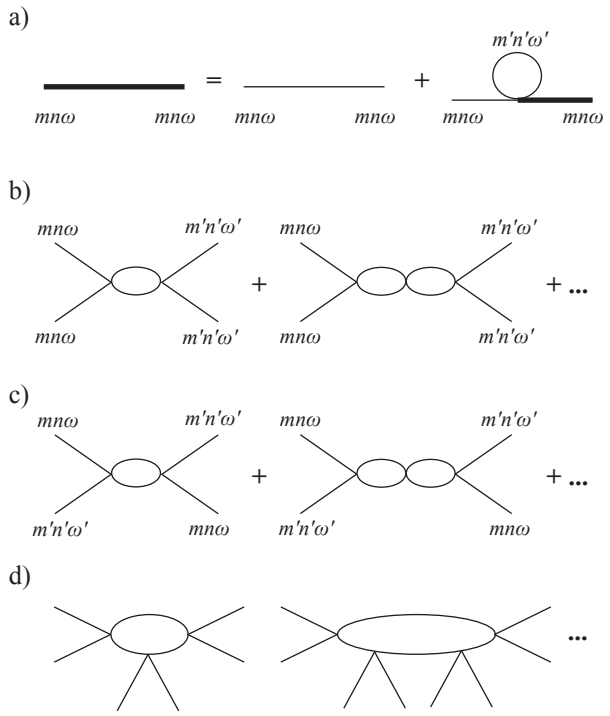

Figure 3.3: (a) Dyson equation for the self-energy at one loop order (i.e., the leading fluctuation correction to r). (b) A geometric series of corrections to the vertex (i.e., to u), which constitute the primary fluctuation corrections for $(m', n', \omega') \neq (m, n, \omega)$. (For the classical case, $\omega' = \omega = 0$.) (c) A geometric series of corrections to u that contribute only when $(m', n', \omega') \approx (m, n, \omega)$. It is these contributions that change the sign of u, thus causing a first-order transition. (d) Higher-order vertices that emerge under coarse-graining.

order parameter. If Φ_0 is the bulk free energy of the disordered state and F_1 that of the ordered state, one can formally write

$$F_1 - F_0 = \int_0^A dA \, \frac{\partial F}{\partial A} = \int dA \sum_{mn} \frac{\delta F}{\delta \psi_{mn}} \frac{\partial \psi_{mn}}{\partial A}. \tag{3.57}$$

The motivation for this rewriting is that $h_{mn} \equiv \delta F / \delta \psi_{mn}$ is the biasing field that would render a certain order-parameter configuration stable. Both the disordered and ordered states are locally stable at zero field; therefore, h should go to zero at both ends but should be nonzero between, so as to "drag" the system from one phase to the other. The advantage of integrating h, as opposed to computing the free energies directly, is that one avoids having to compute terms in the free energy that are the same in both phases. The leading contributions to h can be written as follows:

$$h_{mn} = \frac{1}{6} u A^3 - \frac{1}{2} r A + \frac{1}{2} u A \sum_{mn} \langle \psi_{mn} \psi_{mn} \rangle. \tag{3.58}$$

The last term should, in principle, be computed to the same order as fluctuations have been computed in the disordered state, viz. to one-loop order. At this order there are two diagrams that need to be computed: Fig. 3.3a and Fig. 3.3b. The corrections are substantially different for $(m, n) = (\widetilde{m}, \widetilde{n})$ (i.e., the longitudinal component) and $(m, n) \neq (\widetilde{m}, \widetilde{n})$ (i.e., the transverse, or Brazovskii's anomalous, component). The *longitudinal* corrections have essentially the same form as those we computed in the disordered phase. The *transverse* corrections, however, diverge with system size, as a consequence of the Mermin-Wagner theorem (see the following section). Swift and Hohenberg [58] have shown that *for a finite system* in two spatial dimensions, these corrections are small as long as $K_0 R \leq u^{-2/5}$, a condition that is met for sufficiently weak coupling. Neglecting these contributions, one finds that the free-energy difference between the disordered and ordered states is given by

$$\Delta\Phi = \frac{\alpha}{2}(\sqrt{r_A} - \sqrt{r}) - \frac{1}{2\mathcal{R}}(r_A^2 + r^2), \tag{3.59}$$

where r_A is defined implicitly via

$$r_A = \mathcal{R} + \frac{\alpha \mathcal{U}}{\sqrt{r_A}} + \mathcal{U} A^2 \tag{3.60}$$

and r is given via Eq. (3.54). Solving this pair of equations, one finds that $\Delta\Phi$ changes sign—and the equilibrium phase transition therefore occurs—when $\mathcal{R} \approx -(\alpha \mathcal{U})^{2/3}$.

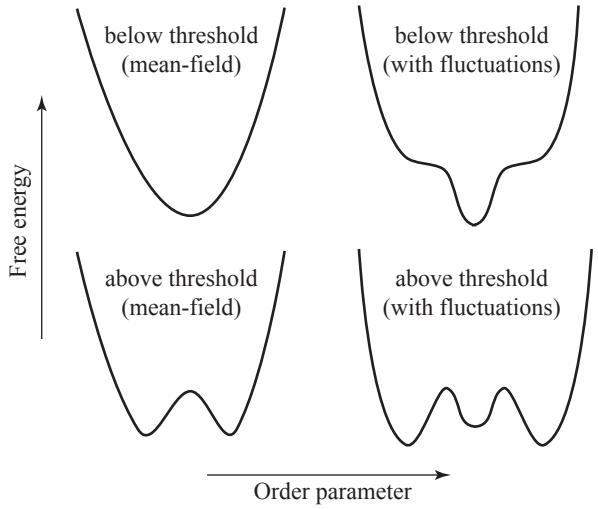

Figure 3.4: Schematic form of the free energy as a function of the order parameter, both above and below threshold, indicating how fluctuations change the character of the phase transition.

3.5.5 Relevance of the Mermin-Wagner theorem

A well-known result in the theory of phase transitions, the Mermin-Wagner theorem (see, e.g., Ref. [59]), states that long-range order is impossible in two dimensions for any thermodynamic system with a continuous symmetry (and short-ranged interactions). This result is a consequence of the large phase space associated with long-wavelength fluctuations of the *direction* of ordering—in the present case, to fluctuations of the phase of the superfluid order parameter and/or the direction of ordering 3.7.1. Therefore, one would not expect an infinitely large sample to exhibit true long-range order at finite temperatures. This result is not, however, particularly relevant to the case at hand, for the following reason. At $T = 0$, the system is effectively three-dimensional rather than two-dimensional, owing to the additional dimension that corresponds to imaginary time; at sufficiently low temperatures, therefore, one expects the distances over which *spatial* fluctuations destroy long-range order to exceed the system size for relatively small systems such as a typical BEC [3]. Even at higher temperatures, one can suppress long-wavelength fluctuations by using a system having multiple layers, so as to increase the effective stiffness against fluctuations of the order parameter.

[3] As in any finite system, the order parameter for the entire system would fluctuate in time; the relevant time scales, however, scale exponentiallywith the number of particles, and are not accessible in realistic experiments.

3.5.6 Quantum Brazovskii transition

The *quantum* case of the Brazovskii transition, which occurs at $T = 0$, differs from the classical case in that the quadratic part S_2 of the action governing it has the form given in Eq. (3.49), viz.,

$$S_2 = \int d\omega \sum_{mn} \widehat{\Phi}_{\omega mn} \left[\mathcal{R} + \omega^2 + \frac{\hbar(m+n-\Lambda_0)^2}{2MR^2} \right] \widehat{\Phi}_{-\omega mn}, \tag{3.61}$$

in which the frequency integration variable ω has been rescaled to absorb certain dimensionful factors. The quartic term in the action, Eq. (3.51), also includes frequency integrals. The presence of these frequency integrals, absent from the classical case, changes the spectrum of fluctuations. Qualitatively, this is because there are now *two* dimensions transverse to the critical surface; therefore, instead of a ribbon of critical modes, one must consider a tube. If one suitably adapts the Brazovskii diagrammatic procedure, one arrives at the following implicit expressions for the fluctuation-corrected parameters:

$$r = \mathcal{R} + [\alpha \mathcal{U} \ln(B/r)], \tag{3.62a}$$

$$u = \mathcal{U} \frac{1 - [\alpha \mathcal{U}/r]}{1 + [\alpha \mathcal{U}/r]}. \tag{3.62b}$$

In these equations, B is a high-energy cutoff (which would be of order Δ_A in the physical system). It is tempting to interpret them as follows: as $\mathcal{R} \to -\infty$, we have that $r \to 0$; therefore, $r \sim B \exp(-|\mathcal{R}|/\alpha\mathcal{U})$, and thus r is always positive, although it does become exponentially small in the $\mathcal{R} \to -\infty$ limit. This would seem to suggest that criticality is not restored at zero temperature. Furthermore, the fluctuation-corrected vertex has the approximate form

$$u \approx \mathcal{U} \frac{B - \alpha\mathcal{U}^2 \exp(|\mathcal{R}|/\alpha\mathcal{U})}{B + \alpha\mathcal{U}^2 \exp(|\mathcal{R}|/\alpha\mathcal{U})}, \tag{3.63}$$

which suggests (cf. Sec. 3.5.4) that metastability should set in when $|\mathcal{R}| = \alpha\mathcal{U} \log(B/\alpha\mathcal{U}^2)$.

As these results are cutoff-dependent, however, one should investigate the quantum Brazovskii action using a more systematic scheme than Brazovskii's, e.g., a renormalization-group scheme such as that developed for the classical Brazovskii problem in Ref. [53]. We describe the appropriate quantum adaptation of this renormalization-group scheme in App. B. The corresponding renormalized values of the various (de-dimensionalized) parameters are shown in Fig. 3.5 as functions of the (de-dimensionalized) bare control parameter $\overline{\mathcal{R}}$. The fact that $\overline{u}$ first becomes negative for a smaller value of $-\overline{\mathcal{R}}$ than the value at which $\overline{r}$ goes to zero indicates that the transition remains first order, and this is one of our main results. This result can, however, be deduced on grounds that are more physically transparent, as we shall now discuss.

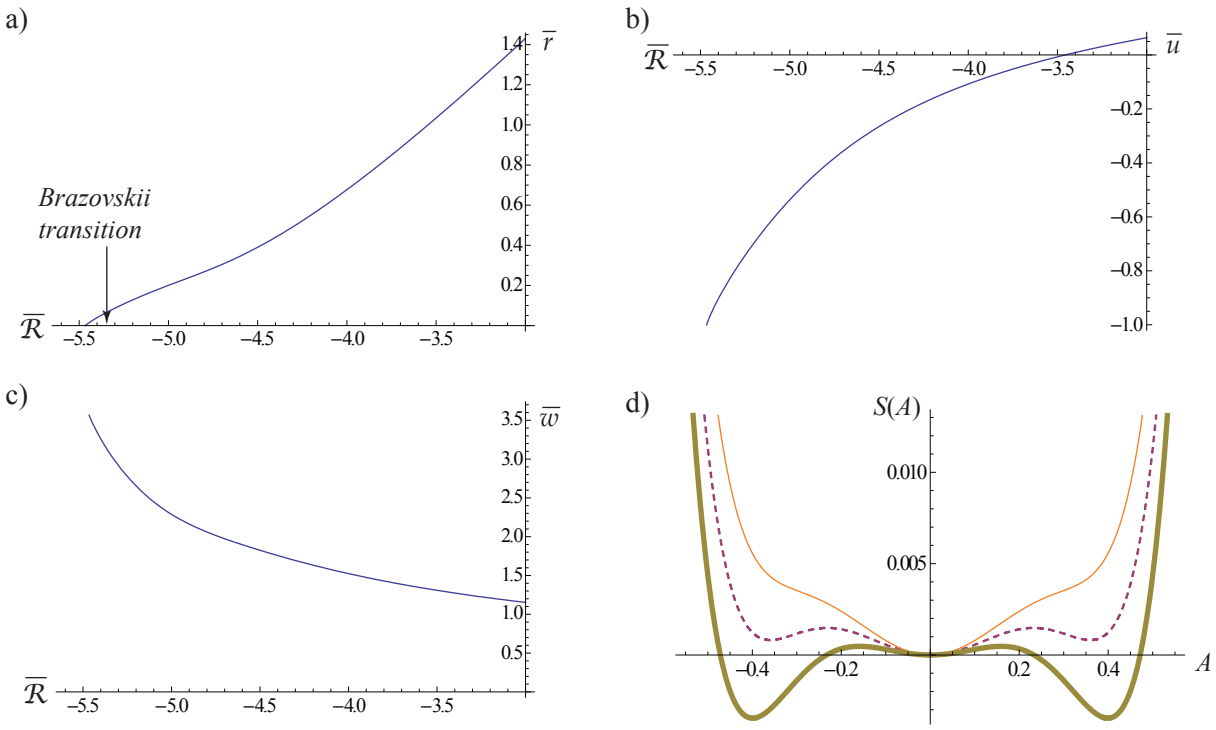

Figure 3.5: (color online) (a)-(c) Dependence of coarse-grained, fluctuation-corrected parameters on the bare control parameter $\mathcal{R}$, which is related to the laser strength, for a fixed value of the bare parameter $\mathcal{U}$. (The bars over the parameters signify that they have been rescaled as described in App. B.) These results are obtained by integrating the renormalization-group equations derived in App. B. Panel (a) shows the flow of the effective "control parameter" $\overline{r}$ (which remains positive). Panel (b) shows the flow of the effective interaction parameter $\overline{u}$, which changes sign as discussed in the text. Panel (c) shows the flow of the emergent six-point coupling $\overline{w}$. Finally, panel (d) plots the free energy as a function of the order parameter A for three values of $\overline{\mathcal{R}}$, viz. -5.3 (thin solid line), -5.35 (dashed line), and -5.4 (thick line). The first-order phase transition takes place at $\overline{\mathcal{R}} \approx -5.36$. These results are interpreted in terms of microscopic parameters in Sec. 3.9.

3.5.7 Analogy with $O(p)$ vector model

(Note that the remarks in this section do not, strictly speaking, apply to the case of a nested surface of low-energy modes; in the nested case, the neglected four-point couplings are not kinematically disallowed. However, the phase space for internal legs is still largest for the forward/back-scattering terms, so that they are the first to change sign.)

At low energies, the only four-point couplings that are relevant, and therefore survive under coarse graining, involve either forward- or back-scattering. Consider order-parameter modes (m, n) that satisfy $2\pi(m+n) = K_0 R$; for these modes the quartic term takes the following form, in which time indices (which follow from locality in time) have been suppressed:

$$\mathcal{U}\left(\sum_{mn} \psi_{mn}\psi_{mn}\right)\left(\sum_{m'n'} \psi_{m'n'}\,\psi_{m'n'}\right)(1+\delta_{m,m'}\,\delta_{n,n'}). \tag{3.64}$$

It is convenient to introduce the notation: $\theta \equiv n/m$ and $\eta \equiv |\Lambda_0 - (m+n)|$, which together provide an alternative labeling of the mode (m, n). In terms of these labels, the action takes the form

$$\begin{aligned} S = &\int d\omega \sum_{\eta\theta} (\mathcal{R} + \omega^2 + \eta^2)\psi_{\eta\theta}\,\psi_{\eta\theta} \\ &+\mathcal{U}\sum_{\eta_i}\left[\sum_{\theta} \psi_{\theta\eta_1}\psi_{\theta\eta_2}\right]\left[\sum_{\theta'} \psi_{\theta'\eta_3}\psi_{\theta'\eta_4}\right](1+\delta_{\theta,\theta'})\delta_{\sum \eta_i,0}. \end{aligned} \tag{3.65}$$

If one had ignored the contribution from terms having four equal values of θ (i.e., the $\delta_{\theta,\theta'}$ term), this action would be an instance of the $O(p)$ model in $(1+1)$ dimensions, with p being the number of cavity modes satisfying the degeneracy condition $2\pi(m+n) = K_0 R$. In the large p limit, terms having $\theta = \theta'$ do not contribute to the renormalization of $\mathcal{R}$: the index θ' (or θ) is summed over in the relevant diagrams, and the single value $\theta = \theta'$ contributes negligibly to this sum. Therefore, the renormalization of r in the present setting should be the same as that in the $O(p)$ model at large p. It is known that in $(1+1)$ dimensions and for $p > 2$, the parameter r is always rendered positive by fluctuations; therefore, criticality is never achieved in the $O(p)$ model, and any phase transition that might occur in the $O(p)$ model—and hence the present model—must be first order. (This remark also applies to the classical Brazovskii case; the absence of criticality does *not* depend on the weak-coupling approximation that Brazovskii's analysis employed, but follows from the low-energy structure of the free energy.)

Unlike the $O(p)$ model, which is isotropic in order-parameter space, the present model *does* undergo a transition (which is first order), owing to the additional contribution to the quartic term involving all four θ's being equal. In order to show that such a transition is feasible free-energetically, one can turn to the

renormalization-group scheme outlined in App. B.

3.5.8 Fluctuation-corrected threshold: summary of results

We now list the fluctuation-corrected values of the threshold for self-organization, for the three cases discussed in previous subsections, in terms of the physically relevant microscopic parameters. In each case, the quantity listed is the fractional change in the threshold pump laser strength, i.e., $(\Omega_{\rm th} - \Omega_{\rm th}^{\rm mf})/\Omega_{\rm th}^{\rm mf}$; for the regimes in which our analysis is valid, this quantity is generally much smaller than unity.

(i) For the ideal gas at $T > 0$, the corrected threshold for the Brazovskii transition is given by

$$\frac{\Omega_{\rm th} - \Omega_{\rm th}^{\rm mf}}{\Omega_{\rm th}^{\rm mf}} \simeq \frac{1}{2}\left[\alpha \frac{K_0^2 R^2}{N\sqrt{\chi}}\right]^{2/3} . \tag{3.66a}$$

This expression is somewhat simpler than that given in Ref. [14] for the *absolute* change in threshold, but is equivalent to it. (In the present expression, we have explicitly included a factor α that is related to the number of cavity modes that couple appreciably to the atoms.) The fluctuation correction can be thought of as consisting of two components: (i) α is a geometric factor, introduced in Eq. (3.55); (ii) the other part of the equation is a measure of the number of particles *per correlation area*, in the sense that (as discussed further in Sec. 3.6.2) the quantity $\sqrt{\chi}/K_0$ is analogous to a (far-from-criticality) correlation length.

(ii) For the interacting BEC at $T > 0$, the shifted threshold is given by

$$\frac{\Omega_{\rm th} - \Omega_{\rm th}^{\rm mf}}{\Omega_{\rm th}^{\rm mf}} \simeq \frac{1}{2}\left[\frac{\alpha}{\sqrt{\chi}} \frac{\{U - \xi N\}\sqrt{k_B T/\hbar}}{(\zeta_{\rm mf} N)^{3/2}} \frac{K_0^2 R^2}{N}\right]^{2/3} . \tag{3.66b}$$

Note that this shift explicitly depends on temperature. At sufficiently low temperatures this shift picks up further corrections, and eventually crosses over to the quantum Brazovskii result discussed in Sec. 3.5.6, which in terms of microscopic parameters becomes

$$\frac{\Omega_{\rm th} - \Omega_{\rm th}^{\rm mf}}{\Omega_{\rm th}^{\rm mf}} \simeq 2.5\left[\frac{\alpha U\sqrt{\hbar^2 K_0^2/2M}}{(\hbar\zeta N\chi)^{3/2}}\right] . \tag{3.66c}$$

In the fourth case (viz., that of an ideal gas at $T = 0$) power-counting suggests that the transition should remain second order, even after cavity-mediated interaction effects are included. We have not discussed this regime in detail in the present paper; we plan to address its properties and achievability in future work.

3.5.9 Signatures of criticality

The Brazovskii transitions, both classical and quantum, being first order, do not exhibit the power-law dependencies (e.g., of the fluctuation correlation length, the order parameter, and its susceptibility) commonly associated with continuous phase transitions. However, as the Brazovskii transitions are only *weakly* first-order (i.e., they involve small discontinuities in the order parameter), the influence of fluctuations on the atomic and optical correlations should be experimentally accessible. In particular, the fluctuation corrections to the density-density correlation function—i.e., Eq. 3.54—should be experimentally detectable in one of two ways. A straightforward way to detect these correlations is to release the atoms from the trap, and analyze the correlations in the noise of the spatial density profile of the atomic system. These correlations can then be related to the density-density correlation functions of interest by means of the scheme described in Ref. [60], which involves the post-processing of absorption images. An alternative approach—unique to the cavity QED setting, and preferable in that it does not automatically destroy the BEC—is through the correlations of the light emitted from the cavity. At weak coupling, the *intracavity*-photon correlations are directly related to the atomic density correlations, as follows. The full action (up to Gaussian order) is of the form $\omega a^\dagger a + (a^\dagger + a)\rho + \rho G \rho$, where G is the atomic correlation function given by Eq. 3.54; one can in principle integrate out ρ, thus arriving at the relation $\langle a^\dagger a \rangle \sim 1/(\omega - G^{-1})$. The fluctuation corrections to G are therefore manifest in the correlations of the emitted light.

The weak-coupling approach, just given, has a serious limitation when it comes to describing *quantum* fluctuations: as discussed in the following section, $\hbar\kappa$ acts, in some ways, as an effective temperature for the atoms in the cavity. Therefore, quantum effects are typically cut off by decoherence on a timescale comparable to $1/\kappa$. However, $1/\kappa$ is also the timescale on which photons leak out of the cavity. It would seem to follow, therefore, that effects associated with coherent, *quantum* fluctuations take place on timescales too rapid to be detected via the leakage of light through the mirrors. This analysis, however, neglects the existence of cavity modes that couple relatively weakly to the atoms (so that they barely affect the effective temperature) and have considerably lower finesse. It is plausible, then, that the correlations of these modes can be used to probe the dynamics of the quantum fluctuations of the remaining degrees of freedom of the system.

3.6 Nonequilibrium effects at the Brazovskii transition

In this section we reinstate the dissipative effects due to the cavity photon leakage rate κ, and consider their impact on the self-organization transition. As we shall discuss, the departure from equilibrium implied by

a nonzero value of κ has three kinds of consequences: (i) it cuts off critical fluctuations, (ii) it affects the timescale on which the system is able to escape from a metastable state, and (iii) it modifies the dispersion of long-wavelength excitations in the ordered state. In this section we consider effects (i) and (ii); our discussion of effect (iii) is postponed to the next section, in which we discuss the properties of the ordered state.

To accomplish this reinstatement, we follow the standard prescription for expressing an effective equilibrium action in the nonequilibrium formalism (see, e.g., Sec. 4.7 of Ref. [4]) and then augment the theory with the term S_κ in Eq. (3.28). Thus we arrive at a theory containing a copy of the equilibrium Brazovskii action involving fields on the $\pm$ contours, coupled to one another via S_κ, the consequences of which we shall now address using perturbation theory.

3.6.1 Critical effects

In this section we focus on the case of the interacting BEC at zero temperature (cf. Sec. 3.5.6), as the analysis is most transparent for this case. We begin with the dissipative term,

$$\begin{aligned} S_\kappa &= \int \frac{d\omega}{(\omega-\Delta_C)^2+\kappa^2} \int d^dx\, d^dx'\, g_\alpha(\mathbf{x})\, g_\alpha(\mathbf{x}') \\ &\quad \times i\zeta\kappa\Delta_C \coth(\hbar\kappa/k_BT)\, n_1(\mathbf{x}\omega)\, n_1(\mathbf{x}\omega), \end{aligned} \tag{3.67}$$

and re-express the atomic field Ψ in terms of the condensate and non-condensed parts, as follows:

$$\Psi_c(\mathbf{x}) = \sqrt{N_0} + \Phi_c(\mathbf{x}), \tag{3.68}$$

$$\Psi_q(\mathbf{x}) = \Phi_q(\mathbf{x}). \tag{3.69}$$

In terms of this decomposition, the primary quadratic contribution to the complete action arising from S_κ then becomes

$$\begin{aligned} i\frac{\zeta N\Delta_C\kappa}{\Delta_C^2+\kappa^2} \sum_{mn} \int d\omega \Big(& 2\Phi^*_{\omega mn,q}\, \Phi_{\omega mn,q} \\ & + \Phi^*_{\omega mn,q}\, \Phi^*_{-\omega mn,q} + \Phi_{\omega mn,q}\, \Phi_{-\omega mn,q} \Big). \end{aligned} \tag{3.70}$$

The most salient feature of this term is that its prefactor is frequency-independent. For a system to be at a *quantum* critical point, it is necessary that the prefactor vanish as $\omega \to 0$ (see, e.g., Ref. [61] and our App. C). When—as in the present case—this condition fails, the collective dynamics on sufficiently long

timescales is classical. Indeed, the term Eq. (3.70) is formally identical to the term

$$ik_B T \int d\omega \, \Phi^*_{\omega,q} \, \Phi_{\omega,q} \tag{3.71}$$

that arises for an otherwise isolated complex field Φ coupled to an equilibrium thermal environment that is at temperature T [see, e.g., Eq. (66) of Ref. [4]]; one can therefore regard the coefficient $\hbar\tilde{\kappa}/k_B \equiv \hbar\kappa\zeta N/(\Delta_C k_B)$ in Eq. (3.70) as an effective system temperature. In particular, quantum correlations on timescales longer than $1/\tilde{\kappa}$ are washed out by the decoherence arising via the leakage of photons from the cavity: this effect is analogous to the decoherence due to a *finite temperature* that is known to occur near to a quantum critical point.

This point is—in principle—immaterial, as interaction effects preclude criticality regardless of the value of κ (as a consequence of Brazovskii's argument); however, at $T = 0$ the fluctuation-corrected equilibrium control parameter is exponentially small, behaving as $\exp\big(-|\mathcal{R}|/\alpha\mathcal{U}\big)$, and therefore it should be possible to tune the system close enough to criticality that the nonequilibrium suppression of criticality due to dissipation is observable.

We now turn to the issue of influence of the nonequilibrium terms given in Eq. (3.70) on the effective quartic *interaction* vertex. At tree-level, the interaction vertex only couples terms having Keldysh indices *cqqq* or *cccq*. However, the nonequilibrium terms generate an effective *ccqq* vertex, via the Feynman diagrams shown in Fig. 3.6. This vertex brings the factor

$$\tilde{u} \equiv \left(\frac{\kappa\zeta N}{\Delta_C} u\right)^2, \tag{3.72}$$

in which u is the fluctuation-corrected equilibrium vertex (see Sec. 3.5.4). The most notable feature of this vertex is that it does *not* change sign when u does. In the regime considered in the present work, we have that $\kappa \ll \Delta_C$, and hence $\tilde{u}$ provides a subdominant correction to u, and therefore cannot prevent the net vertex from changing sign, signaling a first-order transition. It is possible, however, that in the opposite regime, in which $\kappa \gg \Delta_C$, this correction term would dominate; in this regime, this term might be capable of preventing the Brazovskii transition from taking place at all.

3.6.2 Nucleation and state selection

In this section we address the dynamics of the emergence of self-organization associated with the Brazovskii transitions, classical and quantal. As these transitions are first order, one expects them to exhibit regions of two-phase coexistence, in which some parts of the cloud have self-organized and others have not. The time

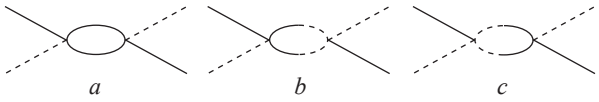

Figure 3.6: Contributions to the nonequilibrium vertex having external indices *ccqq*. For an introduction to the Keldysh diagrammatic notation see Ref. [4].

interval that the system takes to approach the steady state, in which the entire system is self-organized, depends on the energetics of critical droplets of the minority phase, which determines their nucleation rate. There are three regimes of interest, distinguished by the primary mechanism responsible for fluctuations: (i) near zero temperature in an isolated system (i.e., in the regime where both the system temperature and $\tilde{\kappa}$ are smaller than U), quantum tunneling is the primary cause of nucleation; (ii) at temperatures that are high compared with U, in an essentially isolated system ($k_B T \gg \tilde{\kappa}$), it is thermal activation that is the primary cause; and (iii) near zero temperature in the far-from-equilibrium regime (i.e., when $\tilde{\kappa}$ exceeds the temperature and U), nucleation is primarily triggered by extrinsic force noise that originates with fluctuations in the photon population in the cavity. Owing to the formal analogy between $\tilde{\kappa}$ and T, discussed in Sec. 3.6.1 and App. C, cases (ii) and (iii) can be treated by similar means.

In all three cases, an essential ingredient is the energy barrier for thermal (or quantal) nucleation. In many settings this would be easy to read off from the tree-level (i.e., mean-field) Landau free energy (or action); however, in the case at hand, the Landau free energy *does not* predict a first-order transition at tree level. On the other hand, it is not *prima facie* legitimate to use the *fluctuation-corrected* free energy that was calculated above, as this incorporates fluctuations on *all* length scales, including those larger than the droplet itself. In general, therefore, one must follow a procedure like that due to Hohenberg and Swift [53], in which only fluctuations on length-scales smaller than the droplet diameter are self-consistently integrated out.

Motivated by the wish to obtain analytical results, we focus, in the present work, on nucleation kinetics in the regime in which the corrected free energies of the self-organized and uniform phases are sufficiently similar that the critical droplet size is comparable to the system size. In this regime, the error incurred by using the fully renormalized bulk free energy is expected to be relatively small (as, in this case, most of the renormalizations should already have taken place), and one can legitimately use the fully renormalized parameters computed in Secs. 3.5.4 and 3.5.6.

Classical nucleation

In the classical case, one needs to compute the free-energy barrier to the nucleation of a critical droplet, i.e., the smallest possible droplet intrinsically capable of growing until it encompasses the entire cloud. The standard procedure for doing this is to identify appropriate saddle-point configurations of the effective free energy. As these saddle-point configurations involve droplets of the ordered phase immersed in the uniform phase, one is interested in spatially varying configurations $\Phi(\mathbf{x})$, and the position coordinates are therefore the appropriate ones to consider. In these coordinates, the Euler-Lagrange equation corresponding to the Brazovskii free energy takes the approximate form:

$$\xi_0^4(\nabla^2 + K_0^2)^2\Phi(\mathbf{x}) + [r - 2|u||\Phi(\mathbf{x})|^2 + 3w|\Phi(\mathbf{x})|^4]\Phi(\mathbf{x}) = 0, \tag{3.73}$$

in which $\xi_0 \sim \sqrt{\chi}/K_0$ is an effective healing length for the crystalline order parameter. In order to find the saddle-point configuration, we look for solutions of the Euler-Lagrange equation that obey the boundary conditions that $\Phi = 0$ near the edge of the cloud and $\Phi(\mathbf{x}) = A\,\Xi_{\tilde{m}\tilde{n}}(\mathbf{x})$ near the middle of the cloud, where $A = \pm\sqrt{(2u + \sqrt{4u^2 - 12rw})/6w}$ is the value of the order parameter in the ordered state, and $(\tilde{m}, \tilde{n})$ is the mode into which the atoms are self-organized. In the *conventional* Brazovskii problem, the difference in energy between a configuration including a droplet of area $\mathcal{A}$ and the uniform state is given by

$$F_{\rm drop} = (F_0 - F_A)\mathcal{A} + \sigma_\perp L_\perp + \sigma_\parallel L_\parallel, \tag{3.74}$$

in which F_0 $(= 0)$ and F_A are, respectively, the free energy densities of the uniform and self-organized states; $\sigma_\perp$ $(\sigma_\parallel)$ is the energy cost of an interface perpendicular (parallel) to the lamellæ; and $L_\perp$ $(L_\parallel)$ is the length of the interface that lies perpendicular (parallel) to the lamellæ. The concentric-cavity geometry differs from that considered in Ref. [53] in that it is not translationally invariant in its radial direction: both the atomic density and the mode functions depend on $\mathbf{x}$ and so, therefore, do the parameters in the Brazovskii model. As our purpose in the present section is to focus on order-of-magnitude estimates, we shall neglect this complication. A further difference between the present case and the conventional Brazovskii problem is that the modes are checkerboard-shaped rather than lamellar (see Ref. [14], and also Sec. 3.7.1). Thus, a generic interface has some aspects of both transverse and longitudinal character, and the optimal droplet shape varies from mode to mode. In what follows, we focus on the (physically most relevant) modes for which $m \ll n$, and consider droplets of the form sketched in Fig. 3.7.

Returning to Eq. (3.74), we see that the free-energy difference per unit area, ΔF is of order

$$\Delta F \approx -\frac{r_c - r}{r_c}\frac{u^3}{27w^2}, \tag{3.75}$$

in which r_c is the value of the control parameter at which the equilibrium transition occurs. As argued in Ref. [53], the *width* of a longitudinal interface is approximately $\xi_0(K_0\xi_0/2r)$, whereas that of a transverse interface is ξ_0. Near the phase transition, $r \approx (\alpha\mathcal{U})^{2/3}$, which is small relative to $K_0\xi_0$ for weak coupling $\mathcal{U}$; hence, longitudinal interfaces are larger than transverse ones. Furthermore, the interface energy cost per unit area is given by the interface width multiplied by the quantity $f_0 = u^3/(27w^2)$, which is related to the curvature of the free-energy landscape about the minimum corresponding to the self-organized state. Thus, the total interface energy cost is given by the expression

$$\frac{u^3}{27w^2}\xi_0\left(L_\perp + \frac{K_0\xi_0}{2r}L_\parallel\right). \tag{3.76}$$

Because transverse interfaces cost less energy at weak coupling, the optimal droplet shape is needle-like, as shown in Fig. 3.7.

To determine the free-energy barrier for droplet nucleation, we use the well-known Wulff construction (see, e.g., Ref. [62]); in the present case, this amounts to considering bubbles of dimension $\propto \sigma_\parallel$ in the *perpendicular* direction and $\propto \sigma_\perp$ in the *parallel* direction. Thus, the free energy of a configuration including a droplet is:

$$F_{\rm drop} = \gamma\xi_0^2\frac{K_0\xi_0}{2r}\left(-\gamma\,\frac{r_c - r}{r_c} + 2\right)\frac{u^3}{27w^2}, \tag{3.77}$$

where γ is a variational parameter that sets the overall scale of the droplet. By minimizing $F_{\rm drop}$ with respect to γ, we see that the critical bubble is that for which $\gamma = r_c/(r_c - r)$; thus, the free-energy barrier for the thermal nucleation of droplets of the ordered state is

$$F_{\rm drop} = \Delta F\xi_0^2\frac{K_0\xi_0}{2r}. \tag{3.78}$$

The nucleation rate follows directly, being given by $r\exp(-F_{\rm drop}/k_BT)$ or, in the case that nucleation is due to external noise [i.e., case (iii)], by $r\exp(-F_{\rm drop}/\hbar\tilde{\kappa})$. For a discussion of the relevant experimental parameters, see Sec. 3.9.

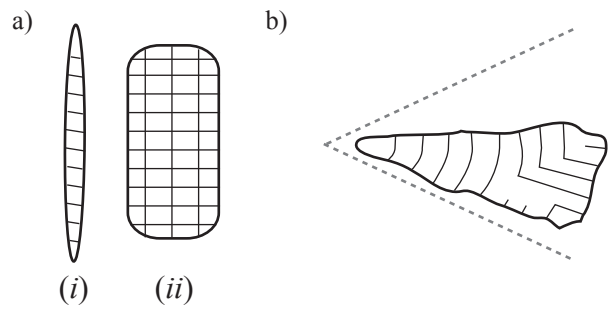

Figure 3.7: (a) Wulff droplets, corresponding to the TEM_{00} mode (i), and to a higher-order mode (ii), respectively. The droplets should become less anisotropic (i.e., less "needle-like") for higher-order modes; it is, however, possible that the optimal droplets in these cases have more complicated shapes. (b) Defected droplets, which are favored for $r \approx r_c$, as discussed in the text. For these, the energetic cost of introducing defects inside the droplet is outweighed by the increase in the fraction of the interface that is transverse.

Qualitative features of the defect morphology

Near coexistence (i.e., for $r \approx r_c$), the critical droplet is arbitrarily large and—even for a highly anisotropic droplet—the energetic cost of the longitudinal interface (which scales linearly with bubble size) becomes greater than that of introducing localized defects, arranged so that the surface of the bubble is made as transverse as can be. A possible arrangement of such defects is shown in Fig. 3.7. It was argued in Ref. [53] that such defects are energetically favorable only for $|(\mathcal{R}-\mathcal{R}_c)/\mathcal{R}_c| \leq (U/\zeta N)^{10/27}$, which is a narrow range compared with the thermal-fluctuation-dominated regime, which obtains for $|(\mathcal{R}-\mathcal{R}_c)/\mathcal{R}_c| \leq 1$.

Quantum tunneling

In the case of quantum tunneling rather than thermal barrier crossing, the argument of Sec. 3.6.2 must be modified in two ways. First, the expression for the tunneling rate should be given by the form $\omega_0 \exp(-S_0)$, where ω_0 is a characteristic collective frequency (e.g., being proportional to the value of the renormalized control parameter r in the disordered phase) and S_0 is the appropriate instanton action (see, e.g., Ref. [55]). A crude approximation to S_0 is the product of the width (which is of order A) and height of the energy barrier; thus the difference between the initial and final values of the order parameter would act as an effective inverse temperature. Second, one must use the coarse-grained values of r, u, and w from the *quantum* rather than the classical model, i.e., from Sec. 3.5.6 rather than Sec. 3.5.4.

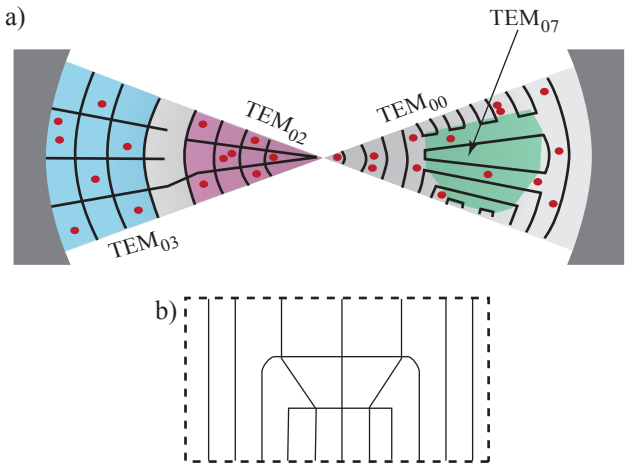

Figure 3.8: (color online) Elementary excitations of the self-organized state in the concentric cavity. (a) Domains that have self-organized into distinct modes can be separated by analogs of grain boundaries (left half of panel) or by continuous textures (right half of panel). (b) Excitations that are analogous to the splay mode in smectic-A liquid crystals (see Sec. 3.7.2). Lines indicate nodes of the cavity electromagnetic field. The curved wavefronts along the radial direction have been drawn as flat lines to emphasize that the sketched feature is small-scale, relative to the size of the cavity.

3.7 Properties of the crystalline state

In this section we examine various properties of the crystalline state exhibited by the coupled atom-light system, including its basic structure, elementary excitations, and topological defects.

3.7.1 Basic properties

Concentric cavity

Soft condensed matter systems that undergo the Brazovskii transition commonly exhibit one-dimensional, lamellar patterns. The present realization does not, owing to the influence of boundary conditions on the optical mode structure, and therefore on the possibilities for atomic crystallization. Instead, in the concentric cavity, the ordered states follow the two-dimensional optical mode patterns, which may be visualized as distorted checkerboard patterns, as shown in Fig. 3.8. Locally, the atomic density selects amongst the cavity modes by crystallizing into the "odd or even squares" of the selected mode (cf. Fig. 3.8 and the discussion in Chapter 2). In physical realizations, the corresponding states of crystallization would not be exactly degenerate, as optical modes having stronger angular variation (i.e., larger m) are of lower finesse; on the other hand, repulsive interactions have a stronger impact on atoms that are crystallizing into modes of lower m. Such effects can readily be accounted for within our model, via the introduction of fictitious fields that would bias the system towards crystallizing into certain modes. In practice, the most straightforward way

to include such effects is by adding the terms

$$S_{\text{fict}} = \sum_{mn} h_{mn}\, \rho_{mn}^2 \tag{3.79}$$

to the Brazovskii action, which would raise (or lower) the threshold laser power in a mode-dependent way.

Other multimode cavities

A well-known example of a multimode cavity is the confocal cavity, in which all the even TEM modes are degenerate [30]. (It is also possible to make multimode cavities in which every p^{th} TEM mode is degenerate.) These cavities have the practical advantage over the concentric cavity that their stability criteria are easier to fulfill (e.g., their mode structures are more robust with respect to mirror misalignment). To the extent that it is legitimate to think of such cavities as each having a continuous family of degenerate modes (i.e., provided they possess a large number of modes that are both degenerate and not heavily suppressed by diffractive losses), the self-organization transition in these cavities should belong to Brazovskii's universality class, and our analysis of the transition itself should extend to these models. Where confocal cavities are likely to differ from concentric ones is in the geometry of the ordered states and of their defects, which is much more involved in the confocal case because of its less-evident symmetry structure.

A feature common to most multimode geometries is that it is possible to tune the system across the point at which the modes are degenerate by gradually changing the mirror spacing. Thus, one can explore the crossover between the multimode physics discussed in the present work and the single-mode physics realized in Ref. [23].

3.7.2 Phonons and nonequilibrium elasticity

Manifestly, the concentric cavity geometry does not possess translational invariance in the radial direction; hence, there are no translational Goldstone modes in the radial direction. The geometry that we have primarily considered in this paper does not possess translational invariance in the angular direction either, because of the hard-wall boundary conditions that we imposed on the mode functions at the edge of the cavity, when computing the mode structure (see Sec. 3.5.1). For the usual experimental situation, in which the cavity mirrors cover a relatively small solid angle, this is the relevant case. In the opposite regime, in which each cavity mirror occupies most of a hemisphere, one *would* essentially recover translational invariance in the angular direction; concomitantly, there would be phonons, corresponding to the "rippled" atomic arrangement shown in Fig. 3.9. For large cavities, such excitations would have a linear, phononlike spectrum, with a speed of sound related to the order parameter for crystallinity.

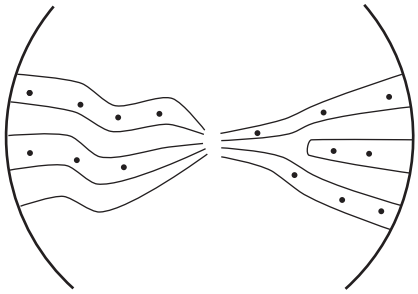

Figure 3.9: Case of the large-solid-angle concentric cavity, in which the atom-light system possesses a continuous symmetry associated with the relative phase between the $+m$ and $-m$ components of each mode function. This symmetry, when broken by the self-organized atomic cloud, leads to the existence of both phonon excitations (shown in the left panel of the figure) and true edge dislocations (shown in the right panel of the figure).

The concentric cavity geometry does, however, possess an analog of *rotational* invariance, in that the energy is unchanged if one reorganizes the crystallization of atoms in mode (m, n) into crystallization in a degenerate mode (m', n'). For a large cavity, having many modes, this symmetry is effectively continuous. Consequently, there are low-energy excitations involving the gradual variation of m and n across the cavity; an example of such an excitation is sketched in Fig. 3.8. The physics of these layer-wandering excitations is analogous to that of the splay mode of smectic liquid crystals [59]; as in the liquid-crystal case, the effective elastic energy for these excitations takes the Landau-Peierls form:

$$F_{\rm el} = K_1 \int d^2x \, (\nabla_\perp^2 \theta)^2 + \cdots \,, \tag{3.80}$$

where θ ($\equiv n/m$) parametrizes the macroscopically occupied mode, and the ellipses indicate terms involving higher powers of the gradient operator. Near the transition, the wandering rigidity K_1 is proportional to the square of the equilibrium order parameter and also to the fourth power of the healing length ξ_0 in Eq. (3.73).

We note in passing that the nonequilibrium character of the phase transition affects the spectrum of phonon and wandering excitations at very long wavelengths. For example, the effective retarded Green function for phonons, which in general has the form

$$G_R(\omega, m, n) \approx \frac{1}{\omega^2 - K_{\rm eff}(m+n)^2 + 2i\omega\tilde{\kappa}} \,, \tag{3.81}$$

has purely imaginary poles when $\sqrt{K_{\rm eff}}(m+n) \leq \tilde{\kappa}$; modes satisfying this criterion are diffusive rather than propagating. This idea, which was discussed in Refs. [63, 42] in the context of excitonic condensates, has nontrivial consequences for, e.g., the spatio-temporal decay of correlations in sufficiently large systems.

3.7.3 Defects

In addition to the low-energy splay excitations (which are analogous, in some ways, to phonons), the ordered state can also have gapped excitations or defects, which in the present case are analogous to grain boundaries (see left panel of Fig. 3.8). When the ordered states on the two sides of such a boundary are of opposite parity, as in the figure, the boundary wipes out a fraction of a row of crystalline order. Its energetic cost is therefore approximately $L\sigma_\perp$, where L is the length of the boundary and $\sigma_\perp$ is the interface energy discussed in Sec. 3.6.2. These defects are analogous to conventional topological defects in the sense that, for certain configurations of the order parameter at the boundary of some region in the cavity (e.g., at the edges of the cavity), the system is forced to have at least one defect somewhere inside this region. These defects are not, however, directly related to the existence of continuously broken symmetries in the system.

Other kinds of topological defects might also be realizable. For instance, in the large-solid-angle case discussed above in Sec. 3.7.2, genuine edge dislocations, of the kind illustrated in Fig. 3.9, may arise. Another possibility is a *texture* of the kind sketched in the right-hand panel of Fig. 3.8: such a texture would be analogous to a closed lamella in the conventional Brazovskii case. It is not clear, however, that such textures are experimentally *feasible*, as they would require that the system self-organize into a high-m mode in some region of the cavity.

3.8 Supersolid aspects of the self-organized state

The spatially ordered state of a BEC in a multimode cavity is a "supersolid" in the following sense. It possesses emergent forms of both crystalline and superfluid order: i.e., it spontaneously breaks two *continuous* symmetries, the rotational invariance of space (to the extent that the cavity admits an effectively continuous family of modes) and the $U(1)$ invariance associated with the phase of the condensate wavefunction. The properties, and even the existence, of supersolids have recently been active issues in condensed-matter research [47, 46, 1, 49, 64]. Amongst traditional condensed-matter systems, the primary candidate for exhibiting supersolidity is solid ^{4}He, which was conjectured to have a supersolid phase in the late 1960s [65, 66]. Shortly thereafter, Leggett [67] predicted that a supersolid would exhibit "nonclassical rotational inertia" when rotated sufficiently slowly, owing to the quantization of angular momentum of a rotating superfluid. Evidence for this phenomenon was reported in Ref. [1]; the interpretation of this and subsequent experiments is, however, still controversial. It has been proposed, for instance, that rather than indicating bulk supersolidity, the missing moment of inertia arises because of superfluidity in dislocation cores [47, 46], because of elastic effects arising from the presence of ^{3}He impurities [48], as a by-product of glassiness [49],

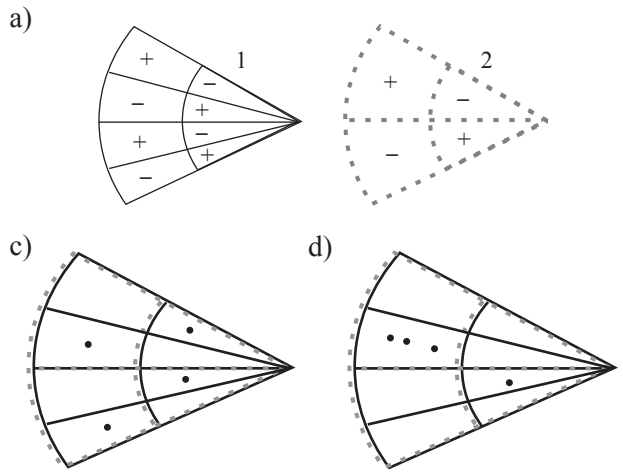

Figure 3.10: Proposed scheme for detecting supersolid order. (a) Profiles of two cavity modes: Mode 1 (into which the atoms self-organize) and Mode 2 (which can be used to detect phase coherence, as discussed in Sec. 3.8). The two modes are degenerate; Mode 2 possesses more nodes along the z direction (i.e., perpendicular to the plane of the figure). The $\pm$ signs describe the phases of the electromagnetic fields in the two modes relative to some reference (e.g., the pump laser) in various regions of the cavity. (b) Atomic configuration in which the atoms emit constructively into Mode 1 and destructively into Mode 2. In the insulating phase, this is the typical configuration, as the number of atoms per site is fixed; hence, there is suppressed emission into Mode 2. (c) Atomic configuration in which the atoms emit constructively into both Mode 1 and Mode 2. Such configurations, which involve multiple occupancy, occur in the superfluid phase but are suppressed in the insulating phase; hence, the amount of light emitted into Mode 2 is a measure of superfluidity.

and so on.

One must distinguish between two types of questions regarding supersolids: (i) whether solid ^{4}He, or any other neutral substance having "realistic" interparticle interactions, is supersolid in the sense defined above, and (ii) what properties a supersolid would possess, should one exist. In the condensed-matter context, attempts to address question (ii) have been vitiated by the uncertainty about whether the substance being studied is in fact supersolid, whereas attempts to address question (i) have been hampered by imperfect understanding of the characteristic phenomenology of supersolids. The advantage of ultracold atomic realizations of supersolidity, such as the present one, is that one can explore question (ii) without first addressing question (i), as the existence of both superfluid and crystalline order is relatively easy to establish. The existence of *crystallinity* can be deduced via the superradiant emission of light (see Sec. 3.5.9), whereas that of superfluidity may be explored using a range of standard techniques (see, e.g., Ref. [23]).

Furthermore, it is in principle possible in the present setting to test for supersolidity in a manner that enables one to distinguish between scenarios in which the *bulk* of the sample is a supersolid, and those that involve phase separation of some kind—e.g., scenarios in which BEC is restricted to, e.g., dislocation lines. This can be accomplished via an analysis of the spatial correlations of the light emitted from the cavity. Such a technique is an adaptation of that developed by Ref. [68] to explore the superfluid-insulator transition in an optical lattice. It uses the fact that the number of particles per site is not fixed in a superfluid; therefore, even if the emission into a particular cavity mode is zero on average because of destructive interference between the contributions from even and odd sites, local atomic number fluctuations would render this destructive interference imperfect and would lead to a nonzero photon population, which can be detected in the light leaking out of the cavity. This idea is sketched in Fig. 3.10; for calculational details, we refer to Ref. [68].

3.8.1 Coupling the superfluid order parameter to the solid order parameter

A well-known manifestation of supersolidity is the nonclassical behavior of the the moment of inertia [67], which results from the requirement that the macroscopic wavefunction be single valued. This effect can be explored directly in the present setting, e.g., by imparting angular momentum to the BEC via an auxiliary laser beam that carries orbital angular momentum. Furthermore, one can study the implications of the presence of crystalline order for the superfluid transition [69] by increasing the density of the atomic cloud in the cavity until it undergoes Bose-Einstein condensation. A third possibility is to displace the superfluid from the center of the overall dipole trap and observe its relaxation [70]; this should provide information about the coupling between the Anderson-Bogoliubov mode of the superfluid and the excitations (both phononlike and topological) of the crystal. In particular, it should be possible to tune the cavity geometry

across a multimode geometry by adjusting the mirror spacing, as discussed in Sec. 3.7.1, thus altering the spectrum of crystalline excitations.

It should be emphasized that all these experiments depend crucially on the cavity's being a *multimode* one, and on the broken spatial symmetry being at least approximately continuous. In a single-mode cavity, in which the broken symmetry is of the discrete (i.e., even/odd) type (and, moreover, the interactions are effectively infinite-ranged), the "solidity" is of a different kind; in particular, there can be neither Goldstone modes nor topological defects in the solid.

3.8.2 Supersolid-"Mott" transition

As discussed in, e.g., Ref. [67], the "normal solid" state that competes with a supersolid is analogous to a Mott insulator with regard to its transport properties. In the setting of self-organized atom-light crystals, for laser intensities well above threshold one expects the emergent lattice potential to be sufficiently deep to cause the supersolid state to have undergone a transition into a nonsuperfluid state. This state can be either a Mott insulating state (which would be a normal solid) or a Bose glass state (which, too, would have many of the properties of a normal solid, particularly a non-quantized moment of inertia). The latter possibility arises even in the absence of extrinsic disorder because vacancies and dislocations in the self-organized lattice might dynamically generate disorder. The Mott insulator state (which is incompressible) and Bose glass state (which is compressible) should be distinguishable via, e.g., their large-scale spatial density profiles.

The BEC-to-Mott transition has recently been addressed—for the case of a single-mode cavity—in Ref. [71]. The case of the concentric cavity has several features in common with the single-mode cavity case; there is, however, one key difference, which follows from the difference in the character of the self-organization transitions in these two cases. Consider the phase diagram in terms of the two physically adjustable parameters, viz., the pump laser strength Ω (or, equivalently, the effective coupling constant ζ) and the scattering length of the atoms, a (which can be tuned, e.g., by approaching a Feshbach resonance). In the case of a *single-mode* cavity, the self-organization transition is continuous; therefore, by tuning the laser to sufficiently near threshold, the emergent lattice depth can be made arbitrarily small. Accordingly, regardless of how large the scattering length might be, there is always a region in which the self-organized lattice is *too* shallow to support a Mott insulator. Put differently, there is always a region of the supersolid phase between the liquid (i.e., the uniform BEC) and the normal solid. By contrast, self-organization in a *concentric* cavity occurs by means of a first-order, Brazovskii transition. The emergent lattice depth therefore jumps discontinuously to some nonzero value at the self-organization transition; if this minimum lattice depth is greater than that required to support a Mott insulator, it is possible to have a *direct* liquid-to-Mott

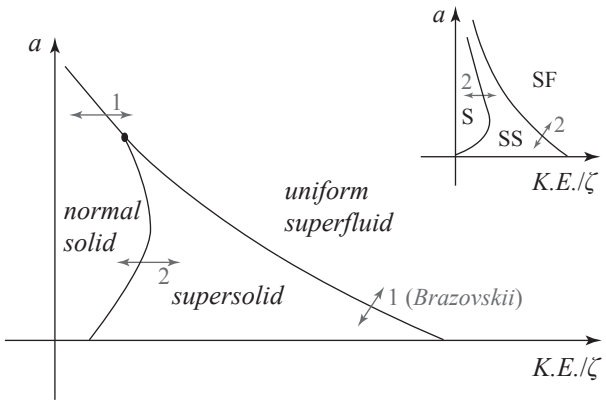

Figure 3.11: Schematic zero-temperature (i.e., quantum) phase diagram for a BEC in a concentric cavity, with the control parameters being the atomic scattering length a and the inverse effective atom-cavity coupling ζ^{-1} (or equivalently the inverse laser intensity Ω^{-2}). For weak, repulsive interactions, the superfluid first undergoes self-organization via the Brazovskii transition, thus forming a supersolid. If the laser intensity is increased further, the supersolid undergoes a transition into a normal solid (i.e., a Mott insulator). However, for strong, repulsive interactions, the uniform BEC can lose phase coherence concurrently with the first-order self-organization transition. This situation is to be contrasted with that for the case of a single-mode cavity (inset), in which there should always be a supersolid (SS) region separating the uniform fluid (SF) and normal solid (S) regions. First- and second-order transitions are marked (1) and (2) respectively.

transition, without an intermediate supersolid phase. The phase structure of our atom-cavity system that results from the foregoing considerations is summarized in the schematic phase diagram shown in Fig. 3.11. Curiously, it has the same morphology as that predicted for the corresponding liquid-to-solid transitions of ^{4}He [72] (but with temperature and pressure serving as the control parameters in the ^{4}He case).

3.9 Experimental feasibility

In this section we discuss typical parameter values for which the Brazovskii transition, and the resulting self-organized state, should be observable in a *multimode* cavity. Recently, the self-organization transition was observed in a *single-mode* cavity using Bose-Einstein-condensed ^{87}Rb atoms. The cavity was characterized by the cavity QED parameters $(g, \kappa, \gamma) = 2\pi \times (10, 1, 3)$ MHz; and the pump laser was detuned from the atomic resonance by $\Delta_A \approx 2\pi \times 10^{13}$ Hz [23]. An appreciable photon population was observed in the cavity for Δ_C up to $2\pi \times 40$ MHz. For these parameters, the mean-field value of the self-organization threshold $\Omega_{\rm mf}$ is approximately $2\pi \times 2$ GHz. For a concentric cavity having these parameters, the range in frequency space of the fluctuation-dominated regime for the *classical* self-organization transition is approximately $2\pi \times (2 - 20)$ MHz. (The precise value depends on the healing-length parameter χ, but only as $\chi^{-1/3}$; hence these results are not very sensitive to the choice of χ.) As previously noted [14], this range is greater than

the frequency width associated either with spontaneous decay or with the intensity-noise of a typical laser (converted to frequency units). For the *quantum* transition, the fluctuation-dominated regime (for ^{87}Rb at unit filling far from a Feshbach resonance) would be of order $0.1 - 1$ MHz; the width of this regime can, however, be extended by tuning the interparticle interaction through a Feshbach resonance.

The nucleation rates, both thermal and quantal, can be expressed—for the case of the interacting system—as $U \exp[-\mathfrak{K}(\Omega_{\rm th} - \Omega_{\rm th}^{\rm mf})/(\Omega - \Omega_{\rm th})]$. In this expression, Ω is the pump laser strength and $\mathfrak{K}$ is a number of order unity; the expression is only valid when the exponent exceeds unity, i.e., for Ω sufficiently near $\Omega_{\rm th}$. For U far from a Feshbach resonance, this expression implies that, for the regime discussed in this work, in which nucleation proceeds via the formation of large, well-defined droplets, the average nucleation timescale should typically exceed the lifetime of the experiment (discussed in the next paragraph). It might therefore prove necessary to enhance U by means of a Feshbach resonance in order to explore the physics of nucleation. Note that this does not imply that the self-organized state is *inaccessible* away from a Feshbach resonance: rather, one expects that the laser strength would have to be increased (decreased) well past threshold before the system entered (left) the self-organized state. In other words, the process of self-organization should exhibit significant hysteresis.

For the experimental parameters just given, Baumann et al. [23] found that the lifetime of the self-organized BEC (i.e., the timescale on which atom loss destroys the BEC) was approximately 10 ms. For detunings $\Delta_C > \kappa$, atom loss is largely due to spontaneous scattering, which occurs at a rate R_γ proportional to $\gamma\Omega^2/\Delta_A^2$. The corresponding timescale is long enough to enable the observation of the family of phenomena discussed in the present work. In order to perform a similar experiment with cavities in the *weak*-coupling regime (i.e., for smaller g), one would have to ensure that the spontaneous decay rate R_γ stays below 1 kHz. This would involve satisfying two conditions: $g^2 N/\Delta_C > 10^3$ and $\kappa \ll \Delta_C$. One could do so by increasing the number of atoms in the BEC or by increasing the finesse of the cavity mirrors (which would reduce κ).

3.10 Systems of coupled layers and the origins of frustration

We have discussed how an equilibrium atomic cloud, confined by the pump laser to a plane near the equatorial plane of the cavity, spontaneously crystallizes globally into one of a family of degenerate quasi-checkerboard arrangements. Now let us consider an atomic cloud confined to a single plane *away* from the equator of the cavity. In this case, spontaneous crystallization still occurs but, as we shall now explain, the particular checkerboard arrangement into which the atoms crystallize varies *statically* across the plane—energetics demands, e.g., that the center and edge of the cloud crystallize in distinct arrangements. This is a consequence

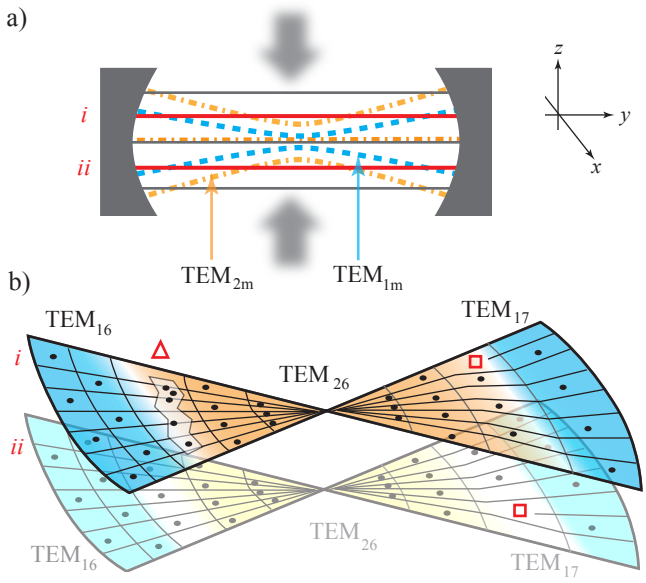

Figure 3.12: (color online) Schematic illustration of the implications of frustration. Atoms are loaded into sheets (i) and (ii), shown as thick lines in panel (a), which are an integer number of pump-laser wavelengths apart. The dashed and dashed-dotted curves are, respectively, antinodal regions of the modes TEM_{1m}, which have low intensity near the centers of sheets (i) and (ii), and TEM_{2m}, which have low intensity away from the centers of sheets (i) and (ii). Near the center of each sheet, atoms crystallize into the TEM_{2m} modes; away from the center, they crystallize into the $\mathrm{TEM}_{1m'}$ modes. Within a sheet, regions may be separated by faults in the ordering, as illustrated in panel (b). For example, on the left side the fault has the form of a discommensuration (see Sec. 3.10). By contrast, the fault on the right side is a grain boundary. Between layers, the opposing parity of adjacent modes leads to frustration, which precludes ordering, as in the regions indicated by a $\triangle$ and a $\square$. Grain boundaries (denoted by $\square$) are more localized faults, and are therefore less costly, energetically, than discommensurations ($\triangle$).

of *frustration*: satisfying local energetic preferences introduces "fault zones" between locally ordered regions.

In our analysis of equatorial-plane atomic distributions (see Fig. 3.8), we were able to focus on the family of degenerate modes TEM_{lm} having $l = 0$. To generalize our analysis beyond the equatorial plane, we must consider all modes that meet the degeneracy condition $l + m + n = K_0 R$. Consider the situation illustrated in Fig. 3.12a, first focusing on the non-equatorial sheet marked (i). Near the center of this sheet, crystallization into modes with $l = 1$ is suppressed because such modes have low intensity, whereas crystallization into $l = 2$ modes is favored because they have maximal intensity; away from the center, the opposite is true. The change in l forces a change in m or n, owing to the degeneracy condition, so the mode functions in the sheet must change across an interfacial zone between the $l = 1$ and $l = 2$ favored regions. Therefore, either a dislocation, associated with a change in m, or an abrupt change in lattice periodicity (i.e., a discommensuration), associated with a change in n, is expected. (This picture assumes that, as is always the case near threshold, the self-organized lattice is not strong enough to trap the entire atomic distribution at the center or the edge of the sheet. The kinetic energy cost of localization, as well as the cost in repulsive

energy, will act to spread the atomic cloud out.)

Now consider a situation in which two symmetrically disposed sheets on opposite sides of the equator are populated with atoms, as in sheets (i) and (ii) of Fig. 3.12. Atoms in sheet (i) and those in sheet (ii) are coupled via the cavity modes. Because $l = 2$ ($l = 1$) mode functions are symmetric (antisymmetric) about the equatorial plane, the atoms in the $l = 2$ ($l = 1$) arrangement in sheet (ii) occupy the same (opposite) checkerboard as those in sheet (i). If there are no dislocations, atoms in the interfacial zone remain disordered, because it is impossible for the atoms to satisfy both desiderata [or, equivalently, because the corresponding cavity modes interfere destructively in sheet (i) and constructively in sheet (ii)]. The introduction of dislocations enables the system to order in part of the interfacial zone, as shown in the right hand side of Fig. 3.12b, and is therefore preferred.

The full many-layer, many-mode system is expected to experience the same kinds of disordering effects as the idealization sketched above: i.e., one expects systems slightly above threshold to develop locally crystalline phases separated by zones riddled with faults.

3.11 Summary

In this chapter, we have shown that the self-organization of BECs in multimode cavities is accompanied by a host of effects, such as fluctuation-driven nonequilibrium first-order transitions (both classical and quantum), topological defects, rigidity, frustration, and supersolidity. We have developed both a nonequilibrium formalism for exploring such systems in general, and an effective equilibrium description valid in the regime of greatest interest, viz., the quantum phase transition undergone by a Bose-Einstein condensate. We have outlined, moreover, how these formalisms may be used to compute the correlation functions of the photons emitted from the cavity, as well as those of the atoms, and how such correlations may be detected experimentally. Finally, we have indicated realistic values of experimental parameters that might be used to realize self-organization and its attendant phenomenology in the laboratory.

Chapter 4

Spins in cavities: associative memories and glassy phases

a frozen swarm
of incommensurate wishes

— Rae Armantrout, "Closer"

In the previous two chapters we explored the physics of mobile, typically Bose-condensed, atoms trapped inside a cavity; we argued that the atoms arrange themselves into crystals, and potentially glasses, when the cavity is driven by a sufficiently strong laser. In the present chapter, we turn our attention from atoms to *spins*: i.e., instead of considering a cloud of mobile spinless atoms, we consider atoms that are frozen in place at random positions inside a cavity, but have internal degrees of freedom ("spins") that can fluctuate in their "orientation." As remarked in the Introduction, one expects the natural analog of crystallization in this setting to be *antiferromagnetism*. As we show, an antiferromagnetic state does indeed arise when the spins are coupled to a *single-mode* cavity: in the ground state, the spins at even antinodes all point one way, whereas those at the odd antinodes point in the opposite direction. However, in the case of a multimode cavity with more than ~ 0.1 modes per spin, one can show that the preferred ground state is in fact a *spin glass*.

We begin this chapter by motivating the study of frustrated spin models with cavity-mediated interactions, and then describe a scheme using three-level Λ atoms that allows the realization of such spin models. We show that the effective spin Hamiltonian realized in this way is a variant of that studied in Refs. [73, 74, 75, 76]. By adapting the results of Refs. [74, 76], we show that, depending on the number of spins per strongly-coupled cavity mode, the low-temperature phase is either a spin glass or a superradiant phase [26, 32, 23] (analogous to a cavity-mediated crystal [14, 15]); we discuss how these phases can be distinguished experimentally. In contrast with condensed-matter realizations, the systems considered here allow one to access both regimes in the same system, by changing the mirror spacing and thereby tuning the number of active cavity modes [30]. We note, moreover, that for *quantum* spins, the effective Hamiltonian can be mapped onto a Bose-Hubbard model possessing strictly off-diagonal disorder [77]. Unlike the

diagonally disordered Bose-Hubbard model [78, 79], the off-diagonally disordered version exhibits multiple distinct insulating phases, including a Mott glass phase and a random-singlet glass phase [77, 80, 81], neither of which has been experimentally observed so far. Finally, we discuss how the spin glass phase can be experimentally detected, sketch the results of a related study by Strack and Sachdev [82] of the quantum spin glass phase in a cavity, and discuss the possible consequences of dissipation on the spin glass transition and phase, noting an analogy with polariton condensation.

The following sections, up to but not including Sec. 4.6.2, are based on the text of the following publication: Sarang Gopalakrishnan, Benjamin L. Lev, and Paul M. Goldbart, Phys. Rev. Lett. 107, 277201 (2011). Copyright (2011) by the American Physical Society. Note that in this chapter and the following chapter, we have adopted units in which $\hbar = 1$.

4.1 Motivation

Realizing models of magnetic phenomena and exploring their phases has been a central objective in ultracold atomic physics since the advent of optical lattices [10]. Such models (e.g., the Hubbard and Heisenberg models) have been of long-standing theoretical interest as they are believed to offer minimal descriptions of strongly correlated materials [83]. Unlike real materials, ultracold atomic systems offer the prospect of realizing the theoretical models essentially *exactly*; because many of the models are not solvable, it is hoped that ultracold-atomic realizations will shed light on their properties. The central effort to realize magnetism, to date, has focused on the fermionic Hubbard model [84]; however, its magnetic ordering temperature is too low to be readily achievable in current experiments. These difficulties have stimulated an interest in alternative paths to quantum magnetism [85, 86, 87], of which the present work is an example.

We introduce a scheme for realizing magnetism—involving Λ-type three-level atoms [see Fig. 4.1(a)] trapped in a multimode optical cavity—that differs from previous schemes in an essential respect, viz. the range and structure of interactions. Whereas previous schemes have involved contact or dipolar interactions [87], the spin-spin interactions in our scheme, being mediated by cavity modes, are both *long-ranged* (indeed, infinite-ranged for a single-mode cavity) and *oscillatory* in sign. In these respects, they resemble the Ruderman-Kittel-Kasuya-Yosida (RKKY) interaction [88], which underlies, e.g., the physics of heavy-fermion materials [89] and metallic spin glasses [90, 76]. The present work is concerned chiefly with the latter class of systems, and, in particular, with the fact that long-range, sign-changing interactions between spins facilitate the realization of various frustrated and bond-disordered models. (Analogous realizations have also been proposed, e.g., in photonic band-gap systems [91] and Coulomb crystals [92].)

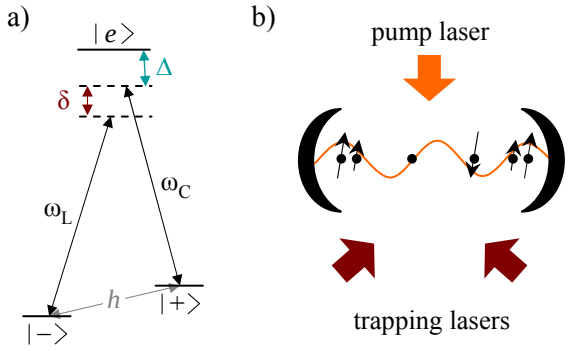

Figure 4.1: (a) Level structure of three-level Λ atoms, dressed by a pump laser at frequency ω_L, cavity mode(s) at frequency ω_C, and a microwave field represented by h. The detuning from two-photon resonance, δ, is assumed to be much smaller than the detuning of laser and cavity photons from the atomic transition, Δ. (b) Proposed experimental setup. Atoms are tightly trapped by trapping lasers, which are far detuned from the atomic transition, and pumped transversely. Spins are self-organized as discussed in the text for a single-mode cavity, with a sinusoidal mode function as depicted: spins at even antinodes interact ferromagnetically with spins at other even antinodes, but antiferromagnetically with spins at odd antinodes. Spin-spin interactions are strongest for spins trapped at antinodes; therefore, ordering is strongest at antinodes and weakest at nodes.

4.2 Model

We consider Λ-type atoms whose lower levels (which will be our two spin states, $|+\rangle$ and $|-\rangle$) are separated by a microwave transition whereas the excited level, $|e\rangle$, is separated from both by an optical transition. The $|\pm\rangle$ states are assumed to be tightly confined at the intensity extrema of trapping lasers that are far detuned from the $|\pm\rangle \to |e\rangle$ transition; i.e., the atomic positional degrees of freedom are assumed to be frozen out. (Thus, the physics considered here differs from that of *mobile* spinful atoms [93, 94, 95].) Disorder can be introduced using diffusers (see, e.g., Ref. [79]). The atoms are confined in an optical cavity having multiple degenerate modes, at a frequency red-detuned from the $|+\rangle \to |e\rangle$ transition by $\Delta \sim 1$ GHz; other modes are typically farther-detuned (e.g., by ~ 15 GHz for a 1 cm cavity). Additionally, the atoms interact with a pump laser oriented *transverse* to the cavity axis, red-detuned from the $|-\rangle \to |e\rangle$ transition by $\Delta + \delta$, where $\delta \simeq 10$ MHz is the detuning from two-photon resonance. (Note that the aforementioned setup generalizes to systems possessing manifolds of ground and excited atomic states, rather than two ground states and one excited state, provided that—as in dysprosium [12]—the two manifolds have similar g-factors.) The microwave $|+\rangle \leftrightarrow |-\rangle$ transition is driven at a weak Rabi frequency that, as we shall see, acts as an effective magnetic field.

Under these conditions, the spin-spin interactions can be understood as follows: an atom in the $|-\rangle$ state can scatter a laser photon into a cavity mode, thus changing its state to $|+\rangle$; this virtual cavity photon, being δ higher in energy than laser photons, is reabsorbed into the laser after a time $\sim 1/\delta$. The reabsorption

involves flipping the state of a $|+\rangle$ atom (typically a different one from the initial atom) to $|-\rangle$. This entire process generates an effective interaction of the form $M(\mathbf{x}_i, \mathbf{x}_j)\sigma_+^i\sigma_-^j/(\Delta^2\delta)$ between two atoms, where $\mathbf{x}_i$ is the position of the i^{th} atom and M is a matrix element (derived below) depending on the cavity mode(s).

We further assume that the cavity photon leakage rate per mode, $\kappa \ll \delta$, and also that the atomic-excited-state decay rate, $\gamma \ll \Delta$. In this "*dispersive*" regime, the conservative virtual-excitation processes fall off as $1/\delta$ and $1/\Delta$ respectively, whereas the dissipative processes fall off as κ/δ^2 and γ/Δ^2 respectively. As argued in Ref. [15], the effect of dissipation in this regime can be understood in terms of heating, and need not be explicitly included in the Hamiltonian. Generally, dissipation does not change the mean-field properties even beyond this regime [41]; we shall revisit this issue in future work. (Note that a weak microwave field must be applied to prevent the spin population from being pumped entirely into the $|+\rangle$ state; however, this field is comparable in strength to the decay processes, and thus much weaker, for small κ/δ, than the interaction terms.) Thus, we neglect, in this work, issues such as the nonequilibrium growth of entanglement [96].

Hence, upon *adiabatic elimination* [31, 15] of the state $|e\rangle$, the Hamiltonian $\mathcal{H}$ of the atom-light system takes the form

$$\mathcal{H} = H_{\text{at}} + \sum\nolimits_{\alpha} \omega_\alpha a_\alpha^\dagger a_\alpha + \frac{\Omega}{\Delta} \sum_{\alpha,i=1}^{N} g_\alpha(\mathbf{x}_i)\sigma_-^i a_\alpha^\dagger + \text{h.c.}, \tag{4.1}$$

where ω_α is the frequency of cavity mode α; a_α destroys a cavity photon; Ω is the strength (i.e., Rabi frequency) of the pump laser; $g_\alpha(\mathrm{x}_i)$ describes the coupling to mode α at the position $\mathbf{x}_i$ of atom i; and the σ operators are Pauli matrices acting on the atomic ground-state manifold. One can rewrite the coupling $g_\alpha(\mathrm{x}_i)$ as $g\Xi_\alpha(\mathbf{x}_i)$, where g is an overall coupling strength (assumed to be the same for all strongly-coupled modes) and $\Xi_\alpha(\mathbf{x}_i)$ a normalized mode profile. The terms in $H_{\text{at}} = \sum_i (h_x\sigma_x^i + h_z\sigma_z^i)$ represent transitions that do not involve the cavity, and are due to the $|+\rangle \leftrightarrow |-\rangle$ microwave driving: h_x is the microwave Rabi frequency, h_z is the detuning, and σ^i are the Pauli matrices for atom i. In what follows we refer to these terms as "fields." Note that the model described above, while similar in some ways to the multimode Dicke model [97], differs from it in the crucial respect that, in the present case, the different modes have *distinct spatial profiles*; it is this feature, not present in the multimode Dicke model, that enables frustration to be realized.

We now proceed to eliminate the cavity modes perturbatively, thus arriving at an effective model for the spins, valid on timescales $\geq 2\pi/\delta$:

$$H = H_{\text{at}} + \sum_{\alpha;i<j} \frac{|\Omega(\mathbf{x}_i)|^2}{\Delta^2} \frac{g_\alpha(\mathbf{x}_i)g_\alpha^*(\mathbf{x}_j)}{\delta} \sigma_+^i\sigma_-^j + \text{h.c.} \tag{4.2}$$

(Note that this result can also be derived from nonequilibrium field theory, as in the spinless case [15].)

Higher-order terms

The ellipses in Eq. (4.2) represent terms that do not involve the pump laser. Of these, the leading term is a "refractive-index" term of the form $(g^2/\Delta)\sum_{\alpha,i}\Xi_\alpha(\mathbf{x}_i)^2 S_i^z$, which acts as an effective magnetic field (and stems from the shift in the cavity resonance frequency because of the presence of atoms in the cavity); one can compensate this field by choosing the microwave driving frequency appropriately. The next-to-leading term, however, can generate spin-spin interactions, and takes the following form:

$$\begin{aligned} H_2 \quad \sim \quad & \frac{g^4}{\Delta^2\delta}\sum_{\alpha\neq\beta,i\neq j}\Xi_\alpha(\mathbf{x}_i)\Xi_\beta(\mathbf{x}_j)\Xi_\alpha(\mathbf{x}_j)\Xi_\beta(\mathbf{x}_i)S_i^z S_j^z \\ & +(\alpha\leftrightarrow\beta) \end{aligned} \tag{4.3}$$

Thus, this term generates an Ising-type spin-spin interaction, which could in principle compete with the term in Eq. (4.6). As with the $\lambda/2$-periodic potential discussed in Sec. 2.4.1, this Ising-type term is negligible in the regime of large detuning and/or weak ordering, which we have focused on; in the regime of small detunings, this term is likely to complicate the phase diagram derived here.

4.3 Analysis of effective Hamiltonian

4.3.1 Single-mode case

In what follows we denote the effective spin-spin coupling as $\zeta \equiv |g\Omega|^2/(\Delta^2\delta)$. Thus, e.g., for atoms in a single-mode cavity for which $\Xi_\alpha(x)\sim\cos(kx)$, the zero-field Hamiltonian is

$$H_{1-\text{mode}} = \frac{1}{2}\zeta\left(\sum\nolimits_i \cos(kx_i)\sigma_+^i\right)\left(\sum\nolimits_j \cos(kx_j)\sigma_-^j\right) + \text{h.c.} \tag{4.4}$$

Because the interaction term can be rewritten as $\sigma_i\cdot\sigma_j \equiv \sigma_x^i\sigma_x^j+\sigma_y^i\sigma_y^j$, the system possesses an $O(2)$ symmetry (as the repumping field is negligible). The cavity-mediated interaction is *ferromagnetic* for atoms λ apart, but *antiferromagnetic* for atoms $\lambda/2$ apart; therefore, the low-temperature ordered state involves all spins at even antinodes aligned along some direction θ on the equator of the Bloch sphere defined by $|\pm\rangle$, and all atoms at the odd antinodes aligned along $\theta+\pi$. The interactions, though disordered (as their *magnitude* is position-dependent), are not frustrated in this case. Note that spin-ordering leads to a macroscopic photon population in the cavity mode, as in the self-organization of an atomic cloud [26, 31, 14, 15]—put differently,

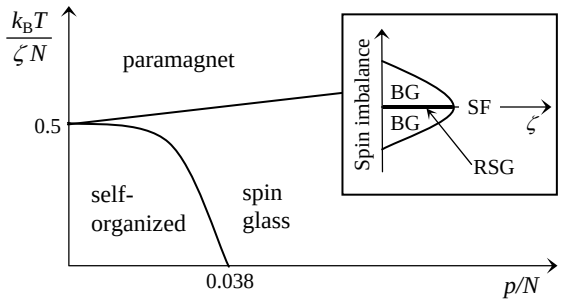

Figure 4.2: Phase diagram of frustrated spin systems in cavities, as a function of the temperature (vertical axis) and ratio of number of modes, p, to number of atoms, N. Inset: schematic quantum phase diagram for an off-diagonally disordered XY model, as a function of hopping (i.e., cavity-mediated interaction strength) and spin imbalance, showing SF ("superfluid," i.e., magnetically ordered), BG (Bose glass), and RSG (random-singlet glass) phases discussed in the text.

magnetism is a self-organization of atomic spins rather than positions. (This can be seen, e.g., by replacing the σ operators in Eq. (4.1) by their expectation values.) In the driven, dissipative system (with $h_x, \kappa \neq 0$) such macroscopic occupation corresponds to superradiance.

4.3.2 Multimode Case

We now turn to multimode cavities, in which the interactions do not factorize as in $H_{1-\mathrm{mode}}$. The simplest case is the ring cavity, which supports two degenerate modes $\Xi_{\pm}(x) \sim e^{\pm ikx}$. In this case the interaction term takes the translation-invariant form

$$H_{\mathrm{ring}} = -\zeta \sum_{i<j} \cos[k(x_i - x_j)]\, \sigma_i \cdot \sigma_j. \tag{4.5}$$

Note that Eq. (4.5) is precisely Eq. (1) of Ref. [76], which approximately describes the RKKY interaction in materials (such as $\mathrm{Y}_x\mathrm{Gd}_{1-x}$) having spin susceptibilities peaked at a single momentum. While this interaction leads to frustration for Ising spins, it does not for XY spins; instead, the ground state is a spin spiral of pitch λ [75, 76].

To realize frustration using XY spins, one must progress to cavity geometries possessing many degenerate modes, such as confocal and concentric cavities [30]. The general Hamiltonian for these is:

$$H_{\mathrm{mm}} = -\zeta \sum_{\alpha, i \neq j} \Xi_\alpha(\mathbf{x}_i) \Xi_\alpha(\mathbf{x}_j) \sigma_i \cdot \sigma_j. \tag{4.6}$$

For XY spins, Eq. (4.6) closely resembles the $O(2)$ generalizations [3, 98] of the Hopfield neural-network model [74, 2]. The mapping to Cook's model [3] is exact for translation-invariant, traveling-wave cavity

geometries such as the ring and confocal cavities; however, the basic features of these models (which are similar to one another) are expected to extend quite generally to $H_{\rm mm}$ [76].

4.4 Associative memories, spin glasses, and self-organization.

The Hopfield and Cook models describe associative memories, consisting of N neurons (i.e., spins in the physical system) that collectively encode p "patterns." In general, p corresponds to the number of cavity modes that are resolvable, given the interaction range (i.e., χ in the notation of Refs. [15]). The associative memory is said to function if, starting with any configuration similar to a stored pattern, the dynamics drives the configuration to the stored pattern, i.e., if a partially self-organized initial configuration at $T = 0$ becomes fully self-organized under the dynamics (this point is discussed further in Ref. [99]). In the Hopfield and Cook models [2, 3, 74], this is the case (as $N \to \infty$) for small p/N (i.e., less than approximately 0.05), e.g., in the single-mode cavity. For larger p/N, metastable states proliferate, and the system becomes a spin glass; the spin glass differs from the self-organized phase in that the ground-state atomic configuration *does not* globally emit superradiantly into any particular cavity mode; nevertheless, it is a distinct phase from the high-temperature paramagnetic phase [90]. A finite-temperature phase transition between the two is known to exist in the case that $p/N \to \infty$, i.e., the Sherrington-Kirkpatrick model [74, 90]. These considerations lead to the global phase diagram shown in Fig. 4.2.

4.5 Tuning and detection

Both the associative memory and the spin glass are low-temperature phases. The former is stable when $k_B T \leq \zeta N$. As is standard in ultracold atom experiments, the temperature is determined (in the $\kappa \ll \delta, \gamma \ll \Delta$ limit) by the system's initial entropy; however, ζ increases with pump laser intensity, and can be tuned across the transition. The spin ordering threshold is similar to that for self-organization, and is achievable, even for relatively large δ, for reasonably long experimental lifetimes [23, 14, 15]. The effective number of modes coupling to the atoms can be decreased by adjusting the length of the cavity away from the confocal/concentric limit; as $\zeta \sim 1/\delta$, only modes having sufficiently small δ couple strongly to the atoms. The spin glass transition temperature T_g in Hopfield-type models is comparable to the single-mode ordering temperature [74].

The self-organized phase should be detectable via the light emitted from the cavity, but the spin-glass phase is not, as it does not exhibit superradiance. One straightforward way to detect this phase is through its slow relaxational dynamics: a possible protocol involves initializing all spins in a certain region in the

$|+\rangle$ state via a local spin addressing protocol [100], and measuring the spin relaxation timescale (observed, e.g., via phase-contrast imaging [101]) as a function of pump intensity. A feature common to both the superradiant and spin-glass phases at low temperatures is the presence of a large number of low-energy excitations; these reveal themselves in condensed-matter systems via the heat capacity. In the cavity QED setting, such excitations can be detected, e.g., via two-photon spectroscopy [102]. Further possibilities for distinguishing the two low-temperature phases via their response functions are considered in Ref. [82].

4.6 Quantum regime

4.6.1 Case of weak disorder

Thus far, we have focused on the classical spin physics realizable using cavity-mediated interactions. We now turn to the quantum regime, in which Eq. (4.6) can be mapped [36] onto a Bose-Hubbard model in the limit $U/t \to \infty$, via the transformation $\sigma_+ \to b^\dagger$:

$$H_{\rm BH} = -w \sum_{ij} t_{ij} (b_i^\dagger b_j + \text{h.c.}) + \mu \sum_i b_i^\dagger b_i. \tag{4.7}$$

According to this mapping, a $|+\rangle$ state corresponds to the presence of a b boson whereas a $|-\rangle$ state corresponds to the absence of a b boson; the chemical potential μ is determined in the standard way from the number of bosons (i.e., $|+\rangle$ atoms). More generally, an n-state atom maps onto a Bose-Hubbard model with a maximum occupation per site of $n-1$:

$$H_{\rm n-level} = -w \sum_{ij} t_{ij} (b_i^\dagger b_j + \text{h.c.}) + U \sum_i (n_i - \bar{n})^2, \tag{4.8}$$

where the "interaction" term U can arise, e.g., because of the quadratic Zeeman shift. Note that, in this bosonic terminology, a "superfluid" state corresponds to a finite expectation value of $\sigma_\pm$ (i.e., to in-plane magnetic ordering). Thus, it is a "superfluid" of spins and *not* of the atoms, which are frozen in place.

A crucial difference between cavity-based realizations of the Bose-Hubbard model and optical-lattice ones [79] is that, in the cavity-based setting, strongly disordered hopping amplitudes are natural (hopping amplitudes being determined by the oscillatory cavity mode functions) even in the *absence* of on-site disorder (as both spin states interact identically with the trapping lasers). This is challenging to achieve in optical lattices [79], as varying the hopping amplitude via the lattice depth inevitably leads to on-site disorder. The phase structure of the disordered Bose-Hubbard model is known to be richer in the absence of chemical potential disorder, especially in one dimension [77]: the off-diagonally disordered model exhibits a Mott

glass phase, as well as a random-singlet glass phase [80, 81] (see Fig. 4.2). These phases are not present in models having on-site disorder, and are thus not directly realizable in optical lattices, but are realizable in the cavity-based setting.

A simple one-dimensional geometry that realizes the model of Ref. [77] involves a chain of atoms trapped perpendicular to the cavity axis. The cavity modes are Hermite-Gaussian along this direction, which we label y; thus, the nth mode has a profile of the Hermite-Gaussian $H_n(y/L)\exp(-y^2/L^2)$, where L is the waist of the TEM_{00} mode. For good confocal cavities $n \sim 10-100$; a more scalable geometry involves atoms trapped along the cavity axis. An atom at position y couples most strongly to modes with "classical turning points" near y; these modes have large amplitudes within a distance L from the turning point, and either decay or oscillate rapidly beyond this distance. Thus the interaction range is given by L and (in particular) is finite, and the analysis of Ref. [77] applies. For the case of a Λ atom having equal spin populations, one can realize the random-singlet glass, which possesses long-range spin-singlet correlations [80, 81]. (In order to realize the Mott glass, one could use, e.g., an atom possessing three ground states.) The three realizable glassy phases can be distinguished, e.g., via internal-state dependent transport or compressibility measurements [79].

4.6.2 Case of strong disorder

We now mention the work of Strack and Sachdev [82] on a spin-glass-forming model that is closely related to that discussed here. This model can be arrived at by adapting Eq. (4.6) to the case of Ising spins:

$$H_{\mathrm{st}} = \frac{\mathcal{C}_1}{4}\sum_i \sigma_x + \frac{1}{2}\sum_{l,m} J_{l,m}\sigma_z^l\sigma_z^m. \tag{4.9}$$

H_{st} can be realized using, e.g., the geometry considered here together with the atomic level structure and laser configuration discussed in Ref. [103]. It was argued in Ref. [82] that, depending on the sizes of the *mean* of J and the *standard deviation* of J relative to the transverse field $\mathcal{C}_1$, three distinct phases are achievable. When the variation in J is unimportant or removable (as in a single-mode cavity), there are two phases: a self-organized phase for strong coupling and a paramagnetic phase for large $\mathcal{C}_1$. When both the average and the variance are large compared with the transverse field, the problem is purely classical, and the ferromagnet-to-spin-glass transition occurs as described in Ref. [90]. Finally, when the mean coupling is close to zero, there is a quantum phase transition between a paramagnet and a spin glass when the variance in couplings exceeds a critical value. Strack and Sachdev show [82] that the spectral properties of the spin glass phase are very different from those of the self-organized phase, owing to the presence of considerable spectral

weight at low frequencies (as discussed in Ref. [90], the presence of low-energy excitations is characteristic of spin glasses).

We should note an important distinction between our treatment of the cavity-mediated interactions in Sec. 4.6.1 and that of Ref. [82]: we explicitly considered a cavity geometry for which the interactions decayed with distance, whereas Ref. [82] (as in our treatment of the classical case) took the interactions to be infinite-ranged but random for generic positions of atoms within the cavity. While this is almost certainly reasonable in practice, assuming the spins are randomly trapped, the question of the true range and distribution of interactions in real cavity geometries merits further attention.

4.7 Effects of dissipation

So far, we have treated the cavity-coupled spin models as if they were in equilibrium; this assumption is valid on short and intermediate timescales, as discussed in Chapters 2 and 3. However, by contrast with the spinless case discussed in previous chapters, the spinful case exhibits nontrivial long-time dynamics rather than simply heating up. The crucial distinction is as follows: in the spinful case, the microwave field is necessary to "repump" the system into the $|-\rangle$ state. However, a *coherent* microwave field would also break the $U(1)$ spin symmetry, by setting a preferred phase relation between the $|\pm\rangle$ states. In order to restore the $U(1)$ symmetry, one must make the repumping incoherent by including noise in the microwaves. Thus, the system achieves a nonequilibrium steady state governed by the balance between two separate sources of fluctuations, viz. the microwave noise and the noise due to dissipation. This situation is closely analogous to that of polariton condensates [63, 42], in which nonequilibrium effects alter the spectrum of the ordered state, the power-law decay of correlations in two dimensions, etc. The dynamics of glassy phases in the presence of these noise terms is a question of particular interest for future work.

4.8 Summary

In this chapter we have extended the self-organization transition from atoms to spins, and argued—using an analogy with associative memories—that an ensemble of spins frozen at random positions inside a multimode cavity should exhibit a spin-glass phase if there are enough cavity modes. We have extended this argument to the case of quantum-mechanical particles, and argued that cavity-mediated interactions provide a general method for realizing models with disordered interactions but no on-site disorder. This equilibrium analysis ignores many important questions about the dynamics of the spin-glass phase, which we hope to address in future work.

Chapter 5

Brazovskii transitions at zero density: the spin-orbit-coupled Bose gas

A quintessence even from nothingness,

From dull privations, and lean emptiness.

— John Donne, "A Nocturnal upon St. Lucy's Day"

In this chapter we return to the Brazovskii transition, which was introduced and discussed in Chapter 3, and address it from a different perspective. In Chapter 3, we argued that the change in the order of the crystallization transition was a dramatic—and easily measurable—manifestation of the importance of fluctuation effects, which are enhanced by the "Fermi-surface"-like character of the low-energy theory [45, 53]. There are, however, two ways in which this result is disappointing—(a) a first-order transition is not a quantum critical point, and thus does not exhibit the universal power-law scaling that is associated with such critical points, and (b) despite quantitative differences, the thermal and quantum transitions are *qualitatively* similar. This raises the question of whether there are Brazovskii-like models (especially experimentally *feasible* ones) in which the Fermi-surface-like character of the low-energy theory persists but does *not* avert quantum criticality.

The purpose of this chapter is to present one such model, which *is* experimentally realizable (and had, indeed, been introduced before our work [25]) in systems of spin-orbit-coupled BECs. This model describes a continuous quantum phase transition, as the chemical potential is changed, between an empty vacuum and a dilute BEC. For a conventional BEC, this transition is well understood [36], but here we consider the consequences of altering the single-particle dispersion so that its minimum lies on a *circle* in momentum space. This dispersion endows the low-energy critical theory with Fermi-surface-like kinematics, and therefore leads (as in Chapter 3) to emergent angle-dependence in the renormalized interactions; however, the transition remains continuous at zero temperature. Having discussed these features of the quantum critical theory, we turn to the case of finite temperatures; here, the Brazovskii argument discussed in Chapter 3 yields, not stripe-ordering as previously, but an instability toward the condensation of *pairs* of bosons. We comment briefly on the distinctions between the present system and that considered in Chapter 3, and finally discuss

the relation of our work to the many other approaches that have been brought to bear on these systems.

This chapter is based on work done in collaboration with Austen Lamacraft and Paul Goldbart; much of its content was published in Ref. [25].

5.1 Motivation

The advent of ultracold gases has vastly increased the range of physically realizable many-body bosonic systems, enabling the exploration of quantum-degenerate Bose gases possessing tunable interactions and band structure as well as internal degrees of freedom. Among such systems, those of particular interest involve single-particle Hamiltonians having degenerate ground states related by symmetries. Bose-Einstein condensation (BEC)—i.e., the macroscopic occupation of a *particular* single-particle state—typically entails breaking these symmetries; hence the order parameter space and defects of such BECs are richer than those of conventional BECs. For instance, spin-1 BECs [104] support fractionally quantized vortices, and in this sense resemble exotic *fermionic* condensates such as triplet superconductors.

Just as these exotic defects stem from broken *internal* symmetries, the defects of the Fulde-Ferrell-Larkin-Ovchinnikov (FFLO) superconductors, such as vortex-dislocation bound states [105, 106], stem from its broken translational and rotational symmetries. The present work addresses purely bosonic analogs of the FFLO states, in which the degenerate single-particle ground states have distinct *spatial* wavefunctions. In particular, we consider the case in which the single-particle Hamiltonian possesses a dispersion minimum on a circle in momentum space, so that BEC occurs at one or more nonzero momenta. Our work is motivated by a recently proposed realization of such a Hamiltonian, viz. a spin-$\frac{1}{2}$ Bose gas subject to a light-induced Rashba spin-orbit coupling [24]. Simpler forms of spin-orbit coupling, having multiple discrete minima, have been experimentally demonstrated [107]. An alternative approach to realizing a circular dispersion minimum would be to load the atoms into the excited band of an optical lattice; in this case, too, multiple discrete minima have been realized [108], and under appropriate conditions (e.g., "SE-even faulted" stackings of bilayer honeycomb lattices [109]) continuous minima are realizable.

5.2 Approach and main results

Spin-orbit coupled BECs were originally addressed in Refs. [110, 111] as examples of unconventional condensation; it was argued in Ref. [111] that, for a pure Rashba coupling and *isotropic* interactions, a fragmented condensate should form. More recently, the case of the Rashba-coupled BEC was treated using mean-field theory [112] and incorporating Gaussian fluctuations [113]; related systems have been studied

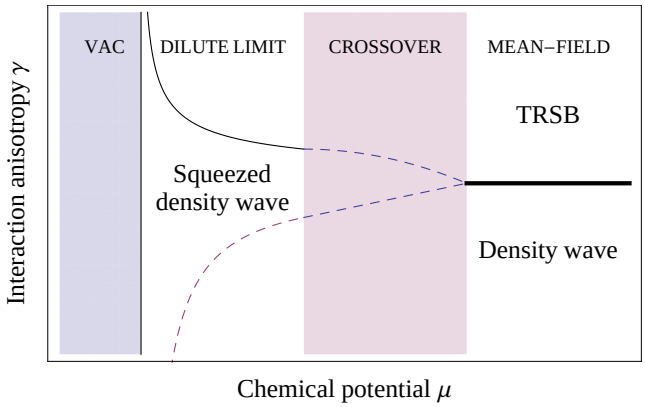

Figure 5.1: Zero-temperature phase diagram as a function of the interaction anisotropy $\gamma \equiv c_2/c_0$ and the chemical potential μ, showing the phases and transitions discussed in the main text. The (dashed) phase boundaries in the crossover region are schematic; the bold line indicates a first-order transition predicted by mean-field theory.

in Refs. [114]. In general, two phases have been found, depending on the spin-dependence of interactions: a time-reversal-symmetry-breaking (TRSB) state and a density-wave state. In the present work, we describe how interaction-renormalization effects *qualitatively* change the phase diagram at low densities (see Fig. 5.1), destabilizing the TRSB state and giving rise to a number-squeezed (and, in finite systems, "fragmented") limit of the density-wave state. These changes are due to the strong, *emergent* angle-dependence of renormalized interactions; such angle-dependent renormalizations are generic in systems whose low-energy modes occur around momentum-space surfaces, e.g., Fermi liquids [45]. (We emphasize that these effects, which arise because of the asymmetric renormalization of interactions, are distinct from the Gaussian fluctuation effects that destroy phase coherence in low dimensions, and are addressed for the present case in Refs. [105, 106, 113].) Our results, while consistent with those of Ref. [111] in the special case of isotropic interactions, hold more generally for *any* interactions that are repulsive in all angular-momentum channels.

Our primary results are as follows. At zero temperature, we find—exploiting the properties of a quantum critical point introduced in Ref. [115]—that the renormalized interactions for a dilute gas *universally* favor a state in which the BEC forms at a pair of opposite momenta. For *finite*, weakly trapped systems, fragmented BEC is energetically favored over simple BEC at either a single momentum or a coherent momentum superposition such as a density wave. In the thermodynamic limit, the fragmented BEC, though favored over a *coherent* superposition, becomes degenerate with *squeezed* states that break translational symmetry. The resulting ground-state energy per particle scales unusually with the density n, i.e., as $n^{4/3}$; note that this scaling is the same as that of the "extremely anisotropic Wigner crystal" [116], which in fact approaches the fragmented state in the zero-density limit. At nonzero temperature, we argue using renormalization-group (RG) methods that the leading instability is toward condensation of boson *pairs*, and estimate the

condensation temperature.

5.3 Model and microscopics

We begin with the following effective model of a d-dimensional Bose gas having a circular dispersion minimum:

$$\begin{aligned} H &= \int d^d k\, \Psi^\dagger(\mathbf{k}) \left[-\mu + \frac{1}{2M} \{ (|\mathbf{k}_{2D}| - k_0)^2 + k_\perp^2 \} \right] \Psi(\mathbf{k}) \\ &\quad + \int \prod_{i=1}^{4} d^d k_i \, U(\{\mathbf{k}_i\}) \Psi^\dagger(\mathbf{k}_1) \Psi^\dagger(\mathbf{k}_2) \Psi(\mathbf{k}_3) \Psi(\mathbf{k}_1 + \mathbf{k}_2 - \mathbf{k}_3), \end{aligned} \tag{5.1}$$

where $\Psi(\mathbf{k}_i)$ are Bose fields of momentum $\mathbf{k}_i$; $\mathbf{k}_{2D} \equiv (k_x, k_y)$; $k_\perp$ encodes all other momentum components; U is a possibly momentum-dependent interaction; and we have set $\hbar = 1$. For Rashba-coupled bosons, *spin*-dependent interactions in the microscopic model imply momentum-dependent interactions because, for modes near k_0, the spin is locked to the momentum. We shall first consider the universal properties of the general Hamiltonian H, and then relate these to the phases of the specific microscopic model considered in Ref. [112]. We focus primarily on the two-dimensional case, in which $k_\perp = 0$, and then touch on the qualitatively three-dimensional case.

We assume that energies associated with temperature T, chemical potential μ, system size, etc. are smaller than the spin-orbit coupling scale $k_0^2/2M$. Typical values of k_0^{-1} are on the order of an optical wavelength [107], which is exceeded by the interparticle spacing in many experiments ($k_0^2/2M$ cannot be *smaller* than these scales if spin-orbit coupling is to play a significant role).

As we are concerned with the low-energy limit, it is convenient to study only the degrees of freedom in a momentum shell of thickness 2Λ centered on the dispersion minimum, giving rise to an energy scale $\Omega_\Lambda \equiv \Lambda^2/2M$ intermediate between $k_0/2M$ and the low-energy scales μ and T. Integrating out degrees of freedom with energies $\geq \Omega_\Lambda$ generates effective interactions for modes with energies $\leq \Omega_\Lambda$; as we discuss below, these interactions are further renormalized, and (for energies $\ll \Omega_\Lambda$, take on universal values that are independent of Λ. A careful treatment of the high-energy renormalization, including the other Rashba bands [117], confirms this picture.

5.4 Zero-density quantum critical point

The model described by H has a quantum critical point (QCP) at $\mu = 0$, corresponding to the phase transition from the empty vacuum to a BEC. This QCP was analyzed in Ref. [115] *for fermions*, but the analysis extends straightforwardly to bosons. Given that $\Lambda \ll k_0$, kinematics constrains the resulting form of the effective interaction vertices within the momentum shell (i.e., those for which all four momenta satisfy $||\mathbf{k}_i| - k_0| \leq \Lambda$) to lie in the following channels: (i) forward scattering processes, which involve momentum transfer $\leq \Lambda$ [denoted $F_{\Omega_\Lambda}(\theta)$ where θ is the angle between the incoming momenta]; and (ii) "Cooper-channel" processes, in which incoming momenta are almost equal and opposite [denoted $V_{\Omega_\Lambda}(\theta)$ where θ is the angle between incoming and outgoing momentum pairs (see, e.g., Ref. [45])]. These channels renormalize differently: owing to the non-polarizability of the vacuum [36], all renormalizations are due to the repeated scattering processes shown in Fig. 5.2a, which have different amplitudes in the forward-scattering and Cooper channels. For forward scattering, intermediate momenta are constrained to lie in the regions shaded in Fig. 5.2c, whereas in the Cooper channel intermediate momenta run over the entire circle of radius k_0.

The outcome of renormalization depends on the sign of the microscopic interactions. *Any* attractive interactions lead to an instability in the Cooper channel [115], and thereby to bound states; this case is not expected to yield universal behavior. If, on the other hand, the initial interactions are *all* repulsive, one arrives at the following expressions for the renormalized interactions, for incoming frequencies of order $\Omega \leq \Omega_\Lambda$ (see Ref. [115]):

$$F_\Omega(\theta) = \frac{F_{\Omega_\Lambda}(\theta)}{1 + [MF_{\Omega_\Lambda}(\theta)/(2\pi \sin\theta)] \ln\left(\frac{\Omega_\Lambda}{\Omega}\right)}, \tag{5.2a}$$

$$F_\Omega(\theta{=}0) = \frac{F_{\Omega_\Lambda}(0)}{1 + MF_{\Omega_\Lambda}(0)\sqrt{k_0/\sqrt{M\Omega}}\, f_1\left(\frac{\Omega_\Lambda}{\Omega}\right)}, \tag{5.2b}$$

$$V_\Omega(m) = \frac{V_\infty(m)}{1 + MV_{\Omega_\Lambda}(m)\left(k_0/\sqrt{M\Omega}\right) f_2\left(\frac{\Omega_\Lambda}{\Omega}\right)}, \tag{5.2c}$$

where $f_1(x)$ and $f_2(x)$ are scaling functions that are of order unity as $x \to \infty$ and approach zero as $x \to 0$; and $V(m) \equiv \int_0^{2\pi} V(\theta) e^{im\theta} d\theta$. Subscripts Ω denote the incoming frequencies. Thus the low-energy (i.e., $\Omega/\Omega_\Lambda \to 0$) values of all couplings are "universal," i.e., independent of their microscopic values. Note that $F(\theta = \pi) = \sum_{m \text{ even}} V(m)$. Thus, given that $\Lambda/k_0 \ll 1$, the couplings assume the following hierarchy: $V_\Omega(m) \sim F_\Omega(\theta = \pi) \ll F_\Omega(\theta = 0) \ll F_\Omega(\theta \neq 0, \pi)$. Hence, interactions between particles at opposite momenta are negligible compared with other interactions [1].

[1] Although F is insensitive to the quantum statistics, V has contributions from odd as well as even angular momentum

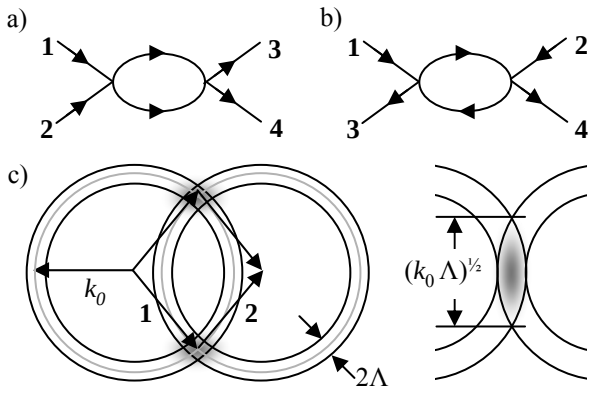

Figure 5.2: (a) Loop correction in the particle-particle channel, which governs the hierarchy of couplings at the QCP. (b) Loop correction in the particle-hole channel. These corrections vanish at $T = 0$. (c) Kinematic constraints due to the dispersion structure: left, case of $\theta \neq 0$: outgoing momenta are constrained to lie in the shaded region, of area $\sim \Lambda^2$; right, case of $\theta = 0$, for which the shaded region's area scales as $\Lambda\sqrt{k_0\Lambda}$.

5.5 Dilute BEC at zero temperature

We now turn from the QCP to phases in its vicinity. Suppose that the system is sufficiently dilute that when renormalization is cut off at a scale set by the chemical potential μ, the interactions are deep in the universal scaling regime. Then the interaction Hamiltonian is given by $H \sim \sum_{\theta,\theta'} F(\theta - \theta') n_\theta n_{\theta'}$, where n_θ denotes the boson density at a momentum of magnitude k_0 and direction θ. The hierarchy of universal coupling constants implies that H is minimized by a "fragmented" state, having precisely $N/2$ bosons at some θ, and $N/2$ at $\theta + \pi$ [2]. Fragmentation is favored owing to a momentum-space analog of Coulomb blockade (cf. Sec. 2.6 of Ref. [118]): bosons with opposite momenta do not interact with one another to leading order in $\sqrt{\Lambda/k_0}$, whereas those at non-opposite momenta do interact.

5.5.1 Ground-state energy and fragmentation

In more quantitative terms we can deduce the ground-state energy from the relation [119] $\mu = (n/2)F_\mu(\theta = 0) \simeq (n/M)(\mu M/k_0^2)^{1/4}$, giving

$$E(N) \simeq \sum_{\sigma=\pm} \frac{\hbar^2 N_\sigma^{7/3}}{M\mathcal{A}^{4/3} k_0^{2/3}}. \tag{5.3}$$

where $\mathcal{A}$ is the system area, and $N_\pm$ respectively denote the number of particles at θ and $\theta + \pi$. Note that this expression is *universal*, i.e., independent of the microscopic interaction strengths, and its unusual scaling is a consequence of the renormalization discussed above. As $E(N)$ is minimized when $N_+ = N_- = N/2$, the

channels in the spin-$\frac{1}{2}$ case. This distinction does not affect the low-energy physics because V's near the fixed point are negligible compared with F's.

[2] Our conclusions thus agree with those of Ref. [111]; however, our argument does not use the assumption that $(\theta, \theta + \pi)$ are associated with orthogonal internal states and thus applies to the higher-band lattice case.

ground state for finite N is fragmented. Such a fragmented state can be understood as a density wave of wavevector k_0 along the direction θ with a randomly varying phase.

Fragmented states are typically unstable relative to simple condensates (i.e., those having a fixed phase relation) because spatial inhomogeneities tend to phase-lock the fragments [118]. In the present case, a phase-locked, coherent superposition would involve fluctuations of order $\sqrt{N}$ in $N_\pm$, and hence cost an energy of order unity relative to the fragmented state even in the thermodynamic limit. Thus, a few scattering sites cannot overcome the tendency toward fragmentation. Similarly, a *weak* harmonic potential (i.e., of characteristic length much larger than the interparticle spacing) would *not* stabilize a coherent superposition relative to a fragmented state, even in the thermodynamic limit, provided that—according to the standard prescription—the trap frequency $\omega \to 0$ so as to keep $N\omega^2$ constant. This is because the typical matrix element between $\pm k$ due to the trap is of order $\exp(-2k_0^2 N)$, which rapidly decreases as $N \to \infty$.

Although a coherent superposition is disfavored in the thermodynamic limit, the energy cost of number fluctuations of order *unity* vanishes as $1/N$. Thus, the thermodynamic ground state (e.g., in a trap) is likely to be a squeezed state with small but nonvanishing phase variance, as opposed to the fragmented state, in which the phase is entirely random. This observation extends to translation-invariant systems, which should therefore exhibit spontaneously broken translational invariance in the thermodynamic limit.

5.5.2 Implications for global phase diagram

The dilute-limit phase diagram is *simpler* than that obtained from mean-field theory: it predicts that BEC occurs at two momenta regardless of microscopic interactions, provided these are repulsive. By contrast, mean-field theory [112] predicts a time-reversal-symmetry breaking (TRSB) state or a density-wave state, depending on microscopic interactions. We now give an account of the crossover between universal and mean-field regimes, and estimate the minimum densities required for mean-field results to apply.

The dilute-gas results apply when, upon renormalization, the pertinent interactions have already achieved their universal forms at a length-scale shorter than the interparticle spacing; thus, a TRSB state is disfavored if $F_\mu(\pi) \leq F_\mu(0)$, regardless of whether the (larger) $F_\mu(\theta \neq 0, \pi)$ couplings have approached their universal values. Note that $F_\Lambda(\theta = 0, \pi)$ are related to the parameters c_0 and c_2 in Ref. [112] as follows: $F_\Lambda(\pi)/F_\Lambda(0) \approx 1 + c_2/c_0$. [These relations, and similar ones for other couplings, can be derived as outlined following Eq. (3) in Ref. [112]. Provided $c_2 \leq c_0$, all microscopic couplings are of comparable magnitude.] Therefore, in terms of c_0 and c_2, the TRSB state is favored only if

$$\frac{c_0}{1 + \frac{M}{2\pi} c_0 \sqrt{k_0/n^{1/2}}} < \frac{c_0 + c_2}{1 + qM(c_0 + c_2)(k_0/n^{1/2})}. \tag{5.4}$$

where q is a constant of order unity.

Note that, in addition to the TRSB phase, the Hamiltonian of Ref. [112] also exhibits a regime in which a coherent superposition is *lower* in energy than the fragmented state, owing to terms of the form $\psi^\dagger_{2\mathbf{k}_0}\psi^\dagger_{-\mathbf{k}_0}\psi_{\mathbf{k}_0}\psi_0$, which involve momenta of order $2k_0$ and thus do not appear in H.

These considerations lead us to the phase diagram shown in Fig. 5.1, in which there is no *direct* transition from the vacuum to the TRSB state. The transition from the vacuum to the density-wave state is unusual in being a *continuous* transition (*known* to be continuous as the properties of the QCP are understood exactly [115]) at which both rotational and translational symmetry are broken. As a general rule (see, e.g. Refs. [105, 52]) transitions that break rotational *and* translational symmetry are first-order. For densities $\geq \Lambda^2$, at which the renormalization effects discussed in the present work are not present, mean-field simulations show evidence of metastability [112]; this would suggest a first-order transition between the density-wave and TRSB states.

5.6 Finite-temperature phase transition

Having discussed the zero-density QCP, we turn to its finite-temperature consequences. We are particularly interested in the "universal" regime [36] in which $T \gg \mu$. This regime was addressed in detail, for the case of a conventional BEC, by Fisher and Hohenberg [119]; their approach consisted of the following two steps—(i) renormalize interactions according to the zero-density QCP up to a scale Λ_T (defined below) that is set by the system temperature, and (ii) perform a standard classical RG treatment of the dilute Bose gas using the renormalized interactions from step (i) as input. (This procedure can be used, e.g., to estimate the condensation temperature.) In the present case, this two-step renormalization has dramatic qualitative consequences—owing to the strong angle-dependence of renormalizations in step (i), the classical RG is *initialized* with highly anisotropic interactions. As we argue below, this anisotropy leads (by a mechanism reminiscent of the Kohn-Luttinger effect [120]) to a pairing instability for bosons.

The crossover between the two steps described above occurs at $\Lambda_T \equiv 1/\sqrt{2MT}$; beyond this scale, the physics is captured by a classical free-energy functional of the form

$$S = \int d^d k \left[-\mu + (|\mathbf{k} - k_0)^2\right] |\psi_{\mathbf{k}}|^2 + S_4, \tag{5.5}$$

where S_4 denotes the set of angle- and channel-dependent couplings, and we have set $2M = 1$. S is a complex-field version of Brazovskii's model [52] (the relevance of Brazovskii's model to the Rashba-coupled Bose gas was previously suggested in Ref. [110]). The initial values for the couplings in S_4 are the renormalized

interactions at a scale $\Omega = T$. At scales $\leq \Lambda_T$, the vacuum is nontrivial, owing to the presence of thermal particles; hence, all couplings are renormalized by the particle-hole channel [Fig. 5.2b]. It is convenient to expand F as well as V in terms of angular momenta. One can then implement the momentum-shell RG procedure described in Ref. [53], by integrating out modes satisfying $\Lambda_T(1-dl) < |k-k_0| < \Lambda_T$ and rescaling $k \to (1+dl)k, \psi \to [1-(3/2)dl]\psi$, and $\mu \to \mu/\Lambda_T^2$. The couplings transform as follows (ignoring the flow of μ):

$$\frac{dF_l(m)}{dl} = 3F_l(m) - \frac{A\,F_l^2(m)}{(1-\mu_l)^2} - \frac{A}{2}\frac{\sum_m V_l^2(m)}{(1-\mu_l)^2}, \tag{5.6a}$$

$$\frac{dV_l(m)}{dl} = 3V_l(m) - \frac{A\,V_l^2(m)}{2(1-\mu_l)^2} - A\frac{\sum_m F_l^2(m)}{(1-\mu_l)^2}, \tag{5.6b}$$

where $A \equiv 2\pi k_0/\Lambda_T$. If the coupling constants at Λ_T are in the universal regime, one can use the fact that $V \ll F$ to drop terms of order V^2. The last term in the flow equations drives all *even* $V(m)$ (which are initially near zero) to negative values at some $\Lambda_2 = \Lambda_T(1 - o(\Lambda_T/k_0))$, triggering a runaway growth of the even-parity $V(m)$ couplings. Such runaway growth is associated with a pairing instability, which should in principle occur simultaneously in all even-m channels. (However, as noted in Ref. [111], the confining trap acts as a kinetic energy term of the form ∇_θ^2, which penalizes higher-m channels.)

The pair-condensation temperature can be estimated by observing that arbitrarily weak attractive interactions in the Cooper channel give rise to pairs [121] whose binding energy is $\Delta \sim MV^2k_0^2$. Pairing is favored for $\Delta \geq T$. As $T/E_0 \simeq (\Lambda_1/k_0)^2 \ll (\Lambda/k_0)^2 \ll V \simeq \ln(\Lambda/\Lambda_1)$, one expects pairs to be tightly bound at length-scales comparable to $1/\Lambda_T$; at longer distances they can be treated as nonoverlapping. The system is thus a dilute gas of pairs, which condense at a temperature given implicitly [119] by $T_c \approx (\hbar^2 n/4m) \times 1/\ln\ln(na^2)$, where a is an effective dimer-dimer scattering range, which is of order Λ.

Pairing would be straightforward to detect experimentally via radio-frequency spectroscopy, which should reveal a peak corresponding to the pair binding energy; moreover, a pair condensate would support half-quantized vortices detectable via rotation.

5.7 Three-dimensional case

For this case, $k_z \equiv k_\perp$ in Eq. (1); thus, the dispersion minimum is *circular* rather than spherical, and imposes the same kinematic constraints as in 2D. The 2D analysis thus generalizes readily; the chief difference is that the forward-scattering couplings in 3D renormalize to nonuniversal T-matrices rather than universal values,

and the ground-state energy thus depends on microscopic couplings. However, Cooper-channel couplings approach the following universal expression as $\Omega/\Omega_\Lambda \to 0$:

$$V_\Omega \sim 1/\left[k_0 M \ln(\Omega_\Lambda/\Omega)\right]. \tag{5.7}$$

Hence, as in 2D, $\sum_m V(m) \sim F(\theta = \pi) \ll F(\theta \neq \pi)$ at low energies. It follows that the dilute-limit ground state universally preserves time-reversal symmetry. This qualitative resemblance to 2D extends to the $T > 0$ case, in which the free-energy functional—in this case, the variant of Brazovskii's model having two transverse dimensions discussed in Ref. [14]—develops a pairing instability as in 2D. As the Cooper-channel couplings approach universal values more slowly, however, the conditions for the dilute limit to obtain are more stringent in 3D than in 2D.

5.8 Related work

In this section we briefly review a few other works that study non-mean-field effects in spin-orbit-coupled BECs. The first of these, Ref. [113], addresses the destabilization of the ordered state by Goldstone modes at finite temperatures; as mentioned above, this effect—which is essentially classical in nature—is distinct from the interaction-renormalization effects considered here, which are inherently quantum-mechanical (the results of even our finite-temperature analysis depended strongly on the "quantum" renormalization step).

We now turn to work that appeared subsequent to ours. Soon after the appearance of our work [25], Ozawa and Baym [117, 122] analyzed the interaction renormalizations in the three-dimensional case [3] in detail, and investigated their consequences for the zero-temperature phase diagram. The second of the Ozawa-Baym papers [122] addresses the general case of dispersions that are anisotropic (so that two points along the dispersion minimum lie slightly below the others), and shows how the TRSB state shrinks to occupy a smaller and smaller fraction of the phase diagram as one approaches the limit of isotropic interactions considered here. In agreement with our findings, they show that the TRSB state does not exist at low density for isotropic interactions.

The nature of the ground state in the isotropic case has also been considered from two other perspectives. Berg, Rudner, and Kivelson [116] considered a simple variational wavefunction, in which (two-dimensional) space is partitioned into non-overlapping rectangles of area $1/n$ and aspect ratio $(n/k_0^2)^{1/3}$, and each particle occupies one rectangle. They found that the variational ground-state energy per particle—which, in the ansatz of Ref. [116], is purely the kinetic energy—scales as $(n/k_0)^{4/3}$, in agreement with our result for the

[3] As noted above, the three-dimensional case still has a *circular* rather than a *spherical* dispersion minimum.

interaction energy; moreover, in the limit of low density, the rectangles approach the limit of stripes. Thus the "anisotropic Wigner crystal" phase of Ref. [116] is similar to the striped phase we discuss, although it lacks long-range phase coherence in the direction transverse to the stripes. As the energies of both the phase-coherent and phase-incoherent states scale identically, however, determining which one is the true ground state would require a computation of the prefactors in both cases, which has not yet been done. (We note, however, that the "Wigner crystal" scaling is generally the same as that of the renormalized interaction energy in low-dimensional dilute systems [123]; yet none of these actually exhibit Wigner crystallization.)

Finally, Barnett et al. [124] considered the case in which the *bare* interactions do not distinguish between the striped and TRSB phases, and argued that in this case an order-from-disorder mechanism should stabilize the TRSB phase. The results of Ref. [124] depend crucially on the symmetric nature of interactions, which is, however, always broken by the renormalization effects discussed in this chapter. However, the arguments of Ref. [124] can presumably be adapted to include the renormalization effects considered here by choosing the bare interactions so that the *renormalized* interactions do not distinguish between the two phases. The consequence of such a replacement would be to expand the region covered by the TRSB phase in Fig. 5.1 slightly; however, in the low-density limit the renormalized interactions *universally* favor the striped phase, and the order-from-disorder mechanism is always anticipated by these asymmetric renormalizations.

5.9 Distinctions between real- and complex-field Brazovskii transitions

In the present thesis, we have discussed two different kinds of quantum transition in which the low-energy modes cluster around a surface in momentum space—the self-organization transition in a concentric cavity and the zero-density critical point for bosons subject to Rashba spin-orbit coupling. To these, one can add a third such transition, viz. the transition from the normal state to the FFLO state in a rotationally symmetric system [105, 106]. While these transitions, and the resulting ordered states, have several features in common, there are also important distinctions between them, which should be kept in mind while drawing parallels; some of these parallels are listed in Table 5.1.

Table 5.1: Distinctions between the cavity-mediated self-organization phenomenon, the condensation of Rashba-coupled bosons, and the transition from a normal to an FFLO state.

	Cavity-mediated crystal	Rashba-coupled BEC	FFLO state
Reference state	Uniform BEC	Vacuum	Interacting fermions
Order-parameter fields	Real	Complex	Complex
Cubic term suppression	Accidental	$U(1)$ symmetry	$U(1)$ symmetry
Transition character	First order	Continuous	?
Ordered-state wavefunction	$A + Bg_\alpha(\mathbf{x})$	$A\cos(\mathbf{k}\cdot\mathbf{x})$	$A\cos(\mathbf{k}\cdot\mathbf{x})$
Half-quantum vortex?	No	Yes	Yes
Paired superfluid?	No	Yes	Yes

5.10 Summary

In this chapter, we have shown that the condensation of a dilute Bose gas with a circular dispersion minimum is greatly affected by the strongly angle- and channel-dependent renormalization of interactions. In two dimensions, these renormalizations (i) render the ground-state energy independent of the bare interaction strengths, (ii) universally lower the energy of a striped and/or fragmented state relative to that of a simple time-reversal-symmetry-breaking Bose condensate, and (iii) give rise, at finite temperatures, to a pairing instability of the bosons, and thus to a condensate of pairs of bosons. It is to be hoped that some of these effects will be realized experimentally in the near future in systems of interacting spin-orbit-coupled bosons.

Chapter 6

Conclusions and outlook

The end is where we start from.

— T.S. Eliot, "Little Gidding"

In the previous chapters we discussed how ultracold atomic systems can be induced to order at nonzero wavevectors; how such ordering can be geometrically frustrated, leading to spin glasses and perhaps structural glasses; and, finally, how the generic low-energy theories associated with such ordering have strongly angle-dependent renormalizations, which constrain the range of achievable ground states. We developed one particular approach to finite-wavevector ordering, which involved using multimode cavities to mediate interatomic interactions favoring configurations in which the atoms are separated by an optical wavelength (i.e., a distance comparable to the typical atomic spacing in experiments); these interactions therefore favor crystallization, and also make geometrical frustration achievable. We then addressed the general question of phase transitions in isotropic systems with finite-wavevector instabilities, generalizing the Brazovskii effect [52] to two different quantum-mechanical settings; this generalization led, in the case of a spin-orbit coupled Bose gas, to a range of new phenomena, including a fluctuation-driven mechanism for the condensation of pairs of bosons.

These phenomena are, however, clearly a small fraction of the wealth of effects associated with finite-wavevector instabilities and cavity-mediated interactions. Even among the topics we have discussed in this thesis, there are several aspects that call for further investigation: for instance, whether the bilayer systems discussed in Chapter 3 really have glassy phases, and how the spin glass phase discussed in Chapter 4 responds to dissipation and pumping noise. It might be of interest to explore the physics of many fermions trapped in multimode cavities. The interplay between superconductivity and the density-wave instabilities induced by the cavity might, e.g., stabilize spatially modulated superfluids such as the FFLO state [105]. A further possibility of some interest is that of cavity-mediated Cooper pairing: e.g., by attempting to use the photon-mediated interactions introduced in Chapter 2 to achieve photon-mediated Cooper pairing, or by using the phonons of the emergent crystalline phase as the "glue" that would bind the Cooper pairs.

Beyond these specific possibilities, there are two general lines of exploration that this work opens up. The first is about "soft" quantum matter; by this I mean to refer to the exploration of themes that are commonly pursued in soft-matter physics, in contexts where quantum mechanics is the primary source of fluctuations. In particular, cavity-mediated interactions are a close parallel to the engineered interactions that are studied in soft-matter settings as a path toward unconventional "self-assembled" lattices [125], quasicrystalline phases [126], etc. Many such phenomena have only been studied in the classical limit, and it is plausible that quantum fluctuations will alter them considerably, giving rise to forms of order that have not hitherto been studied in any context. (Note that *cavity*-mediated interactions are just one class of interactions mediated by auxiliary degrees of freedom, which might in general be atomic as well as optical.) The second general line of exploration is quantum glassiness in ultracold atomic settings: because ultracold atomic systems are either isolated or controllably coupled to their environments, they provide a uniquely rich setting for exploring how concepts such as thermal equilibrium emerge from the isolated dynamics of large quantum systems, and when—as perhaps in certain glassy systems [21, 127]—they fail to emerge, so that the dynamics is irreducibly quantum-mechanical at all temperatures.

Appendix A

Determining the dispersion parameter χ in multimode cavities

The parameter $1/\chi$, which sets the healing length for crystallinity, is a measure of how weak the atomic coupling ζ_{lmn} to $l \neq 0$ modes is, relative to the coupling to $l = 0$ modes. The value of χ is determined by the following effects: (1) the atoms, being confined near the equatorial plane of the cavity, couple most strongly to modes that have the highest amplitude there, and thus to the lowest-order modes along the z direction (i.e., g is in effect a function of l once $\Xi(\mathbf{x})$ is projected onto the equatorial plane); (2) higher-order modes along the z direction have lower finesse and hence couple more weakly to the atoms (i.e., κ is a function of l); (3) the effective laser-cavity detuning, $\Delta_C - g^2 N/\Delta_A$, is a function of l because g is; (4) for a *nearly* concentric (or confocal, planar, etc.) cavity—the experimentally relevant case—Δ_C is a function of l because higher-order modes have a lower resonant frequency. Thus, ζ is in general a complicated function of l.

For the specific case of a concentric cavity, one can generalize the mode structure given in Sec. 3.5.1 by imposing, e.g., finite-well rather than hard-wall boundary conditions on θ. In this case, it is clear that both g_l/g_0 and κ_l/κ_0 (in which the subscripts denote the appropriate value of l) must go as approximately $(1 - \text{const} \times l^2)$, where the constant is approximately $1/l_{\text{max}}^2$, the number of higher-order modes that are of sufficiently high finesse to couple significantly to the atoms. Thus, χ can be taken to be approximately $1/l_{\text{max}}^2$, up to a factor of order unity; the physically relevant quantities ξ_0 and Ω_{th}, which depend on $\chi^{1/3}$ and $\chi^{1/4}$ respectively, should not be sensitive to this neglected factor.

Note that this analysis ignores effect (4). According to Eq. (19.24) of Ref. [30], this term would lead to a frequency shift $\Delta_C(l)/\Delta_C(0) \propto -l$, with a proportionality constant depending on the distance from concentricity. Thus ζ should have a *positive* linear term in l in addition to the negative quadratic term; the potential effect of such a term is to favor some family of $l = l_0 \neq 0$ modes, even at the equator, over $l = 0$ ones. Similar considerations apply for other geometries, such as the confocal or planar cavities.

Appendix B

Renormalization-group equations for the quantum Brazovskii model

In this Appendix we outline our derivation of the renormalization-group (RG) flow equations for the quantum Brazovskii model discussed in Sec. 3.5.6. Our procedure parallels that discussed in Appendix A of Ref. [53] for the *classical* Brazovskii model; this work, in turn, was based on techniques developed by Shankar [45] for the Fermi liquid. The objective of the renormalization-group procedure is to arrive at a spatially coarse-grained effective theory in terms of modes for which $m + n \approx \Lambda_0$. This is done by progressively integrating out modes for which $|m + n - \Lambda_0| \geq B$, where B is referred to as the renormalization-group "scale." The microscopic, or "bare," theory has an RG scale that is associated with the physical high-energy cutoff (e.g., Δ_A in the cavity QED case); this scale is progressively decreased by the integrating out of "shells" of modes, i.e., modes for which $B_{\rm new} \leq |m+n-\Lambda_0| \leq B_{\rm old}$, thus yielding effective theories involving progressively fewer modes. As one integrates out these shells of modes, the theory maintains its basic structure, but the various coupling constants flow; therefore, the coupling constants are functions of B. For example, the microscopic values of the parameters, $\mathcal{R}$ and $\mathcal{U}$, are their values at a value of B determined by Δ_A, whereas the fully coarse-grained parameters r and u are those corresponding to $B = 0$. At each step in the RG procedure, we integrate out all the *frequency* components associated with that spatial shell; in making this choice [which has the advantage of preserving the causality structure of the microscopic theory (as mentioned in Ref. [61])] we follow Refs. [61, 45].

We begin with the observation that the action can be written as follows:

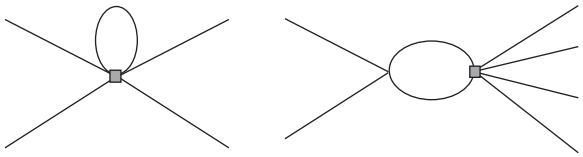

Figure B.1: Feynman diagrams involving the six-point vertices associated with the couplings w_i ($i = 1, 2, 3$), to one-loop order. The six-point vertices are denoted as grey squares. The diagram shown on the left renormalizes the four-point vertices; that on the right renormalizes the six-point vertices.

$$S = S_2 + S_4 + \cdots , \tag{B.1}$$

where

$$\begin{aligned} S_2 &= \frac{(2\pi)^d}{2} \int d1\, r(1)\Phi(1)\Phi(1), \\ S_4 &= \frac{(2\pi)^d}{4!} \int d1\, d2\, d3\, d4\, u(1234)\Phi(1)\Phi(2)\Phi(3)\Phi(4) \\ &\qquad \times\delta(1+2+3+4), \end{aligned} \tag{B.2}$$

and notation of the form $d1$ is to be interpreted in the following way:

$$\int d1 \equiv \frac{1}{(2\pi)^d} \int_{|m+n-\Lambda_0|<B} \Lambda_0^{d-1} d\eta \int_{-\infty}^{\infty} d\omega \int d\theta, \tag{B.3}$$

where η and θ are, respectively, the quasi-radial and quasi-angular variables discussed in Sec. 3.5.7, and are treated here as continuous. We now perform the RG transformation, which involves two steps: (i) integrating out all modes satisfying $B/b \leq |m+n-\Lambda_0| \leq B$ for $b = 1+l$ with $l \ll 1$; and (ii) rescaling the spatial coordinates and the fields in the action so that the new action is similar in form to its predecessor under the RG transformation. Under this rescaling, $\eta \to b\eta$ and $\Phi \to \Phi/b$. Under the combined effects of integrating out the shell of modes (at one-loop order, via the diagram in Fig. 3.3) along with the rescaling, the coefficient of the quadratic term transforms as follows:

$$r(B) \longrightarrow r(B/b) = b^2\big(r(B) + \Delta_2\big), \tag{B.4}$$

where

$$\Delta_2 \equiv \alpha\, u_1(B) \int_{B/b}^{B} d\eta\, \frac{1}{r(B)+\eta^2}. \tag{B.5}$$

By setting $b = 1+l$ and differentiating with respect to l, we arrive at a differential version of the RG equation for r, viz.,

$$\frac{dr}{dl} = 2r(B) + \frac{B\,\alpha u_1(B)}{\sqrt{r(B)+B^2}}. \tag{B.6}$$

We have introduced the notation u_1 instead of u because, as we shall now see (and as we anticipated in

Sec. 3.5.4), the renormalized value of u depends on whether the four θs entering the vertex are identical or not. The *generic* vertex, in which not all four values of θ are the same, is associated with the coupling u_1; the special vertex, in which all four values of θ are the same, is associated with the coupling u_2. Similarly, we shall denote the six-point vertices respectively as w_1, w_2, and w_3, depending on whether two, four, or all six of the incoming propagators have the same value of θ. The RG equations for (u_1, u_2) can be derived via the same procedure as those for r; they are as follows:

$$\frac{du_1}{dl} = 2u_1 - \frac{\alpha u_1^2 B}{r(B)+B^2} + \frac{\alpha w_1 B}{\sqrt{r(B)+B^2}}, \tag{B.7}$$

$$\frac{du_2}{dl} = 2u_2 - 2\frac{\alpha u_1^2 B}{r(B)+B^2} + \frac{\alpha w_2 B}{\sqrt{r(B)+B^2}}. \tag{B.8}$$

Similar equations can be derived for the three w couplings; these involve the diagrams in Fig. 3.3d and Fig. B.1. Before writing these down, however, we introduce the following convenient changes of variables, which serve to de-dimensionalize the RG equations (following Ref. [53]):

$$\mathcal{B} \equiv B(\alpha\mathcal{U})^{-1/2}\, e^{-l}, \tag{B.9}$$

$$\overline{r}(\mathcal{B}) \equiv r(l)(\alpha\mathcal{U})^{-1}\, e^{-2l}, \tag{B.10}$$

$$\overline{u}_{1,2}(\mathcal{B}) \equiv u_{1,2}(l)\,\mathcal{U}\, e^{-2l}, \tag{B.11}$$

$$\overline{w}_{1,2,3}(\mathcal{B}) \equiv w_{1,2,3}(l)\,\mathcal{U}^{-1}\,\alpha^2 e^{-2l}. \tag{B.12}$$

In terms of the new variables, the full set of RG equations is as follows:

$$\frac{d\overline{r}}{d\mathcal{B}} = -\frac{\overline{u}_1}{(\overline{r}+\mathcal{B}^2)^{1/2}}, \tag{B.13}$$

$$\frac{d\overline{u}_1}{d\mathcal{B}} = \frac{\overline{u}_1^2}{\overline{r}+\mathcal{B}^2} - \frac{\overline{w}_1}{(\overline{r}+\mathcal{B}^2)^{1/2}}, \tag{B.14}$$

$$\frac{d\overline{u}_2}{d\mathcal{B}} = \frac{2\overline{u}_1^2}{\overline{r}+\mathcal{B}^2} - \frac{\overline{w}_2}{(\overline{r}+\mathcal{B}^2)^{1/2}}, \tag{B.15}$$

$$\frac{d\overline{w}_1}{d\mathcal{B}} = -\frac{2\overline{u}_1^3}{(\overline{r}+\mathcal{B}^2)^{3/2}} + \frac{3\overline{u}_1\overline{w}_1}{\overline{r}+\mathcal{B}^2}, \tag{B.16}$$

$$\frac{d\overline{w}_2}{d\mathcal{B}} = -\frac{4\overline{u}_2^3}{(\overline{r}+\mathcal{B}^2)^{3/2}} + \frac{\overline{u}_2\overline{w}_2}{\overline{r}+\mathcal{B}^2} + \frac{4\overline{u}_1\overline{w}_1}{\overline{r}+\mathcal{B}^2}, \tag{B.17}$$

$$\frac{d\overline{w}_3}{d\mathcal{B}} = -\frac{12\overline{u}_1^3}{(\overline{r}+\mathcal{B}^2)^{3/2}} + \frac{8\overline{u}_1\overline{w}_2}{\overline{r}+\mathcal{B}^2}. \tag{B.18}$$

The appropriate microscopic values (i.e., initial conditions for these equations) are as follows: $\overline{r}(\infty) = \overline{\mathcal{R}}, \overline{u}_{1,2}(\infty) = 1, \overline{w}_{1,2,3}(\infty) = 0$. Numerically integrating the equations yields the coarse-grained parameters, which are plotted in Fig. 3.5 and discussed in the main text.

Appendix C

Effective temperatures

In this Appendix we briefly explain why, and for what purposes, $\tilde{\kappa}$ in Sec. 3.6 behaves as an effective temperature. The basic claim we shall review is as follows: consider a quadratic Keldysh action that has a $q-q$ component of the (low-frequency) form

$$i \sum_{\nu} \Gamma_{\nu} \int d\omega \, \phi_{\nu,q}(\omega) \, \phi_{\nu,q}(-\omega), \tag{C.1}$$

for some real set of parameters Γ. (The generic set of indices parameterized by ν can describe positions, momenta, mode indices, etc.) The long-time dynamics of such a theory is then described by a Langevin equation, having a white noise term of strength Γ.

In what follows, we shall suppress the ν index; the argument, which is adapted from Ref. [4], can be made independently for each ν. First, note that Eq. (C.1) can be rewritten in the time domain as

$$i\Gamma \int d\omega \, \phi_q(t) \, \phi_q(t). \tag{C.2}$$

This term appears in the system's partition function $Z \equiv \int D\phi_q(t) \, D\phi_c(t) \, \exp iS$, in the form

$$Z = \int D\phi_q(t) \, \exp\left(-\Gamma \int dt \, \phi_q(t) \, \phi_q(t) \right) \times \cdots , \tag{C.3}$$

in which the ellipses denote other terms in the action. The expression above can be rewritten, by means of a Hubbard-Stratonovich transformation, as

$$\int D\phi_q(t) \, D\xi(t) \, \exp\left\{ -\Gamma \int dt \, \left(\frac{\xi(t)^2}{\Gamma} - 2i\xi(t) \, \phi_q(t) \right) \right\} \times \cdots . \tag{C.4}$$

Once this is done, the full partition function, which also includes terms *linear* in ϕ_q (from the retarded and advanced components) can be written as follows:

$$Z = \int D\xi(t)\, D\phi_c(t) \exp\left(-\frac{1}{\Gamma}\int dt \xi(t)^2\right) \tag{C.5}$$
$$\times \int D\phi_q(t)\, \exp\left\{i\int dt\, dt' [\phi_c(t')\, G(t',t) - \xi(t)]\phi_q(t)\right\},$$

where G represents some (unspecified) integral kernel that couples ϕ_c and ϕ_q. Note that the $c-c$ term in the action is absent, via causality, as discussed in Ref. [4]. If one now integrates out ϕ_q, one finds that the partition function is given by

$$Z = \int D\xi(t)\, D\phi_c(t)\, \exp\left(-\frac{1}{\Gamma}\int dt\, \xi(t)^2\right) \tag{C.6}$$
$$\times \delta\left[\phi_c(t)\, G(t,t') - \xi(t')\right].$$

Accordingly, the dynamics of the system is described, at long times, by a sum over classical histories in the presence of a Langevin white noise term ξ, the fluctuations of which are given by

$$\langle \xi(t)\, \xi(t')\rangle = \Gamma\, \delta(t-t'). \tag{C.7}$$

It follows that the long-time dynamics of the system is *classical* rather than quantal; thus any phase transition that the system undergoes is a thermal rather than a quantum phase transition. By contrast, for any system that undergoes a true *quantum* phase transition, the coefficient of the $q-q$ component of the Keldysh action *vanishes* at low frequencies, typically as a power law, $|\omega|^\alpha$ (see, e.g., Ref. [61]). This corresponds to power-law decay of noise correlations in the time domain.

A closely analogous argument (see, e.g., Ref. [4]) shows that, assuming the $q-q$ component of the action is frequency-independent as $\omega \to 0$, the rate of escape from a metastable state is given by an effective Arrhenius formula with a temperature proportional to Γ.

References

[1] Kim, E. and Chan, M. H. W. *Science* **305**, 1941 (2004).

[2] Hopfield, J. J. *Proceedings of the National Academy of Sciences* **79**(8), 2554–2558 (1982).

[3] Cook, J. *Journal of Physics A: Mathematical and General* **22**(12), 2057 (1989).

[4] Kamenev, A. and Levchenko, A. *Adv. Phys.* **58**, 197–319 (2009).

[5] Phillips, W. D. *Rev. Mod. Phys.* **70**, 721–741 (1998).

[6] Cornell, E. A. and Wieman, C. E. *Rev. Mod. Phys.* **74**, 875–893 (2002).

[7] Ketterle, W. *Rev. Mod. Phys.* **74**, 1131–1151 (2002).

[8] DeMarco, B. and Jin, D. S. *Science* **285**, 1703–1706 (1999).

[9] Chin, C., Grimm, R., Julienne, P., and Tiesinga, E. *Rev. Mod. Phys.* **82**, 1225–1286 (2010).

[10] Bloch, I., Dalibard, J., and Zwerger, W. *Rev. Mod. Phys.* **80**(3), 885–964 (2008).

[11] Gorshkov, A. V., Hermele, M., Gurarie, V., Xu, C., Julienne, P. S., Ye, J., Zoller, P., Demler, E., Lukin, M. D., and Rey, A. M. *Nat. Phys.* **6**, 289–295 (2010).

[12] Lu, M., Youn, S.-H., and Lev, B. L. *Phys. Rev. Lett.* **104**, 063001 (2010).

[13] Dalibard, J., Gerbier, F., Juzeliūnas, G., and Öhberg, P. *Rev. Mod. Phys.* **83**, 1523–1543 (2011).

[14] Gopalakrishnan, S., Lev, B. L., and Goldbart, P. M. *Nat. Phys.* **5**, 845–850 (2009).

[15] Gopalakrishnan, S., Lev, B. L., and Goldbart, P. M. *Phys. Rev. A* **82**(4), 043612 (2010).

[16] Gopalakrishnan, S., Lev, B. L., and Goldbart, P. M. *Phys. Rev. Lett.* **107**, 277201 (2011).

[17] Loh, E. Y., Gubernatis, J. E., Scalettar, R. T., White, S. R., Scalapino, D. J., and Sugar, R. L. *Phys. Rev. B* **41**, 9301–9307 (1990).

[18] Andrews, M. R., Townsend, C. G., Miesner, H.-J., Durfee, D. S., Kurn, D. M., and Ketterle, W. *Science* **275**, 637–641 (1997).

[19] Hadzibabic, Z., Krüger, P., Cheneau, M., Battelier, B., and Dalibard, J. *Nature* **441**, 1118 (2006).

[20] Endres, M., Cheneau, M., Fukuhara, T., Weitenberg, C., Schauss, P., Gross, C., Mazza, L., Banuls, M. C., Pollet, L., Bloch, I., and Kuhr, S. *Science* **334**, 200–203 (2011).

[21] Pal, A. and Huse, D. A. *Phys. Rev. B* **82**, 174411 (2010).

[22] Law, K. T. and Feldman, D. E. *Phys. Rev. Lett.* **101**, 096401 (2008).

[23] Baumann, K., Guerlin, C., Brennecke, F., and Esslinger, T. *Nature* **464**, 1301–1306 (2010).

[24] Campbell, D. L., Juzeliūnas, G., and Spielman, I. B. *Phys. Rev. A* **84**, 025602 (2011).

[25] Gopalakrishnan, S., Lamacraft, A., and Goldbart, P. M. *Phys. Rev. A* **84**, 061604 (2011).

[26] Domokos, P. and Ritsch, H. *Phys. Rev. Lett.* **89**(25), 253003 (2002).

[27] Nagy, D., Kónya, G., Szirmai, G., and Domokos, P. *Phys. Rev. Lett.* **104**(13), 130401 (2010).

[28] Snoke, D. and Littlewood, P. *Physics Today* **63**(8), 42–47 (2010).

[29] Metcalf, H. J. and van der Straten, P. *Laser cooling and trapping*. Springer, (1999).

[30] Siegman, A. E. *Lasers*. University Science Books, (1986).

[31] Asbóth, J. K., Domokos, P., Ritsch, H., and Vukics, A. *Phys. Rev. A* **72**(5), 053417 (2005).

[32] Black, A. T., Chan, H. W., and Vuletić, V. *Phys. Rev. Lett.* **91**(20), 203001 (2003).

[33] Nagy, D., Szirmai, G., and Domokos, P. *Eur. Phys. J. D* **48**, 127 (2008).

[34] Lev, B. L., Vukics, A., Hudson, E. R., Sawyer, B. C., Domokos, P., Ritsch, H., and Ye, J. *Phys. Rev. A* **77**(2), 023402 (2008).

[35] Abrikosov, A. A., Gorkov, L. P., and Dzyaloshinski, I. M. *Methods of Quantum Field Theory in Statistical Physics*. Prentice-Hall, (1963).

[36] Sachdev, S. *Quantum Phase Transitions*. Cambridge University Press, (1999).

[37] Mottl, R., Brennecke, F., Baumann, K., Landig, R., Donner, T., and Esslinger, T. arXiv:1203.1322, (2012).

[38] Dicke, R. H. *Phys. Rev.* **93**, 99–110 (1954).

[39] Keeling, J., Bhaseen, M. J., and Simons, B. D. *Phys. Rev. Lett.* **105**, 043001 (2010).

[40] Bhaseen, M. J., Mayoh, J., Simons, B. D., and Keeling, J. *Phys. Rev. A* **85**, 013817 (2012).

[41] Nagy, D., Szirmai, G., and Domokos, P. *Phys. Rev. A* **84**, 043637 (2011).

[42] Szymańska, M. H., Keeling, J., and Littlewood, P. B. *Phys. Rev. B* **75**(19), 195331 (2007).

[43] Schwinger, J. *J. Math. Phys.* **2**, 407 (1961).

[44] Keldysh, L. V. *Soviet JETP* **20**, 1018 (1965).

[45] Shankar, R. *Rev. Mod. Phys.* **66**(1), 129–192 (1994).

[46] Toner, J. *Phys. Rev. Lett.* **100**(3), 035302 (2008).

[47] Fil, D. V. and Shevchenko, S. I. *Phys. Rev. B* **80**(10), 100501 (2009).

[48] Syshchenko, O., Day, J., and Beamish, J. *Phys. Rev. Lett.* **104**(19), 195301 (2010).

[49] Hunt, B., Pratt, E., Gadagkar, V., Yamashita, M., Balatsky, A. V., and Davis, J. C. *Science* **324**, 632 (2009).

[50] Góral, K., Santos, L., and Lewenstein, M. *Phys. Rev. Lett.* **88**(17), 170406 (2002).

[51] Yi, S., Li, T., and Sun, C. P. *Phys. Rev. Lett.* **98**(26), 260405 (2007).

[52] Brazovskii, S. *Soviet JETP* **41**, 85–89 (1975).

[53] Hohenberg, P. C. and Swift, J. B. *Phys. Rev. E* **52**(2), 1828–1845 (1995).

[54] Walls, D. F. and Milburn, G. J. *Quantum Optics*. Springer, (2008).

[55] Altland, A. and Simons, B. D. *Condensed Matter Field Theory*. Cambridge University Press, (2006).

[56] Castro Neto, A. H. and Caldeira, A. O. *Phys. Rev. A* **42**(11), 6884–6893 (1990).

[57] Biroli, G., Parcollet, O., and Kotliar, G. *Phys. Rev. B* **69**(20), 205108 (2004).

[58] Swift, J. and Hohenberg, P. C. *Phys. Rev. A* **15**(1), 319–328 (1977).

[59] Chaikin, P. M. and Lubensky, T. C. *Principled of Condensed Matter Physics*. Cambridge University Press, (1995).

[60] Altman, E., Demler, E., and Lukin, M. D. *Phys. Rev. A* **70**(1), 013603 (2004).

[61] Mitra, A., Takei, S., Kim, Y. B., and Millis, A. J. *Phys. Rev. Lett.* **97**(23), 236808 (2006).

[62] Landau, L. and Lifshitz, E. M. *Statistical Physics Part 1*. Pergamon, (1980).

[63] Szymańska, M. H., Keeling, J., and Littlewood, P. B. *Phys. Rev. Lett.* **96**(23), 230602 (2006).

[64] Reppy, J. D. *Phys. Rev. Lett.* **104**(25), 255301 (2010).

[65] Andreev, A. F. and Lifshitz, I. M. *Soviet JETP* **29**, 1107 (1969).

[66] Chester, G. V. *Phys. Rev. A* **2**(1), 256–258 (1970).

[67] Leggett, A. J. *Phys. Rev. Lett.* **25**(22), 1543–1546 (1970).

[68] Mekhov, I. B., Maschler, C., and Ritsch, H. *Nat. Phys.* **3**, 319–323 (2007).

[69] Dorsey, A. T., Goldbart, P. M., and Toner, J. *Phys. Rev. Lett.* **96**(5), 055301 (2006).

[70] McKay, D., White, M., Pasienski, M., and DeMarco, B. *Nature* **453**, 76–79 (2008).

[71] Fernández-Vidal, S., De Chiara, G., Larson, J., and Morigi, G. *Phys. Rev. A* **81**(4), 043407 (2010).

[72] Bijlsma, M. J. and Stoof, H. T. C. *Phys. Rev. B* **56**(22), 14631–14644 (1997).

[73] van Hemmen, J. L. *Phys. Rev. Lett.* **49**(6), 409–412 (1982).

[74] Amit, D. J., Gutfreund, H., and Sompolinsky, H. *Phys. Rev. Lett.* **55**(14), 1530–1533 (1985).

[75] Ioffe, L. B. and Feigel'man, M. V. *Soviet JETP* **88**, 604–630 (1985).

[76] Weissman, M. B. and Wolynes, P. G. *Phys. Rev. B* **46**(21), 14209–14212 (1992).

[77] Altman, E., Kafri, Y., Polkovnikov, A., and Refael, G. *Phys. Rev. Lett.* **100**(17), 170402 (2008).

[78] Fisher, M. P. A., Weichman, P. B., Grinstein, G., and Fisher, D. S. *Phys. Rev. B* **40**(1), 546–570 (1989).

[79] Pasienski, M., McKay, D., White, M., and DeMarco, B. *Nat. Phys.* **6**, 677–680 (2010).

[80] Bhatt, R. N. and Lee, P. A. *Phys. Rev. Lett.* **48**(5), 344–347 (1982).

[81] Fisher, D. S. *Phys. Rev. B* **50**(6), 3799–3821 (1994).

[82] Strack, P. and Sachdev, S. *arXiv:1109.2119* (2011).

[83] Dagotto, E. *Rev. Mod. Phys.* **66**(3), 763–840 (1994).

[84] Jördens, R., Niels Strohmaier, N., Günter, K., Moritz, H., and Esslinger, T. *Nature* **455**, 204–207 (2008).

[85] Struck, J., lschlger, C., Le Targat, R., Soltan-Panahi, P., Eckardt, A., Lewenstein, M., Windpassinger, P., and Sengstock, K. *Science* **333**(6045), 996–999 (2011).

[86] Medley, P., Weld, D. M., Miyake, H., Pritchard, D. E., and Ketterle, W. *Phys. Rev. Lett.* **106**, 195301 (2011).

[87] Gorshkov, A. V., Manmana, S. R., Chen, G., Demler, E., Lukin, M. D., and Rey, A. M. *Phys. Rev. A* **84**, 033619 (2011).

[88] Ruderman, M. A. and Kittel, C. *Phys. Rev.* **96**(1), 99 (1954).

[89] Tsunetsugu, H., Sigrist, M., and Ueda, K. *Rev. Mod. Phys.* **69**(3), 809–864 (1997).

[90] Binder, K. and Young, A. P. *Rev. Mod. Phys.* **58**(4), 801–976 (1986).

[91] John, S. and Quang, T. *Phys. Rev. Lett.* **76**, 1320–1323 (1996).

[92] Bermudez, A., Almeida, J., Schmidt-Kaler, F., Retzker, A., and Plenio, M. B. *Phys. Rev. Lett.* **107**, 207209 (2011).

[93] Black, A. T., Thompson, J. K., and Vuletić, V. *Phys. Rev. Lett.* **95**, 133601 (2005).

[94] Zheng, S.-B. *Phys. Rev. A* **68**, 035801 (2003).

[95] Zoubi, H. and Ritsch, H. *Phys. Rev. A* **80**, 053608 (2009).

[96] Kastoryano, M. J., Reiter, F., and Sørensen, A. S. *Phys. Rev. Lett.* **106**(9), 090502 (2011).

[97] Tolkunov, D. and Solenov, D. *Phys. Rev. B* **75**(2), 024402 (2007).

[98] Nakamura, Y., Torii, K., and Munakata, T. *Phys. Rev. E* **51**(2), 1538–1546 (1995).

[99] Gopalakrishnan, S., Lev, B. L., and Goldbart, P. M. *Phil. Mag.* **92**, 353–361 (2011).

[100] Weitenberg, C., Endres, M., Sherson, J. F., Cheneau, M., Schauss, P., Fukuhara, T., Bloch, I., and Kuhr, S. *Nature* **471**, 319–324 (2011).

[101] Vengalattore, M., Leslie, S. R., Guzman, J., and Stamper-Kurn, D. M. *Phys. Rev. Lett.* **100**(17), 170403 (2008).

[102] Pino, J. M., Wild, R. J., Makotyn, P., Jin, D. S., and Cornell, E. A. *Phys. Rev. A* **83**(3), 033615 (2011).

[103] Dimer, F., Estienne, B., Parkins, A. S., and Carmichael, H. J. *Phys. Rev. A* **75**, 013804 (2007).

[104] Kawaguchi, Y. and Ueda, M. *Phys. Rev. A* **84**, 053616 (2011).

[105] Radzihovsky, L. and Vishwanath, A. *Phys. Rev. Lett.* **103**, 010404 (2009).

[106] Radzihovsky, L. *Phys. Rev. A* **84**, 023611 (2011).

[107] Lin, Y.-J., Jiménez-Garcia, K., and Spielman, I. *Nature* **471**, 83 (2011).

[108] Wirth, G., Ölschläger, M., and Hemmerich, A. *Nat. Phys.* **7**, 147 (2011).

[109] Mele, E. J. *Phys. Rev. B* **81**, 161405 (2010).

[110] Stanescu, T. D., Anderson, B., and Galitski, V. *Phys. Rev. A* **78**, 023616 (2008).

[111] Wu, C. and Mondragon-Shem, I. Zhou, X.-F. *Chin. Phys. Lett.* **28**, 097102 (2011).

[112] Wang, C., Gao, C., Jian, C.-M., and Zhai, H. *Phys. Rev. Lett.* **105**, 160403 (2010).

[113] Jian, C.-M. and Zhai, H. *Phys. Rev. B* **84**, 060508 (2011).

[114] Ho, T.-L. and Zhang, S. *Phys. Rev. Lett.* **107**, 150403 (2011).

[115] Yang, K. and Sachdev, S. *Phys. Rev. Lett.* **96**, 187001 (2006).

[116] Berg, E., Rudner, M. S., and Kivelson, S. A. *Phys. Rev. B* **85**, 035116 (2012).

[117] Ozawa, T. and Baym, G. *Phys. Rev. A* **84**, 043622 (2011).

[118] Leggett, A. J. *Quantum Liquids.* Oxford University Press, (2006).

[119] Fisher, D. S. and Hohenberg, P. C. *Phys. Rev. B* **37**, 4936–4943 (1988).

[120] Kohn, W. and Luttinger, J. M. *Phys. Rev. Lett.* **15**, 524–526 (1965).

[121] Cappelluti, E., Grimaldi, C., and Marsiglio, F. *Phys. Rev. Lett.* **98**, 167002 (2007).

[122] Ozawa, T. and Baym, G. *Phys. Rev. A* **85**, 013612 (2012).

[123] Kolomeisky, E. B. and Straley, J. P. *Phys. Rev. B* **46**, 11749–11756 (1992).

[124] Barnett, R., Powell, S., Graß, T., Lewenstein, M., and Das Sarma, S. *Phys. Rev. A* **85**, 023615 (2012).

[125] Batten, R. D., Huse, D. A., Stillinger, F. H., and Torquato, S. *Soft Matter* **7**, 6194–6204 (2011).

[126] Barkan, K., Diamant, H., and Lifshitz, R. *Phys. Rev. B* **83**, 172201 (2011).

[127] Oganesyan, V. and Huse, D. A. *Phys. Rev. B* **75**, 155111 (2007).